Laser Nanowarming: A platform technology for ultra-rapid rewarming of cryopreserved zebrafish embryos

A Dissertation
SUBMITTED TO THE FACULTY OF
UNIVERSITY OF MINNESOTA
BY

Kanav Khosla

IN PARTIAL FULFILLMENT OF THE REQUIREMENTS
FOR THE DEGREE OF
DOCTOR OF PHILOSOPHY

Adviser: John C. Bischof

June 2019

Acknowledgments

This work is the culmination of my educational and research achievements over the past nine years at the University of Minnesota. I came to the US as a 17-year-old boy, despite never being away from my family home in India for more than a week. Any success I achieve is solely due to the unconditional love and support I got from my parents Aarti and Pradeep Khosla. I must also thank my sister Kasvi who, despite being six years younger than me, was always a source of inspiration and wisdom.

Adjusting to life in the US was made a lot easier by finding family support in my uncle Dr. Inder Sud and his wife Peg Sud. They both were incredibly generous with their time and resources. To get me started they paid for my college tuition, cellphone bill, bike, and dorm supplies. To this day, they continue to provide valuable advice when it comes to making life and career choices. I want to thank my best friend Samrat Kochhar for helping me explore new things and always being supportive during difficult times. I don't think this dissertation could be written without the constant feedback got on my writing from my girlfriend Elizabeth Tryczak. She has transformed me with her kindness and empathy, guiding me to become better in my personal and professional life. I will be forever indebted to the Sud family and my friends in Minnesota for welcoming me into their lives and helping build a life in the US.

There was no a better place than the Bioheat Mass Transfer lab to invest my time and energy. I want to thank my adviser Dr. John Bischof for giving me an opprotunity. Without his mentorship and support from my colleagues, none of this work could have been accomplished. I would like to acknowledge Dr. Zhenpeng Qin, Li Zhan, Dr. Yiru Wang, Yilin Liu and Joe Kangas for their collaborative efforts on our current and future

work. I find it reassuring to know that with their input, we can take this technology to the next level.

I was fortunate to have some great collaborators on this project. I thank Dr Mary Hagedorn for bringing our labs together to work on this incredibly complex problem and guiding me through the years to better understand the zebrafish embryo. I also would like to acknowledge Marc Tye, the manager at the UMN Zebrafish Core, for training me and supporting this work over the years.

This work was generously funded by the NIH, Institute of Engineering in Medicine and the Department of Mechanical Engineering.

Dedication

This dissertation is dedicated to my mother Aarti Khosla, M.A. & M.Phil. in History

Abstract

This work describes the development of a platform technology called Laser Nanowarming that has enabled the cryopreservation of Zebrafish embryos for the first time. By injecting propylene glycol (PG) and biocompatible gold nanorods (GNR) followed by rapid cooling (90,000 °C/min), embryos were cryogenically stabilized to liquid nitrogen temperatures. Since the effective concentration of PG inside the embryos is approximately 2M, the embryos require rapid rewarming, which was achieved by using a 1064nm powerful millisecond laser pulse that can generate rates up to 14 million °C/min. We leverage biocompatible and photonic GNR that can create rapid and uniform warming throughout the embryo and overcome the damage induced by ice crystallization. We have since adapted this technology to demonstrate successful outcomes in Human Dermal Fibroblasts (HDF) cells as well as Coral larvae (*F. Scutaria*) and continue to use it to enable the cryopreservation of Pancreatic Islets, Drosophila Embryos, Shrimp Nauplii and other fish embryos. Our future work is geared towards improving the long-term survival rate of biological specimens as well as developing efficient high throughput methods. If successful, this technology can transform the way germplasm are banked and create a huge impact in the fields of species conservation, biomedical research and aquaculture.

Table of Contents

List of Tables

List of Figures

Statement of Contribution

This dissertation represents the accumulated research work of the author with contributions from collaborators. The author worked closely with his adviser Dr. John Bischof on experiment planning, data analysis and manuscript writing of each chapter. The contributions of the author and others are presented below by chapter.

Chapter 1: Introduction & Review

This chapter introduces challenges faced by researchers to cryopreserve aquatic embryos as well as briefly describes principles behind laser assisted gold nanoparticle heating. There is also a discussion on the impact of this work on fields of biomedical research and aquaculture. Most of the work in this chapter is taken from the introduction and discussion sections from the following peer reviewed publications and reproduced here with the permission of the journal publisher:

1. **Khosla, K**., Wang, Y., Hagedorn, M., Qin, Z., & Bischof, J. (2017). Gold nanorod induced warming of embryos from the cryogenic state enhances viability. *ACS nano*, *11*(8), 7869-7878. DOI: 10.1021/acsnano.7b02216 Copyright © 2017 American Chemical Society
2. **Khosla, K.,** Zhan, L., Bhati, A., Carley-Clopton, A., Hagedorn, M., & Bischof, J. (2018). Characterization of Laser Gold Nanowarming: A Platform for Millimeter-Scale Cryopreservation. *Langmuir*. DOI: 10.1021/acs.langmuir.8b03011 Copyright © 2018 American Chemical Society

Chapter 2: Laser Warming of Frozen Zebrafish Embryos

This chapter describes the development protocols for laser and gold nanoparticle-based warming that were used in developing this unique approach to rapidly rewarm vitrified

zebrafish embryo. This work led to the first ever successful attempt at maintaining viable and developing embryos after warming. Most of the work in this chapter is taken from the following peer reviewed publication and reproduced here with the permission of the journal publisher:

1. **Khosla, K**., Wang, Y., Hagedorn, M., Qin, Z., & Bischof, J. (2017). Gold nanorod induced warming of embryos from the cryogenic state enhances viability. *ACS nano*, *11*(8), 7869-7878.

DOI: 10.1021/acsnano.7b02216

Chapter 3: Characterization of Laser Gold Nanowarming: A Platform for Millimeter-Scale Cryopreservation

This chapter describes the results from multiple studies conducted to characterize and optimize parameters needed for successful cryopreservation with the laser nanowarming approach. This study also helped position laser nanowarming as a universal platform to cryopreserve various biomaterials within 10 µm to 2mm size range. Most of the work in this chapter is taken from the following peer reviewed publications and reproduced here with the permission of the journal publisher:

1. **Khosla, K.,** Zhan, L., Bhati, A., Carley-Clopton, A., Hagedorn, M., & Bischof, J. (2018). Characterization of Laser Gold Nanowarming: A Platform for Millimeter-Scale Cryopreservation. *Langmuir*. DOI: 10.1021/acs.langmuir.8b03011

Chapter 4: Improvement in long term survival of frozen zebrafish embryos post laser nanowarming

This chapter details the changes and optimizations made in injection and freezing protocols, that led to significant improvements to survival rate up to 5 days post laser warming. Additionally, there is also data showing live and viable embryos spawning from two laser warmed adult fish. Most of the work in this chapter is being prepared as the following manuscript for submission and review:

1. **Khosla, K.,** Kangas, J., Zhan, L., Liu, Y., Daly, J., Hagedorn, M., & Bischof, J. (2019). Improvement in long term survival of zebrafish embryos post laser nanowarming (in preparation)

Chapter 5: Conclusion and Future Work

This chapter will discuss the overall results from the development of laser nanowarming technology and its application to cryopreserve zebrafish embryos. In addition, we also discuss our future work and its implications for other biological systems.

Appendix A

This appendix describes the development of a cryojig device and experimental and modeling work conducted by the author to design studies associated with laser nanowarming of zebrafish embryos systems. This work has been a part of the peer reviewed publication and is reproduced here with permission:

1. **Khosla, K**., Wang, Y., Hagedorn, M., Qin, Z., & Bischof, J. (2017). Gold nanorod induced warming of embryos from the cryogenic state enhances viability. *ACS nano*, *11*(8), 7869-7878.

Appendix B

This appendix shares details such as CAD drawings and BOM for the cryojig

Appendix C

This appendix shares the cover page of a peer reviewed publications from our coral cryopreservation and laser warming work with our Smithsonian Collaborators. The author contributed significantly to this work and it led to the first ever instance of successful cryopreservation of coral larvae.

1. Daly, J., Zuchowicz, N., Lendo, C. I. N., **Khosla, K.**, Lager, C., Henley, E. M., ... & Hagedorn, M. (2018). Successful cryopreservation of coral larvae using vitrification and laser warming. *Scientific reports*, *8*(1), 15714. DOI: 10.1038/s41598-018-34035-0 Open access via Creative Commons Attribution 4.0 International License

Chapter 1: Introduction & Review

This chapter introduces challenges faced by researchers to cryopreserve aquatic embryos as well as briefly describes principles behind laser assisted gold nanoparticle heating. There is also a discussion on the impact of this work on fields of biomedical research and aquaculture. Most of the work in this chapter is taken from the following peer reviewed publications and reproduced here with the permission of the journal publisher:

Khosla, K., Wang, Y., Hagedorn, M., Qin, Z., & Bischof, J. (2017). Gold nanorod induced warming of embryos from the cryogenic state enhances viability. *ACS nano, 11*(8), 7869-7878. DOI: 10.1021/acsnano.7b02216

Khosla, K., Zhan, L., Bhati, A., Carley-Clopton, A., Hagedorn, M., & Bischof, J. (2018). Characterization of Laser Gold Nanowarming: A Platform for Millimeter-Scale Cryopreservation. *Langmuir*. DOI: 10.1021/acs.langmuir.8b03011

1.1 Cryopreservation by vitrification

Vitrification, the freezing of material to a "glassy" rather than crystalline phase, is an important enabling approach for cryopreservation[1-2]. Vitrification relies on cooling rapidly below the glass transition temperature without growth of ice (a kinetic process) despite passing through a thermodynamic regime favorable to nucleation and ice growth (*i.e.* passing through heterogenous, T_{het}, and homogenous, T_{hom}, nucleation temperatures). Figure 1.1a shows the phase diagram for a hypothetical cryoprotective agents (CPA) where, once below the glass transition temperature T_g, biomaterials are considered *"cryogenically stable"* for long-term storage since no additional ice crystallization can occur. To rewarm, one has the same challenge in reverse: as the biomaterial rises above the devitrification temperature (i.e. reversion from glassy to crystalline phase), again passing through the homogeneous and heterogenous nucleation temperatures, one must reach the melt temperature without the occurrence of significant ice crystallization or re-crystallization. Avoiding ice growth in the temperature range between T_g and T_m can be achieved by increasing both CPA concentration (which reduces the difference between T_g and T_m) and/or warming rates (which reduces the time to allow ice crystallization).

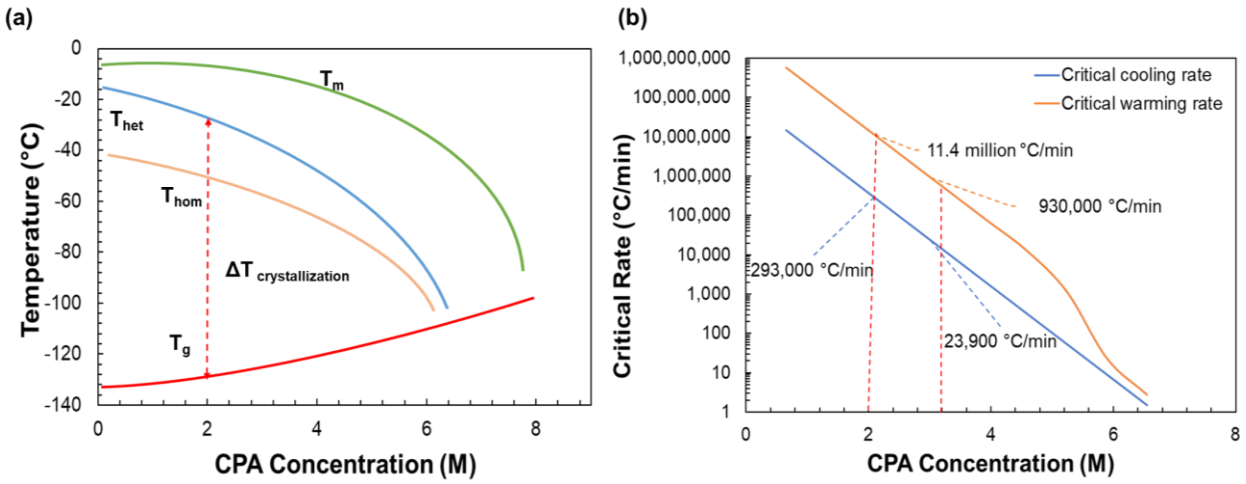

Figure 1.1. Predicting ice formation for low concentration CPA (< 4M). (a) Phase diagram for a theoretical CPA with T_M- Melt temperature, T_{Hom}- Homogenous nucleation temperature, T_{Het}- Heterogeneous nucleation temperature, T_G- Glass transition temperature and $\Delta T_{crystallization}$– temperature range during which the probability of ice crystallization is highest (modified from Fahy et al 1984[1]). (b) Critical rates for PG obtained from literature showing experimental results obtained from a DSC for greater than 5M. Note: There is no experimental data available for concentrations less than 5M for PG, so theoretical predictions were made using Boutron's data and model[3-7]. Using this approach, we predict critical cooling rates (CCR) of 293,000 °C/min and 23,000 °C/min and critical warming rates (CWR) of 11,400,000 °C/min and 930,000 °C/min for 2M PG and 2M and 1M Trehalose, respectively.

In theory, there is an inverse relationship between the cooling and warming rates needed to prevent ice growth and the CPA concentration used for vitrification. The lowest concentration of CPAs that will cool and warm the sample without ice formation is used to prevent toxicity to biological samples. For example, upwards of 6 to 8 M CPA is used with large centimeter-sized tissues and organs in order to prevent ice crystal growth in the temperature range between T_g and T_m[8]. For these larger cm-scale systems, boundary cooling and warming (*i.e.* convective boundary conditions) achieve only 10 – 100 °C/min rates. Nevertheless, a high concentration (~ 8M) CPA vitrification approach was originally found to be effective in mouse embryo cryopreservation.[9] Later work found that lower concentrations closer to 2M can also be used if rates of cooling and warming are

dramatically increased. This is important as it reduces CPA concentration and therefore toxicity in many specialized cells such as embryos[10-11] and oocytes[12]. The critical rates of cooling and warming (*i.e.* CCR and CWR) necessary to achieve vitrification and avoid devitrification (*i.e.* ice crystallization from vitrified glassy phase) in higher concentration (≥ 5M) CPAs have been studied using differential scanning calorimetry (DSC) for propylene glycol (PG)[4-5], DMSO[13-14], ethylene glycol[3], linear poly alcohols[15], and diethylformamide.[16] Nevertheless, the CCR and CWR rates have never been directly measured for low concentration CPAs (< 4M) due to the inaccessibility of high rates (> 100s °C/min) during experimentation. Figure 1b plots the CCR and CWR needed to avoid ice formation (≤ 0.2% of mass of CPA solution) for varying concentrations of PG. Rates here were obtained experimentally from ≥ 5M DSC measurements[3, 7] and theoretically extrapolated for ice crystallization in PG/water (< 5M) using Boutron's equations[3-7]. Several other theoretical estimates for CCR available in literature for different CPAs (2-3M) range from 10,000 to 500,000 °C/min[6, 17-18]. Importantly, CWRs often need to exceed CCRs by at least an order of magnitude to avoid ice crystallization because of the presence of small ice nuclei within cryogenically stabilized specimens. In short, achieving CCR and CWR is critical for successful cryopreservation and there continues to be a need for accurate, quantitative measurements of both CCR and CWR for low concentration (< 4 M) CPA solutions.

Table 1.1. Effect of CPA concentration on critical rates and type of failure modes[6, 18-19].

CPA Concentration	Critical cooling rate (°C/min)	Critical warming rate (°C/min)	Failure mode
High (> 6M)	10-100	100-1,000	Biological (Toxicity)
Low (< 2M)	10,000- 100,000*	100,000-10,000,000*	Physical (Cooling)

*These are expected rates and are yet to be measured

1.2 Challenges to cryopreserve zebrafish embryos

Nevertheless, a great deal is known about the barriers to successfully cryopreserve zebrafish embryos including: (i) the large size of the embryo, resulting in a low surface-to-volume ratio impeding water and cryoprotectant efflux/influx; (ii) compartments, such as the blastoderm and yolk, with differing permeability properties, specifically the yolk syncytial membrane which is a barrier to most cryoprotectants[20]; (iii) large-sized cells, such as the yolk, which may increase the likelihood of membrane disruption by intracellular ice-formation upon cooling and ice-crystal growth upon warming[21]; and (iv) susceptibility to chilling injury[22]. To address the permeability barrier, microinjection has been shown to be a safe and non-toxic method for introducing cryoprotectants up to 2 M into the yolk compartment[23], and the chilling sensitivity can be outrun by rapid cooling. However, the large size of the yolk impedes rapid cooling and warming, thereby yielding to lethal ice-crystal formation[10, 23]. Multiple studies have shown that slow freezing is not a possible method of cryopreservation for embryos because of the relatively high nucleation temperature of intraembryonic water[24-26].

1.3 Significance of zebrafish in aquaculture and biomedical research

Cryopreservation has been used successfully for decades to preserve both bio- and genetic diversity in a planet under siege from local and global stressors. This need is especially apparent in aquatic ecosystems due to coastal pollution, over-fishing, climate change, and acidifying oceans. Today, about 80% of marine fish stocks are over-exploited [27], and the International Union of Conservative Naturalists lists fresh water fish species as one of the most threatened group of vertebrates on the planet [28]. An important safeguard to these species is the creation of a frozen germplasm bank, through cryopreservation, which can

retain viability for years (or even centuries) without DNA damage, an important way to safeguard existing species and their genetic diversity [21]. More specifically, these 'frozen banks' offer samples of preserved and protected genetic pools that can be used to 'seed' shrinking populations all over the world. Additionally, it allows for easy and inexpensive transport of genetic materials among living and/or managed populations and improving access to biomaterials for scholarly research.

Since the beginning of cryopreservation, fish sperm cryopreservation has been commonly practiced[29-32]. However, sperm cryopreservation only maintains half the genome, and until now, fish embryo cryopreservation has never been successful and has remained an elusive goal [33]. The key to successful cryopreservation requires a series of steps that allow some water within the cell to be replaced with a cryoprotectant that prevents damage from freezing. The partially dehydrated cell is then able to withstand the extraordinary stress of cooling and low temperature storage, essentially entering a state of suspended animation. Although many reports claim successful cryopreservation of fish embryos, no protocols have yet been sufficiently defined to allow replication by other groups [34].

Developing techniques for the cryopreservation of teleost germ plasm is timely and the need is pressing. At present, aquaculture is largely dependent upon wild fish populations or continuous maintenance of living cultures. Unfortunately, the availability and productivity of these systems is continually threatened by accidents, natural disasters, breeding failure and disease. In the past decade, laboratories around the world have produced tens of thousands of mutants, transgenic, and wild-type zebrafish (*Danio rerio*) lines for a wide range of vertebrate genetics and biomedical research. Zebrafish possess high fertility rates, their embryos develop externally and rapidly (within 3 days[35]), and their

embryos are transparent. Transparency allows easy optical monitoring during a growth cycle and providing a valuable tool for understanding embryogenesis and organ development. The mapping of the zebrafish genome shows that 70% of the genes have a human orthologue. For disease-causing genes, 82% have an orthologue in humans,[36] and positional cloning of zebrafish genes has allowed researchers to utilize many candidate genes, similar to those of humans, to cause mutations and further improve the ability to study diseases.[31, 36-38] For example, due to the structural and genetic similarity of the zebrafish eye and the human eye, researchers have used zebrafish to study cataracts and glaucoma.[39-40] Scientists have also been able to utilize gene engineering tools in zebrafish to cause an optical reaction to calcium ions in the brain that can be tracked by fluorescence microscopy in order to study and predict brain activity and behavior.[41] Many high-impact studies are now using zebrafish models to complement some cancer models. [42-45] For instance, researchers have used transgenic and xenograft models to study many different aspects of human cancers like lymphoblastic T-cell leukemia, pancreatic cancer, melanoma and rhabdomyosarcoma.[44, 46] The transparency of zebrafish also allows researchers to non-invasively visualize cancer progression and even angiogenesis.[44, 47-48] Researchers are even using these models to look for genetic and chemical modifiers of cancer and to test the efficiency of pharmaceuticals.[39, 48] Maintaining all these valuable genotypes is expensive, risky, and beyond the capacity of even the largest stock centers. For example, valuable genetic lines created for productivity and disease resistance, such as transgenic fish and hybrids [49], must be maintained in live-culture systems. These strains can take years to generate, which is costly in terms of space, maintenance, and research effort, and are subject to loss through genetic drift. Systematic germ plasm cryopreservation can have a

profound impact on aquaculture by: (1) allowing the maintenance of large gene pools and reducing inbreeding; (2) reducing pressure on wild populations from collection activities; (3) maintaining a constant supply of animals (i.e., some animals are unavailable in the wild during certain times of the year like corals and fish); (4) decreasing aquaculture costs by reducing the facilities needed; (5) reducing the impact (e.g., contamination with antibiotics) of aquaculture sites upon wild populations and food resources; and (6) sustaining productivity by minimizing the impact of live-culture failures resulting from human error, natural disasters, breeding failure and epidemics. At its 2007 workshop "Achieving High-Throughput Repositories for Biomedical Germplasm Preservation," the NIH recognized these problems and boosted its efforts to promote research focused on finding effective solutions of which cryopreservation is currently the only long-term alternative. Cryopreserving zebrafish embryos was a clearly identified goal of this report [33].

1.4 Need for laser warming for biomaterials

Today, there are many commercially available devices that approach or achieve the necessary CCR required for vitrifying low concentration CPA solutions (w/ or w/o cells). Some example devices include the cryotop[50], Open Pulled Straw[51], Quartz Micro Capillary[52], and copper grids[12]. For instance, the cryotop system can achieve rates greater than 69,000 °C/min for 0.1µL systems such as mouse oocytes (D_{cell}=80 µm)[53-54] but is unable to provide the high warming rates by convection alone needed to prevent visible ice crystal formation during warming for volumes greater than 0.1µL. Likewise, zebrafish embryos (V=1µL, D_{cell}=1mm) can be microinjected with 2M PG glycol and rapidly cooled below cryogenic temperatures with the cryotop, but convective warming consistently leads to failure (0% survival) since it is not fast enough to prevent ice formation within the larger

embryo[11]. In short, even with fast cooling, faster warming remains essential to either prevent or "outrun" ice crystal growth especially in low concentration CPA systems[55].

To further emphasize this point, Peter Mazur's group pioneered a new laser warming technique that can "rescue" samples that were cooled with less than optimal CPA or simply cooled at rates below CCR such that some ice may have formed during cooling. More specifically, mice oocytes were successfully rewarmed despite being cooled at or below the CCR[56]. This was possible through Mazur's ultra-rapid laser warming technique using India Ink (*i.e.* carbon black) as a laser absorber. Briefly, India Ink, a broad-band laser absorber, was deployed with CPA (~2.3M) around the oocytes to provide "extracellular" absorption of the laser to achieve warming rates of 10^7 °C /min. This work demonstrated excellent viability (96%) of mouse oocytes (D_{cell} = 80 μm) vitrified by rapid cooling with a cryotop and then warmed with a laser[54]. Comparatively, just 28% of mice oocytes (V = 0.1μL) survived that were rewarmed at a rate of 117,000 °C/min convectively with the cryotop. This shows that despite the ability of the cryotop to provide fast cooling rates for 0.1 μL samples without ice formation with under 3M CPA, it failed to provide an ultra-rapid warming rate needed to stop ice crystallization during rewarming. Importantly, this suggests that rapid warming rates provided by laser warming could drastically reduce the need for higher concentrations of CPA.

Although Mazur's extracellular heating approach worked on smaller oocytes, it fails on millimeter-sized cellular systems like fish embryos due the large thermal gradients introduced by heating only in the extracellular space[54]. To address this issue, our research group developed a combined intracellular and extracellular warming approach using biocompatible and plasmonically designed gold nanorods (GNRs) that absorb specifically

and reproducibly at 1064 nm, a wavelength where pulsed laser systems with appropriate energy already exist. This approach was used to successfully rewarm cryopreserved zebrafish embryos, which are 1000x larger than mammalian embryos, using a single 1064nm laser pulse. We chose a 1064nm laser specifically to ensure that water and other cellular structures don't absorb or scatter laser beam at this wavelength and absorption is isolated to nanoparticles only. Most laser based photothermal therapies take advantage of this so called "therapeutic window" [57-58]. Plasmonic nanoparticles have been well-developed for many biomedical applications but have not been extensively applied to cryopreservation applications.[59-60] These nanoparticles can effectively generate heat when the laser wavelength matches the gold nanoparticle's surface plasmon resonance energy. Once resonant, the laser produces oscillations in the gold nanoparticle to induce heat dissipation (Q_{nano}). By placing many nanoparticles (N = particles/m^3) together in one system, a collective heat generation or specific absorption rate (SAR, W/m^3) can be achieved as shown below in Equation 1.1 in the absence of any diffusive or other losses. The laser fluence rate, I (W/m^2), varies as the laser light attenuates inside the specimen based on Beer's law. The C_{abs} (nm^2) term represents the absorption cross section of a single nanoparticle. The μ_{abs} (cm^{-1}) represents the bulk absorption coefficient for the entire absorbing system, which in our case is the embryo:

$$SAR = NQ_{nano} = NC_{abs}I = \mu_{abs}I = \rho c\left(\frac{dT}{dt}\right)_{initial} \qquad (1.1)$$

To fully benefit from this heat generation, the biocompatible PEGylated GNRs are microinjected directly into the zebrafish embryos with low concentration CPA, thereby helping to distribute the laser energy throughout the embryo during warming[11] as opposed to only externally (*i.e.* India Ink). Specifically, external absorbers are sufficient to

successfully warm a mouse oocyte, but not the zebrafish embryo whose volume is ~ 1000 times larger than a mouse oocyte.[54] Gold nanorods (GNR) were chosen as they are easy to produce and have among the highest absorption cross section (C_{abs}) for laser in the near infra-red spectrum (800-1200 nm) for gold nanoparticles.[61] The biocompatibility of PEGylated GNR is supported by numerous studies showing that after removal of toxic CTAB, these nanoparticles are safe for use in numerous biomedical applications including intravenous injections[62-65]. Thus, gold nanoparticle-based laser warming (i.e. laser nanowarming) has the potential to provide a platform for both extra- and intra-cellular heating to successfully cryopreserve a variety of up to mm sized biomaterials in µL sized droplets.

Chapter 2: Laser Warming of Frozen Zebrafish Embryos

This chapter describes the development protocols for laser and gold nanoparticle-based warming that were used in developing this unique approach to rapidly rewarm vitrified zebrafish embryo. This work led to the first ever successful attempt at maintaining viable and developing embryos after warming. Most of the work in this chapter is taken from the following peer reviewed publication and reproduced here with the permission of the journal publisher:

Khosla, K., Wang, Y., Hagedorn, M., Qin, Z., & Bischof, J. (2017). Gold nanorod induced warming of embryos from the cryogenic state enhances viability. *ACS nano*, *11*(8), 7869-7878.

DOI: 10.1021/acsnano.7b02216

Abstract

Zebrafish embryos can attain the cryogenic state by microinjection of cryoprotectants followed by rapid cooling, but the massive size of the embryo has consistently led to failure during the convective warming process. Here we address this zebrafish cryopreservation problem by using gold nanorods (GNRs) to assist in the warming process. Specifically, we micro-injected the cryoprotectant propylene glycol into zebrafish embryos along with GNRs and the samples were cooled at a rate of 90,000 °C/min in liquid nitrogen. We demonstrated the ability to unfreeze the zebrafish rapidly (1.4×10^7 °C/min) by irradiating the sample with a 1064 nm laser pulse for 1 ms due to the excitation of GNRs. This rapid warming process led to the outrunning of ice formation, which can damage the embryos. The results from 14 trials ($n = 223$) demonstrated viable embryos with consistent structure at 1 hr (31%), and continuing development at 3 hr (17%) and movement at 24 hr (10%) post-warming. This compares starkly with 0% viability, structure, or movement at all time points in convectively warmed controls ($n = 50$, $p < 0.001$, ANOVA). Our nanoparticle-based warming process could be applied to storage of fish, and with proper modification, it can be potentially be used for other vertebrate embryos.

Results

2.1 Characterization of GNR

Figure 2.1 shows the characterization of our nanoparticle laser absorber - polyethylene glycol (PEG) coated GNRs. This includes a transmission electron microscopy image, extinction spectra, specific absorption cross section (C_{abs}) and a table summarizing size, optical and thermal properties of the GNR-PEG.

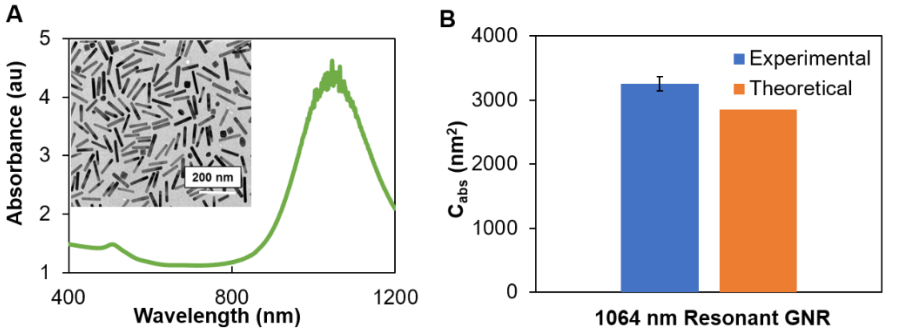

C

Parameter	Experimental	Theoretical
D (n = 526)	18 ± 2 nm	18
L (n = 526)	111 ± 11 nm	111
D_h	22.0 ± 0.1 nm	NA
ζ	22.0 ± 0.1 nm	NA
C_{abs}	3248.9 ± 110.3 nm^2	2853.2 nm^2
μ_a	38.9 ± 0.1 cm^{-1}	34.2 cm^{-1}

Figure 2.1. Gold nanorod (GNR) characterization based DDA modeling and experiments. (a) Extinction spectrum of the GNR was measured from 400nm to 1200nm, showing a plasmon peak at 1064nm. Inside transmission electron microscopy image of GNR, were coated with polyethylene glycol suspended in millipore water. (b) The GNR absorption cross section (Cabs) measured by cuvette heating experiment shown alongside the values obtained from DDA simulation. (c) Table compares experimental and theoretical (DDA) values for GNR properties. It shows the mean diameter D, and length of gold L, nanorods measured from transmission electron microscopy images (n = 526). It also indicated the hydrodynamic diameter (D_h) obtained from dynamic light scattering and the surface charge from zeta potential (ζ) measurements. Negative value of zeta potential is consistent with values reported in literature for PEG coated GNR. In addition, absorption cross section (Cabs) and absorption coefficient (μ_a = NCabs) were calculated by using GNR concentration (N = 1.2 x 10^{18} particles/m^3).

The extinction spectrum confirmed the plasmon absorbance peak at 1064 nm. The Transmission Electron Microscopy images were taken and analyzed with Image J to

establish the GNR diameter and length as 18 ± 2 nm and 111 ± 11 nm, respectively. Dynamic light scattering measured the average hydrodynamic diameter for GNR as 22.0 ± 0.1 nm. The hydrodynamic diameter was slightly higher than the diameter reported by Transmission Electron Microscopy which is common for such measurements.[66] The zeta potential was measured to be -15.0 ± 1.1 mV, with the negative value consistent with values reported in literature for PEG-coated GNRs.[64]

To estimate the heat generated within the embryo by laser GNR warming, comparisons were made between theoretical and experimental results of GNR optical properties that influence warming. First, the nanoparticle property C_{abs}, was predicted to be 2853.2 nm^2 from Discrete Dipole Approximation (DDA) using the same dimensions of GNR-PEG (L = 111 nm, D = 18 nm), assuming negligible polydispersity. [67] Next, we experimentally determined the average C_{abs}= 3248.9 ± 110.3 nm^2, by bulk laser heating a cuvette with GNR solution (n = 3). For a GNR concentration of N =1.2 x 10^{18} particles/m^3, See Selection of GNR Concentration in Appendix A.3), the experimental and theoretical values for the bulk absorption coefficient ($\mu_a = NC_{abs}$) were found to be 38.9 ± 0.1 cm^{-1} and 34.2 cm^{-1} respectively. This 10% difference between the experimental and theoretical C_{abs} can be attributed to polydispersity and nanoparticle size assumptions (Fig. 2.1B) as previous studies have shown.[67] To predict the behavior of the embryo during warming, we elected to use the experimentally determined nanoparticle μ_a = 38.9 ± 0.1 cm^{-1} in our model.

2.2 Distribution of GNR after Injection

We assessed the distribution of the GNRs after they had been injected into the zebrafish embryo. For diffusion inside the embryo, diffusion coefficients for larger spherical gold nanoparticles within zebrafish embryos (GNP: D=86 nm, V=33x10^5 nm^3) were found to be D_{GNP} = 6 x10^{-9} cm^2/s.[68] Since our chosen GNR (L=111nm, D=18nm, V=28x10^3 nm^3) is

orders of magnitude smaller than larger spherical GNP, D_{GNR} was found using Wilke-Chang diffusivity [69] to be: $D_{GNR} = D_{GNP} (V_{GNP}/ V_{GNR})^{0.6}$ or ~ 10^{-7} cm^2/s. The results show that diffusion from a spherical source after 4 hours is roughly 6 x $(D_{GNR} t)^{0.5}$ > 2 mm or 5 times the radius of an embryo thus suggesting uniform dispersion in any given compartment. Confocal fluorescence images in Figs. 2.2 a-c, showing the distribution of fluorescent GNR injected inside the embryos after 4 hours support the uniform distribution.

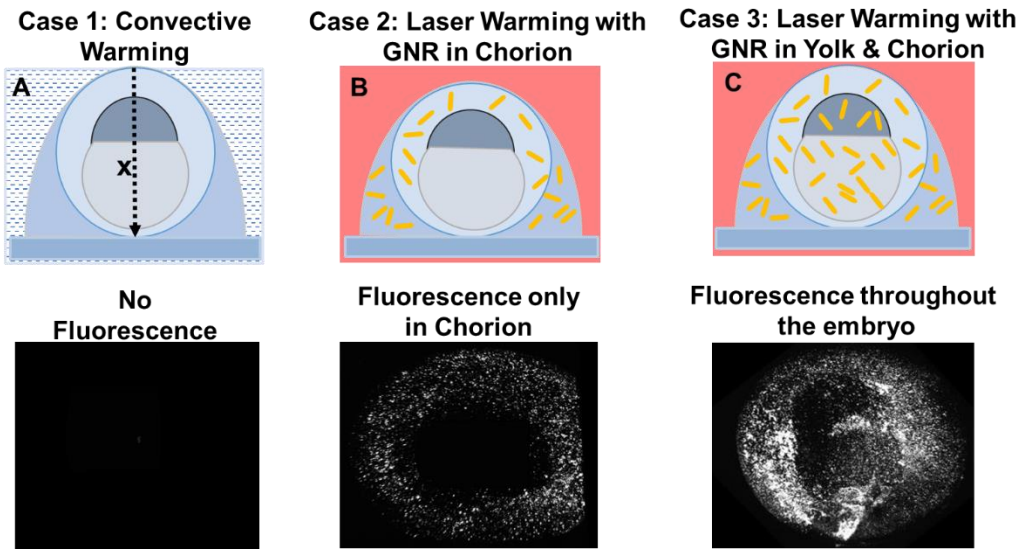

Figure 2.2. Distribution of GNR in different cases of loading. Figures a-c show the distribution of GNR absorbers for the cases studied: (a) Case 1 shows the embryo under standard convective warming conditions without any GNR; (b) Case 2 shows an embryo with GNR present only in the chorion and droplet; and (c) Case 3 shows an embryo with GNR distributed in the chorion and embryo i.e. in yolk and blastoderm. Images to the bottom of (a), (b) and (c) represent the respective cases of zebrafish embryos injected with florescent GNR with emission wavelength at 670 nm.

Fig. 2.2a is blank as expected as no GNR are injected in the convective case, while Figs. 2.2 b and c show compartmental distribution of GNR. For instance, in Case 2 the GNR appear only in the peripheral chorionic space where they were injected. However, in Case 3, the GNR are more widely distributed in the yolk and chorionic space although some variability in viewing within the yolk is noted likely due to its high reflectivity at the

imaging wavelength of 640 nm. Overall, the most uniform distribution of GNR is clearly found for Case 3.

2.3 Thermal Modeling and Characterization

A finite element heat transfer model was constructed to allow for a more detailed assessment of thermal rate response and uniformity in the embryo system during cooling and warming. First, we created a symmetric ¼ model of the embryo as shown in Fig. 2.3A for cooling and warming cases. Next, we modeled cooling on a modified Cryotop with assumed convective boiling conditions in liquid nitrogen (h = 5,000 W/m^{2}°C) which yields a cooling rate of 90,000 °C/min (Fig. 2.3B). This cooling rate exceeds the suggested 50,000 °C/min required for vitrification of 2M Propylene Glycol (PG) on the Cryotop system, [7] and is experimentally supported by achieving transparent embryos. The predicted rates are also broadly in agreement with experimental data with small bead thermocouples (D = 25 µm, time constant = 0.002 s) on smaller systems (0.1 µL) reporting a cooling rate close to 69,000 °C/min using the commercially available Cryotop. [70]

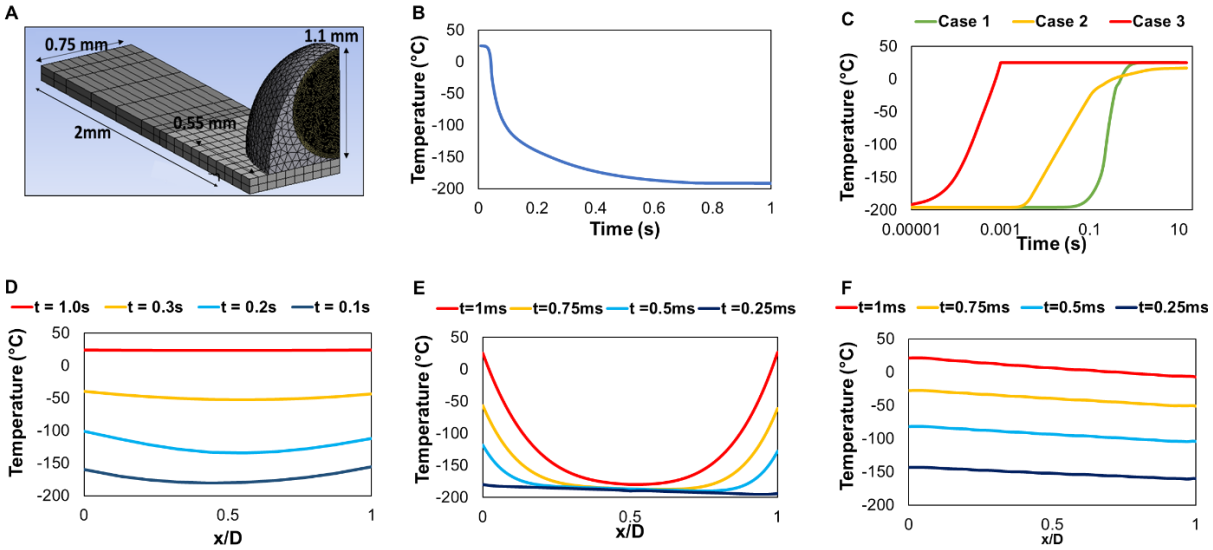

Figure 2.3. Thermal model for zebrafish embryo warming with and without GNR absorbers (A) Finite element mesh of embryo and Cryotop blade, was used to predict cooling rates of 90,000 °C/min (B). Model predicted warming rates for Case 1 (21,000 °C/min), Case 2 (51,000 °C/min) and Case 3 (1.3 x 107 °C/min) are shown in (C). The uniformity of warming is

shown in Figures D – F. For instance, (D) shows uniform but slow cooling for Case 1; (E) shows highly non-uniform warming in the middle *vs*. chorion (edge) setting dangerous thermal gradients (and stress) in Case 2. For Case 3, warming is both uniform and rapid (greater than 10^7 °C/min).

To allow for the larger zebrafish embryo, modifications were made to increase the width of the Cryotop blade to 1.5 mm by attaching wider plastic strips. The modeling results indicate that the embryo equilibrates with liquid nitrogen (-196°C) within 1s. Importantly, once equilibrated at liquid nitrogen temperatures, the embryos were stored for several minutes prior to warming. On the warming side, the model showed that Case 1, which represents a traditional convective warming in a water bath (h=1,900 W/m^2), produced a warming rate of 21,000 °C/min (Fig. 2.3C). For Cases 2 and 3, varying heat generation (SAR, W/m^3) was applied to compartments containing GNR while also accounting for laser attenuation based on Beer's law. A bulk SAR of 4.4 x 10^{11} W/m^3 was estimated for rapid laser warming zebrafish embryos injected with GNR (Fig. 2.1C, μ_a = 38.9 cm^{-1}, N =1.2 x 10^{18} particles/m^3) by a 1ms laser pulse I ~ 1.1 x 10^8 W/m^2 (See *Estimation of SAR* in Methods). The model showed that Case 2 had warming rate of 51,000 °C/min which was much lower than Case 3 which had a warming rate of 1.4 x10^7 °C/min (Fig. 2.3C). Only Case 3 can achieve warming rates higher than the required 10^7 °C/min to prevent crystallization. Rates for both warming and cooling were evaluated between 0°C and -100°C, since this is the range where the risk of ice crystallization and therefore injury is the highest [54, 71-72].

In addition to being rapid, warming also had to be uniform to avoid the danger of cracking due to thermal stress where ≥ 3.2 MPa (critical stress) leads to a brittle state (*i.e.* ≤ -100 °C) (See Fig. A3, in Appendix A). Based on this critical stress, a maximum allowable temperature difference of 51ºC was determined and used as a threshold for success in the three warming cases. A further analysis of spatial temperature distribution within the

embryo during warming for each case is shown in Fig. 2.3D-F. For instance, in Case 2 the temperature difference within the embryo was greater than 51°C during simulation of warming causing it to fail. Fig. A3 in Appendix A will show the thermal stress for the three different cases, which shows that both Cases 1 and 3, remain below the maximum allowable stress of 3.2 MPa. However, in Case 2, the non-homogenous distribution of warming leads to temperature gradients and thermal stress above the critical stress, suggesting that the embryo will crack. In summary, only Case 3 is capable for producing sufficiently fast and uniform warming throughout the larger zebrafish embryo to prevent both crystallization and cracking. Importantly, Case 3 produced warming rates 40% higher than those estimated for the significantly smaller mouse oocytes warmed by India Ink absorption of laser irradiation. [54]

2. 4 Biocompatibility of GNR-PEG and Optimal Stage for Injection

Although Janik and co-workers demonstrated high survival from injections of 2.3 M Propylene Glycol (PG) into the zebrafish embryo, [73] the biocompatibility after injection of the GNRs (or other absorbers) into zebrafish embryos at the necessary concentrations was not available, and required measurement as shown in Fig. 2.4. GNRs are traditionally manufactured with cetyl-trimethylammonium bromide (CTAB) coating which can cause toxicity, [74-75] whereas GNRs with polyethylene glycol (PEG) are considered biocompatible. [76] To test this further India Ink and both kinds of gold nanorods (CTAB- and PEG-coated) were injected into zebrafish embryos. In addition, to test the robustness of an embryonic development stage to injection, embryos at 16 cell, High cell, 50 % epiboly, and 8 somite stages were injected (n=100/stage) with GNR coated with PEG (N =1.2 x 10^{18} particles/m^3). We used morphological and developmental changes through Day 5- such as presence of swim bladder and ability to swim normally, straight alignment

of trunk musculature, presence of normal heart and gills- to determine the toxicity of these components. Morphological screening has long been the benchmark within the zebrafish community to understand mutagenetic changes. [77]

As shown in Fig. 2.4A, microinjection of PEG-coated GNRs yielded the highest embryo survival at day 5 (63%), as compared to those injected with CTAB-coated GNRs (12%) and India Ink (20%). There was no difference in survival between PEG-coated GNR and embryo medium (EM) injection ($p > 0.1$, ANOVA), suggesting that PEG-coated GNRs are biocompatible.

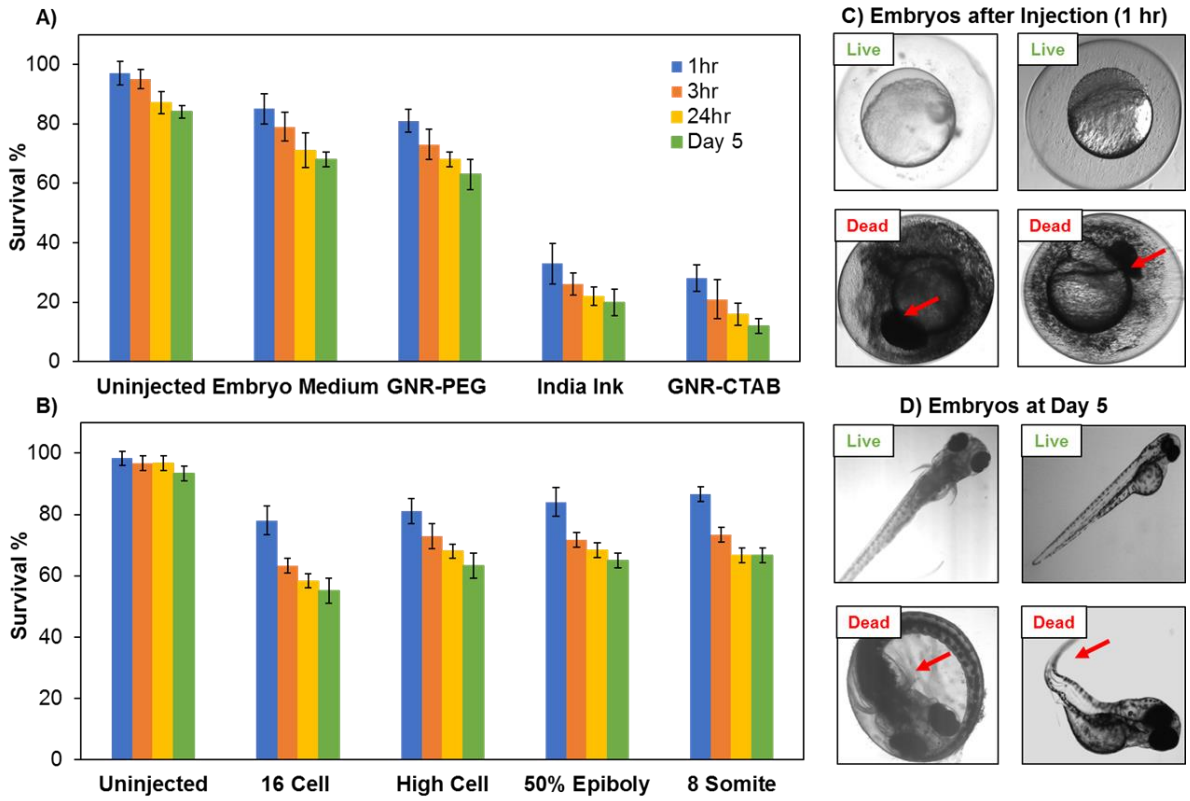

Figure 2.4. Survival after micro-injection of laser absorbers. (A) Three different laser absorbers (GNR-PEG, India Ink and GNR-CTAB) were microinjected into zebrafish embryos at the High cell stage and their survival monitored up to Day 5 with uninjected and embryo medium injected controls. GNR-PEG consisted of GNR coated with polyethylene glycol (PEG) and GNR-CTAB consisted of GNR coated with cetyl-trimethylammonium bromide (CTAB). All absorbers were suspended in embryo media prior to injection. The GNR-PEG preparation produced more normal embryos at Day 5 than the GNR-CTAB and India Ink preparations ($p < 0.001$, ANOVA). No statistical difference ($p > 0.1$, ANOVA) was found between PEG-coated GNR and embryo

medium control injection. In contrast, the higher number of normal embryos at Day 5 using GNR-PEG *vs*. GNR-CTAB or India Ink was statistically significant ($p < 0.001$, ANOVA). For all groups and controls, n=100 embryos were tested. (B) Using the same injection protocol as in A, the most biocompatible GNR-PEG absorber was injected into embryos at different developmental stages and compared to an uninjected control for survival out to Day 5. For survival at the High cell, 50% epiboly and 8 somite stage no statistical difference ($p > 0.1$, ANOVA) was found. By comparison the 16 Cell stage yielded the least survival ($p < 0.001$, ANOVA). In laser warming experiments, the High cell stage was used to inject embryos with propylene glycol and GNR-PEG. (C) Examples of live and dead zebrafish embryos 1 hr after injection of GNR-PEG and PG. (D) Examples of live and dead zebrafish embryos at Day 5 after injection.

In contrast, the higher number of normal embryos at Day 5 using GNR-PEG *vs*. GNR-CTAB or India Ink was statistically significant ($p < 0.001$, ANOVA). Fig. 2.4B showed that embryos injected at the 8-somite stage had the highest survival (67%), followed by 50% epiboly (65%), High cell (63%) and 16 cell (55%). There was no statistical difference in survival between the High cell, 50% epiboly and 8 somite developmental stages ($p > 0.1$, ANOVA). Therefore, the High cell stage was used for injections in further experiments, which gave enough time for carrying out same day experiments. The reported error bars are the standard deviations of the mean survival. Fig 2.4C shows examples of zebrafish embryo morphology 1 hr after a standard injection of GNR and PG. The presence of a dividing blastodermal cells and negligible leakage represents live and developing embryos, whereas darkened cells or massive leakage represents dead embryos indicative of toxicity and injection failure. Fig 2.4D shows examples of zebrafish morphology at Day 5 after the injection. Live embryos at this stage hatched and swam, whereas dead embryos did not hatch.

2.5 Cooling & Laser Warming of Zebrafish Embryos

Figure 2.5 shows an overview of the cooling and laser rewarming process while images of developmental stages examined in this paper after injection (Fig. 2.4C) and warming (Fig. 2.6) are also shown. Following the methods of Janik *et al*, the embryos (High cell stage) were microinjected with 14 M of PG and 1.7 x 10^{19} particles/m^3 of GNR (< 100 nL), to achieve a resulting concentration of 2 M PG and 1.2 x 10^{18} particles/m^3 GNR in the chorion and yolk of the embryo.[73]

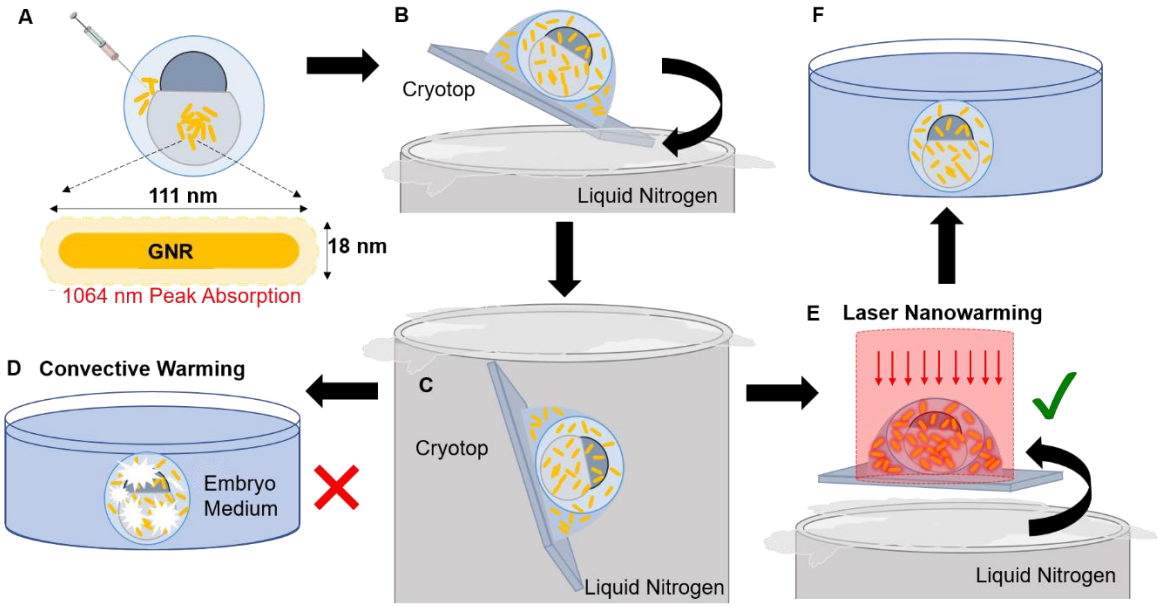

Figure 2.5. Overview of zebrafish embryo cryopreservation and laser GNR rewarming. The process includes: (a) microinjection of 1064 nm resonant GNR and PG into the yolk and chorionic space of the embryo; (b) rapid cooling with the modified Cryotop to prevent ice formation, and storage in (c). Warming consists of either: (d) convective warming in embryo medium at 28 °C firmly yields intra embryonic ice crystallization and death, or (e) laser GNR warming which yields rapid and uniform warming inside the embryo to outrun any ice formation. (f) After which embryo allowed to develop up to five days in embryo medium

The embryos were then placed in embryo medium and cultured for 3 – 4 hours to between 25% and 30% epiboly. At this point, embryos were placed onto the tip of a modified Cryotop with minimal surrounding liquid and plunged into liquid nitrogen where modeling suggests equilibration within 1s. The embryos were then held in liquid nitrogen for at least 2 minutes. Both the rapid cooling and subsequent laser warming were accomplished by an

automated stage device (See Fig. A1 in Appendix A). The time associated with moving the Cryotop from liquid nitrogen into the laser by the stage took ~ 0.3s. A calculation based on h = 100 W/m^2°C (forced convective coefficient in air), L = 400 µm (radius of the embryo), k = 1.0 W/m°C (thermal conductivity of vitrified solutions), showed that the Biot number, Bi = hL/k < 0.1. This in turn suggested that the system was thermally "lumped." A calculation using a lumped model, assuming 0.3 s exposure to the room temperature environment during positioning, suggested only about a 10 ºC change from the -196 °C storage temperature. This is well below the recrystallization range (> -100 °C) and insufficient to trigger devitrification as previously reported for similar systems. [71]

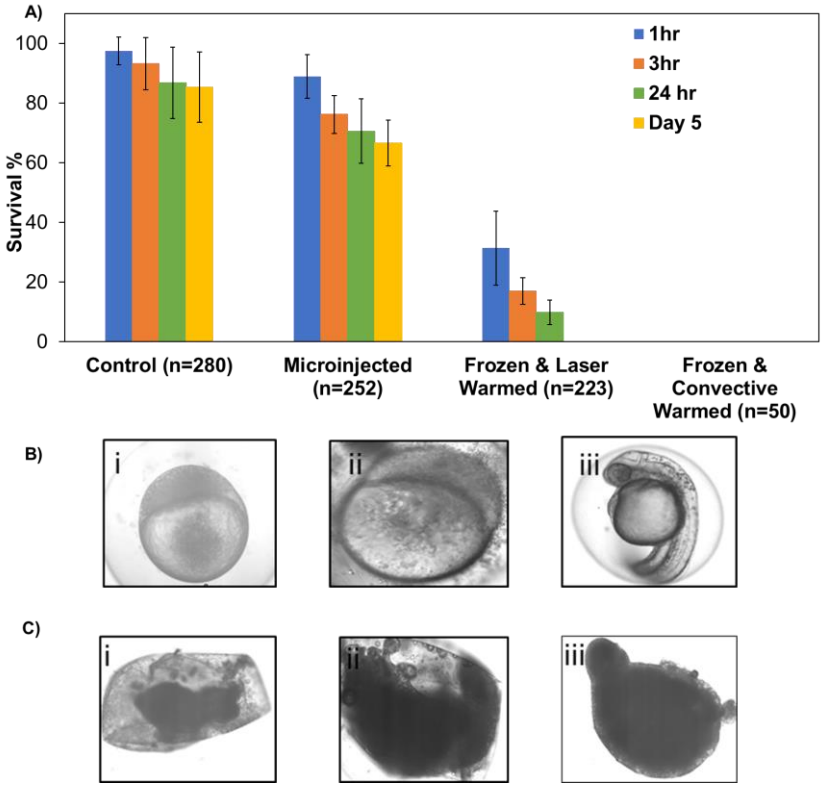

Figure 2.6. Comparison of survival after convective and laser warming of cryopreserved zebrafish embryos. (A) Survival of fish embryos up to Day 5 using four treatments: i) embryo medium only (uninjected), ii) microinjection with PEG-coated GNRs in 2M PG and no cooling (control), iii) microinjection with PEG coated GNRs in 2M PG, cooling, and laser warming, and iv) microinjection with PEG coated GNRs in 2M PG, cooling, and convective warming. Note, survival at 1 hr post-warming was 31% and indicated intact morphology after cooling, at 3 hr post-warming 16% of the embryos were intact and continued developing and at 24

hours after laser GNR warming 5% developed into larval fish. Convective warming did not produce any intact embryos post-warming at any time point ($p < 0.001$, ANOVA). (B) Examples of the morphology of a live fish embryo post laser warming. The images (i, ii and iii) identify the changes in morphology and development after cooling and laser warming at 1, 3, and 24 hr post-warming. At 24 hr, the embryos moved in their chorion validating post-warming viability (See Supporting Video). (C) Example of the morphology of dead fish embryos post convective warming at 1, 3, and 24 hr (i, ii and iii) post convective warming respectively.

After stabilizing the cryopreserved and GNR injected zebrafish in liquid nitrogen, they were subsequently warmed by either standard convection or a 1 ms laser pulse with a fluence rate estimated as $I \sim 1.1 \times 10^8$ W/m^2 (See A.2 Laser characterization in Appendix A). Importantly, this fluence rate was established from laser calibration generated the optimal SAR of 4.4×10^{11} W/m^3 (See *Estimation of SAR* in Methods) which is needed to warm ($\Delta T = -196 - 25 = 221°C$) the embryo. Fig. 2.6A represented the percentage of surviving embryos post-warming at 1, 3 and 24 hr equal to 31% (n=62), 17% (n=37), and 10% (n=22), respectively. Importantly, embryos microinjected, frozen and then warmed by convective warming yielded no morphological structure upon rewarming, thereby demonstrated 0 % survival. Results shown in Fig. 2.6B shows the morphology of a viable embryo at 1, 3, and 24 hr after laser GNR warming, whereas Fig. 2.6C shows a dead and leaking embryo after convective warming. An important outcome was the significant change in consistent structure and survival after 1 hr and 24 hr post laser-GNR warming versus standard rapid convective warming ($p < 0.001$, ANOVA). The embryos at 24 hr developed into young juvenile and moved within their chorion- a clear demonstration of viability associated with a live and developing embryo.

Discussion

We demonstrated the cryopreservation and rewarming of zebrafish embryos that developed and moved at 24 hr post-warming. The approach uses micro-injection (GNRs and cryoprotectants), cooling to -196°C and then ultra-rapid warming with laser irradiation.

Further results demonstrated the biocompatibility of PEG-coated GNRs compared to other laser absorbers like India ink and GNRs coated with cetyl-trimethylammonium bromide (CTAB). These results are supported by other studies showing that GNRs, after removal of toxic CTAB, are sufficiently biocompatible for use in numerous biomedical applications including intravenous injection in humans.[62, 78] The characterization of GNRs along with the heat transfer modeling allowed estimation of the cooling and warming rates that can be achieved by this method.

The results show reproducible survival of embryos out to 24 hr after cryopreservation and laser GNR warming (Fig. 2.6). We considered the laser warmed embryos at 1 hr as membrane intact, but not necessarily viable which is reasonable since approximately 50% of them did not survive up to the 3 hr time point. However, a subset of these embryos advanced to 24 hr in development. Specifically, they continued through cell division advancing from 25% epiboly to 100% epiboly, somite, heart and eye formation and development of the nervous system, which allowed the warmed embryos to move their tails in a normal twitch-like fashion within their chorion. This movement was definitive proof of viability of the warmed embryos beyond 24 hours. We have not measured chilling injury in this study, however, we note that chilling injury requires many minutes to develop at 0 °C in a similar stage embryo. [79] The cryotop cooled embryo will spend less than 0.1 s in the temperature range of 0 to -100 °C where chilling injury might occur. We believe there is insufficient time for the chilling injury to develop. While further study of chilling injury is warranted, we do not believe it is an important form of injury in this work. While each of the 14 trials showed survival out to 3 hr, the loss of fish embryos between 1 and 24 hr might be attributed to the hardening of the chorion, perhaps because of the laser. Putative

changes within the chorion could prevent transport of water and oxygen thus reducing viability and hatching. The chorion was left in place during these experiments because it protected the embryo from mechanical damage. However, future studies will assess our ability to remove the chorion by gentle enzymatic action [80] and replacement with a protective matrix (*i.e.* alginate or other). This should facilitate the next phase of study, which will focus on characterization of the biology of recovered embryo.

This work represents a laser nanoparticle technology to successfully warm cryopreserved zebrafish embryos and produce live zebrafish embryos at 24 hr. In short, this work produced reproducible data showing live teleost embryos after warming which has consistently failed during years of trials of traditional convective warming (Fig. 2.6). The technology relies on a precise matching of the laser wavelength (1064 nm) with the GNR absorber and concentration to evoke a controlled and localized heat generation or SAR within the embryo. This heating is further tailored by selecting the precise pulse width (τ = 1 ms) to ensure heating from liquid nitrogen to melt (ΔT) occurs at a rate at or above the critical warming rate estimated to avoid crystallization ($\Delta T/\tau > 10^7$ °C/min).[54] By micro-injecting the gold nanorods throughout the embryo, the specific absorption rate is spread to avoid slower rates in the center of the embryo, which can lead to both crystallization and thermal stress (*i.e.* cracks) during warming. Importantly, these GNRs need to be sufficiently biocompatible to allow intra-embryonic injection unlike previously used absorbers that have been deployed around oocytes and embryos (*i.e.* India Ink) (See Fig. 2.4).

Methods

Animal Care & culture

Wild type zebrafish (*Danio rerio)* embryos were obtained from the University of Minnesota Zebrafish Core. All care and welfare for the animals met NIH animal care standards. Full details of approved protocols are listed with the Zebrafish Core-IACUC (protocol # 1506-32642A). Zebrafish parent clutches and their embryos were maintained at 28°C under standard conditions as described in Westerfield.[80]

Microinjection of Cryoprotectant and GNR

The microinjection of solutions into zebrafish embryos has been well-established in the literature.[80] The High cell stage (t = 3 hr after fertilization) was chosen to be a robust developmental stage for microinjection while still allowing maximal uniformity of distribution of the injection throughout the embryo. The chorion was not removed in the experiments to mechanically protect the embryo during handling. The embryos were injected laterally through the chorion into the yolk. The volumes of cryoprotectant and GNRs introduced were 9 nL in the yolk and 90 nL into the chorionic space surrounding the embryo. Embryos (n=100 per group) were injected with solutions with N =1.2 x 10^{18} particles/m^3 of GNRs, both coated with CTAB and PEG, and 0.2% V/V India Ink (Higgins Ink, Model #HI44-011). Since India Ink would plug up the injection needles, a slightly lower concentration was used than what was reported in the literature.[54] All the injected solutions were prepared in standard embryo medium.[80] Embryos for laser warming were microinjected with PG (2M) and GNR-PEG (N =1.2 x 10^{18} particles/m^3) using the same protocol as described above. To test the efficacy of the injection and warming processes, the experimental groups included: (i) non-injected non-frozen embryos (n=383); (ii) micro-injected (EM alone) non-frozen embryos tested for toxicity (n= 200); (iii) micro-injected (PG and GNRs) non-frozen embryos and tested for toxicity (n=234); (iv) micro-injected

(PG and GNRs) embryos, frozen and "convectively warmed" (n=50); and (v) micro-injected (PG and GNRs) embryos, frozen and "laser warmed" (n=223).

Estimation of SAR

To warm a zebrafish embryo from liquid nitrogen temperatures to room temperature (ie ΔT = 221 °C) by a laser pulse (τ = 1ms), the required SAR can be estimated as SAR = $\rho C_p \Delta T/\tau$ = 4.4 x 10^{11} W/m^3, where ρ = 990 kg/m^3 and C_p = 2 kJ/kg K are properties of ice. Since SAR depends on GNR optical properties and laser fluence rate, comparisons were first made between theoretical predictions and experimental results of GNR optical properties. First, the absorption cross section, C_{abs}, was predicted from Discrete Dipole Approximation (DDA) method as previously reported for GNR and GNP. [67] Here we assumed the dipole density was 4 dipoles/nm and the average of 9 different laser GNR orientations (from 0° to 90°) were used to account for random GNR distribution inside the embryo. Next, we experimentally measured C_{abs} using GNR warming of GNR solution with a cuvette heating method. [67] This required measuring temperature change resulting from laser warming (1064 nm CW laser, I1064SR0500B, Innovative Photonic Solutions) in a GNR solution (N=3.6 x 10^{18} particles/m^3). In all our embryo warming cases, similar concentration of GNR (N=1.2 x 10^{18} particles/m^3) was injected, and the experimentally determined absorption coefficient (μ_a = 38.9 cm^{-1}) for the embryo was found. From this, the laser fluence rate needed to generate the required SAR (ie 4.4 x 10^{11} W/m^3), was found to be I = SAR/ μ_a = 1.1 x 10^8 W/m^2. From the laser calibration (See Fig. A2 in Appendix A), the operating input conditions capable for generating the required fluence rate were found. We could verify the required laser fluence rate by testing numerous vitrified droplets of the same size as the embryo under the laser and observing them melting and not re-freezing. Very occasionally, refreezing was observed in droplets and embryos presumably due to

differential laser absorption between the cryotop and the GNR loaded system. In this case we raised the laser fluence rate by the smallest possible increment of 5 V to achieve melting without re-freezing. This was always achieved in ≤ 4 increments or ≤ 7.5% total change in voltage from our nominal 270 V setting. In the future, higher reproducibility in GNR loading, cryotop design and laser conditions are expected to reduce any possible re-freezing even further. We consistently used these same laser conditions ($I = 1.2 \times 10^8$ W/m^2, 1 ms pulse time, $N = 1.2 \times 10^{18}$ particles/m^3) in all of zebrafish embryo and HDF warming experiments to generate the adequate amount of heating (SAR).

GNR Biodistribution

To assess the nanoparticle distribution within the embryos they were microinjected with fluorescent GNR (L = 110 nm, D = 20 nm) coated with dylight 650 (emission peak at 670 nm) (nanoComposix, San Diego) and imaged with a fluorescence laser confocal microscope at 640 nm excitation (Nikon C2si, NY). After the initial convection from the micro-injection, the GNR continued to move by passive diffusion for 3-4 hours prior to imaging.

Embryo Survival Analysis

Twelve hundred embryos were examined at different time points after micro-injection for survival. The selected time points were: 1 hr, 3 hr, 24 hr and 5 days after microinjection (for toxicity tests). For the first 3 time points, embryos were considered alive if they were developing and moving within the chorion between consecutive time points. At the Day 5-time point, an embryo was considered normal in development if it had hatched and was able to swim upright in the water column, had proper cardiac development, eye and tail musculature development, fins, and a functional swim bladder. Any fish that did not match

these criteria was considered abnormal in their development and a failed survival as shown in Fig 2.4 (C and D).

Cooling and Laser Warming Experiment

Recent studies measured cooling rates of 69,000 °C/min or higher for a liquid nitrogen cooling 0.1 µL droplet [54, 70-71] on a Cryotop (Kitazato Corp., Fuji, Japan). Since the critical cooling rate for vitrification of 2M PG is 50,000 °C/min [7] and the Cryotop can exceed it, we chose to use the Cryotop for this study. As the commercially available Cryotop is only 0.4 mm wide it was not wide enough for a zebrafish embryo (D > 1 mm, considering the chorion), and modifications were made to extend the width of the polypropylene blade to 1.5 mm. Simulated cooling rates with this modified design suggest rates more than 50,000 °C/min are possible (Fig. 2.3B), and this approach was used in all subsequent embryo cooling. To move embryos rapidly into the liquid nitrogen and quickly bring them from the liquid nitrogen under the laser beam, an automatic microprocessor-controlled stage was built (Fig. A1 in Appendix A), that is functionally equivalent to previous manual designs.[54] Further details of how this device reproducibly positions the cryotop laden with an embryo under the laser beam are provided in the Appendix A

The embryos were placed on the thin, flat blade of the modified Cryotop. It was then attached to the automated device and quickly immersed in liquid nitrogen within a styrofoam reservoir. The embryo was held in liquid nitrogen for at least two minutes and assessed visually to ensure transparency as an indication of successful cryopreservation at liquid nitrogen temperatures. In rare cases, embryos would turn white or opaque, suggesting ice crystal formation during cooling and these were discarded. After equilibration, the embryos were quickly and reproducibly moved by the same automated stage from liquid nitrogen to a position of focus under the laser beam such that warming

could be achieved in one laser pulse. The movement was only initiated after the optimal laser parameters had been validated such as voltage, pulse time and spot size to achieve the fluence rate to produce the warming rates needed. Specifically, one laser pulse at 270 V, 1 ms pulse time, and 2 mm spot size was used to warm embryos. The laser fluence rate provided by the laser was determined to be approx. 1.1 x 10^8 W/m^2. After the laser warming, the Cryotop was removed and the embryo was placed into embryo medium for further analysis. This experiment was repeated for 14 separate trials on a total of 223 embryos. For the convective warming case (n = 50), microinjected embryos were cooled as before with the modified Cryotop into liquid nitrogen. However, after equilibration, the embryos were immersed into embryo medium at 25 °C for warming. The experimental and control groups were then cultured at 28 °C and monitored regularly up to Day 5 at the same time points as noted for biocompatibility testing.

Conclusion

The results from this study demonstrated a method to reproducibly revive zebrafish embryos after cryopreservation using laser-assisted gold nanoparticle warming. The microinjection of PG and GNRs allowed introduction of safer and more effective cryoprotectants and laser absorbers inside the embryo. The use of the Cryotop to achieve rapid cooling allowed the embryos to survive low temperature storage. In tandem, a comprehensive thermal model was used to predict rapid cooling (90,000 °C/min) with ultra-rapid warming (1.4 x 10^7 °C/min). With further studies and optimization to increase the 5-day survival rate, a prototype instrument and associated protocols can be developed to provide a simple and effective cryopreservation technology for zebrafish research facilities around the world like the Zebrafish International Resource Center. In addition, this technology has broad implications as a platform technology to preserve germplasm of

many vertebrate and non-vertebrate systems. It may also be adapted to larger cell and small tissue systems (up to 1.4 mm, See Chapter 3) by solving the associated cooling problem for these larger systems. The ability to preserve such germplasm will provide an important tool for preserving the biodiversity of the planet while also maintaining important genetic research models.

Chapter 3: Characterization of Laser Gold Nanowarming: A Platform for Millimeter-Scale Cryopreservation

This chapter describes the results from multiple studies conducted to characterize and optimize parameters needed for successful cryopreservation with the laser nanowarming approach. This study also helped position laser nanowarming as a universal platform to cryopreserve various biomaterials within 10 µm to 2mm size range. Most of the work in this chapter is taken from the following peer reviewed publications and reproduced here with the permission of the journal publisher:

Khosla, K., Zhan, L., Bhati, A., Carley-Clopton, A., Hagedorn, M., & Bischof, J. (2018). Characterization of Laser Gold Nanowarming: A Platform for Millimeter-Scale Cryopreservation. *Langmuir*. DOI: 10.1021/acs.langmuir.8b03011

Abstract

Preventing ice formation during cryopreservation by vitrification has led to the successful storage and banking of numerous cellular and tissue-based biomaterials. In their breakthrough work, Peter Mazur's group achieved over 90% survival by using a laser warming technique for 100 µm mice oocytes that were cooled in 0.1 µL droplets with 2.3M CPA and extracellularly loaded India Ink (laser absorber). Laser warming can provide rapid and uniform warming rates to "outrun" damaging ice crystal growth. Here we generalize Mazur's technique for microliter sized droplets using laser nanowarming to rewarm millimeter-scale biomaterials when loaded extracellularly and/or intracellularly with biocompatible 1064 nm resonant gold nanoparticles. We first show that droplets containing low concentration cryoprotectants (such as 2M Propylene Glycol +/- 1M Trehalose) can be rapidly cooled at rates up to 90,000 °C/min by plunging into liquid nitrogen to achieve either a visually transparent (*i.e.* vitrified) or a cloudy with ice (*i.e.* non-vitrified) state. Both modeling and experiments were then used to characterize the process for different laser energy (2-6J), pulse length (1-20ms), droplet volume (0.2-1.8µL), cryoprotectant (2-3M) and gold concentration (0.77-4.8 $x10^{17}$ nps/m^3) to assess physical and biological success. Physical success was achieved by finding conditions that minimize cloudiness and white spots within the droplets during cooling and warming as signs of damaging ice formation and ice crystallization respectively. Biological success was achieved using human dermal fibroblasts to find conditions that achieve ≥ 90 % cell viability normalized to controls post warming. Thus, physical and biological success can be achieved using this platform cryopreservation approach of cryotop cooling and laser gold nanowarming in mm scale systems.

Results and Discussion

3.1 Relationship between average laser energy and GNR concentration

Figure 3.1 shows an overview of the laser nanowarming process that can be used to cryopreserve a variety of biomaterials encapsulated in a microliter sized droplet. Specifically, a sample droplet containing various biomaterials, CPAs, and GNRs are loaded onto the cryotop and then plunged into LN_2 by the motor for rapid cooling.

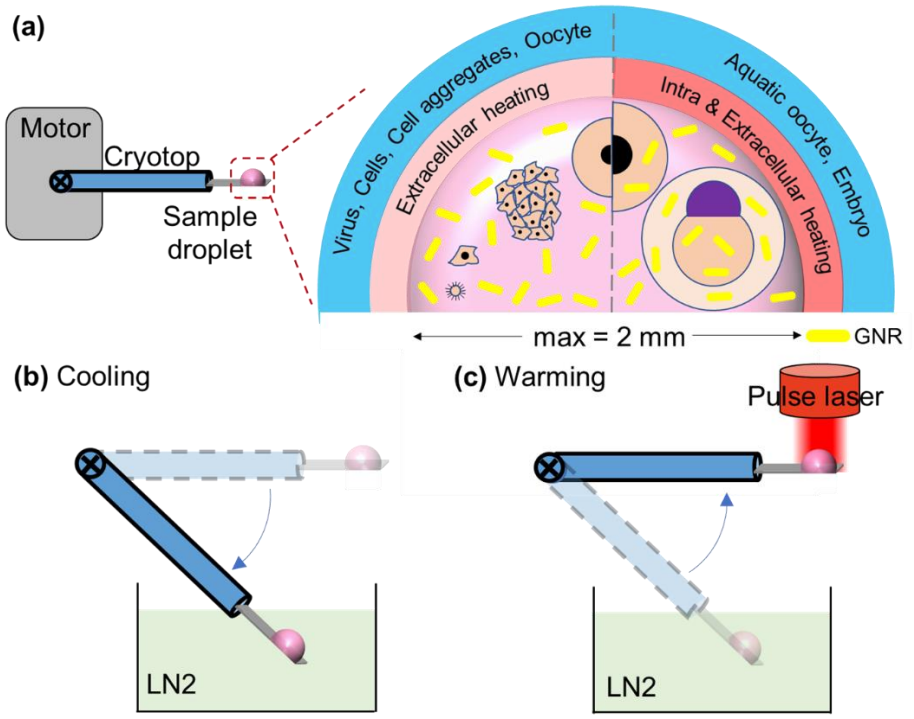

Figure 3.1. Overview of laser nanowarming system. (a) Sample droplet consists of biomaterial(s), CPA, and gold nanorods with a maximum volume of 1.8 µL loaded onto a customized cryotop for rapid cooling and laser warming. Various biomaterials in different sizes including cells, cell aggregates, oocytes, coral larvae, and embryos which can be loaded in the droplet for extracellular and/or intracellular laser nanowarming. (b) A motor automatically and reproducibly immerses the sample droplet into LN_2 for rapid cooling at ~ 90,000 °C/min (for 1µL droplet). (c) The motor elevates the cryogenically stabilized droplet into focus for pulsed laser irradiation yielding ultra-rapid rewarming at rates up to 2 x 10^7 °C/min

To initiate laser warming, the sample droplet is brought up by the motor into laser focus. For smaller samples like viruses, cells, and cell aggregates, the GNRs can be present extracellularly. For larger samples like fish embryos, the GNRs must be present both intra and extracellularly to achieve uniform and rapid warming. The key physics of the

rewarming process are governed by the heat generation term which is generally referred to as the Specific Absorption Rate: $SAR(x,y,z) = NC_{abs}I\,(x,y,z)\left(\frac{W}{m^3}\right)$, where N is the GNR concentration (nps/m^3, 10^6 nps/mL), C_{abs} is the absorption cross section (m^2), and I is the laser fluence rate (W/m^2). We first selected our droplet volume to be 1 µL as it covers the size of most gametes and embryos. Since we were unable to completely vitrify (*i.e.* freeze clear or transparent) 1 µL droplets of 2M PG alone using the cryotop, we increased the concentration to 3M PG which was successful in 1 µL droplets. However, biomaterials like coral larvae and other germplasm can be particularly sensitive to CPAs higher than 2M[81]. Therefore to reduce toxicity and increase stability, we substituted 1M Trehalose for the extra 1M PG as this has shown benefit in other vitrified systems[82]. Figure 3.2a shows a plot of the average laser energy used to rewarm 1µL droplets of 2M PG and 1M Trehalose. In this case, we were rewarming a droplet containing variable GNR concentrations from 0.77 x 10^{17} nps/m^3 (0.14mM), 1.3 x 10^{17} nps/m^3 (0.23mM), 2.6 x 10^{17} nps/m^3 (0.46mM), 3.8 x 10^{17} nps/m^3 (0.69mM), and 4.8 x 10^{17} nps/m^3 (0.87mM).

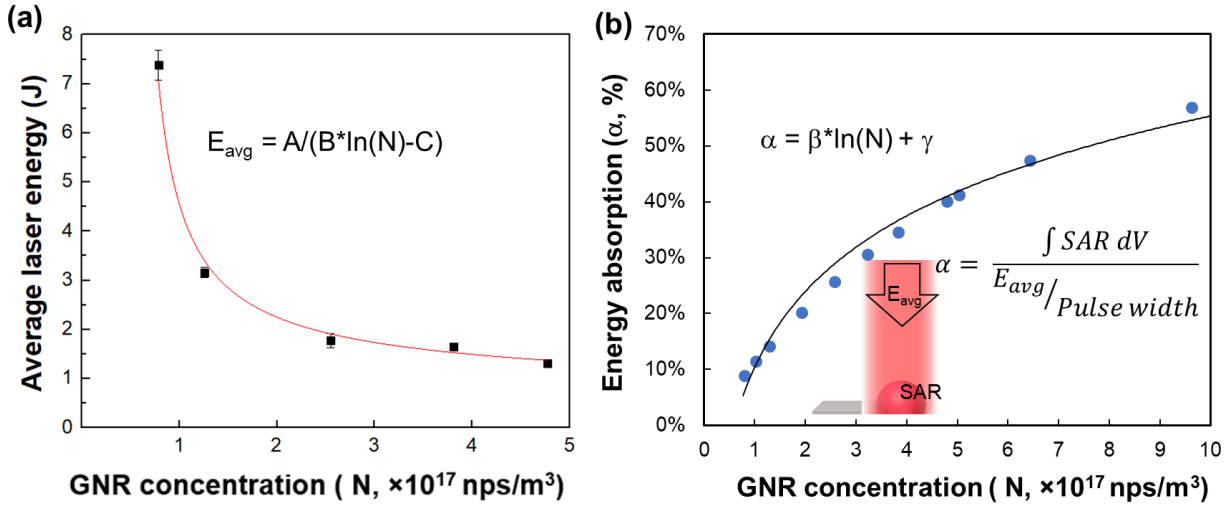

Figure 3.2. Correlation between GNR concentration and laser energy needed to avoid crystallization during warming. (a) Laser energy averaged upon different laser settings that melt the droplet without crystallization decreases with increasing GNR concentration, indicating

higher energy absorption percentage for higher GNR concentration as shown in (b). The fitted empirical function can be used to estimate laser energy required for other GNR concentrations. The fitting function is E_{avg}=1.5/(0.49ln(N)-18), with R^2=0.96. (b) Energy absorption percentage α, defined as the percentage of single laser pulse energy that is absorbed by the GNR-loaded droplet with 1 µL volume, increases with increasing GNR concentration. The fitting function is α=0.19ln(N)+0.1, with R^2=0.99.

The average laser energy represents the mean value of energy per pulse for different laser settings that resulted in rewarming of the droplet without any ice crystallization (*i.e.* going from clear to cloudy). For instance, a droplet with GNR concentration of 1.3 x 10^{17} nps/m^3 was successfully rewarmed at 3.2 J. This energy can be provided by multiple different voltage and pulse widths such as 300V and 1ms, 250V and 1.6ms, 180V and 5.3ms, and many others. (Appendix A1 for laser calibration). All these laser conditions resulted in rewarming the droplet above the T_m without any visible crystallization. The warming rate could be adjusted by simply changing the laser pulse width at a given GNR concentration and laser energy. Interestingly, as GNR concentration increases, the average laser energy needed for warming is expected to decrease since there are more nanoparticles in the droplet to absorb the laser energy. The fitting function reveals a strong correlation (R^2 = 0.96) between average laser energy (E_{avg}, J) and GNR concentration (N, nps/m^3) as $E_{avg} = \frac{1.5}{0.5ln(N)-19}$. In addition, we used modeling to find the ratio between the energy from a single laser pulse (E_{avg}) and the heat generated inside the droplet, which can be written as $\alpha = \frac{\int SAR\, dV}{E_{avg}/_{Pulse\ width}}$. Figure 3.2b plots the percent of the laser energy absorbed by a 1µL droplet (α) for varying GNR concentrations. As expected, a strong correlation (R^2=0.98) was also found as $\alpha = 0.19ln(N) + 0.1$, which can be used to estimate the amount of energy that will be absorbed by the droplet for different GNR concentrations. For instance, a droplet with a GNR concentration of 0.77 x 10^{17} nps/m^3, 1.3 x 10^{17} nps/m^3,

2.6 x 10^{17} nps/m^3, 3.8 x 10^{17} nps/m^3, and 4.8 x 10^{17} nps/m^3 will yield α of 8%, 14%, 26%, 35%, and 40%, respectively. This translates into 0.59J, 0.44J, 0.46J, 0.58J and 0.53J, respectively, as the energy absorbed by the respective GNR concentrations if the total energy per pulse is 3.2 J. This non-linear correlation between GNR concentration and droplet energy absorption efficiency (α) is attributed to the exponential attenuation of laser intensity within the droplet following Beer's law.

3.2 Relationship between average laser energy and CPA concentration

As laser warming has shown the ability to successfully rewarm biomaterials cryopreserved with suboptimal conditions (i.e. some ice formation)[11, 54], we studied the average laser energy needed to successfully rewarm (i.e. melt droplets) under variable cooling conditions that can in some cases yield ice formation. For this study, we selected a 1 µL droplet with two different GNR concentrations: N=1.3 x 10^{17} nps/m^3 and 2.6 x 10^{17} nps/m^3, both with variable CPA. More specifically, Figure 3.3a shows images of droplets of deionized (DI) water with 1M PG, 2M PG, 2M PG and 0.2M Trehalose, 2M PG and 0.5M Trehalose, 2M PG and 1M Trehalose and 5M PG, right before laser warming is initiated. The DI water, 1M PG, 2M PG and 2M PG and 0.2M Trehalose are all crystallized while the droplet of 2M PG and 0.5M Trehalose is partially crystallized, and droplets of 2M PG and 1M Trehalose and 5M PG are completely transparent.

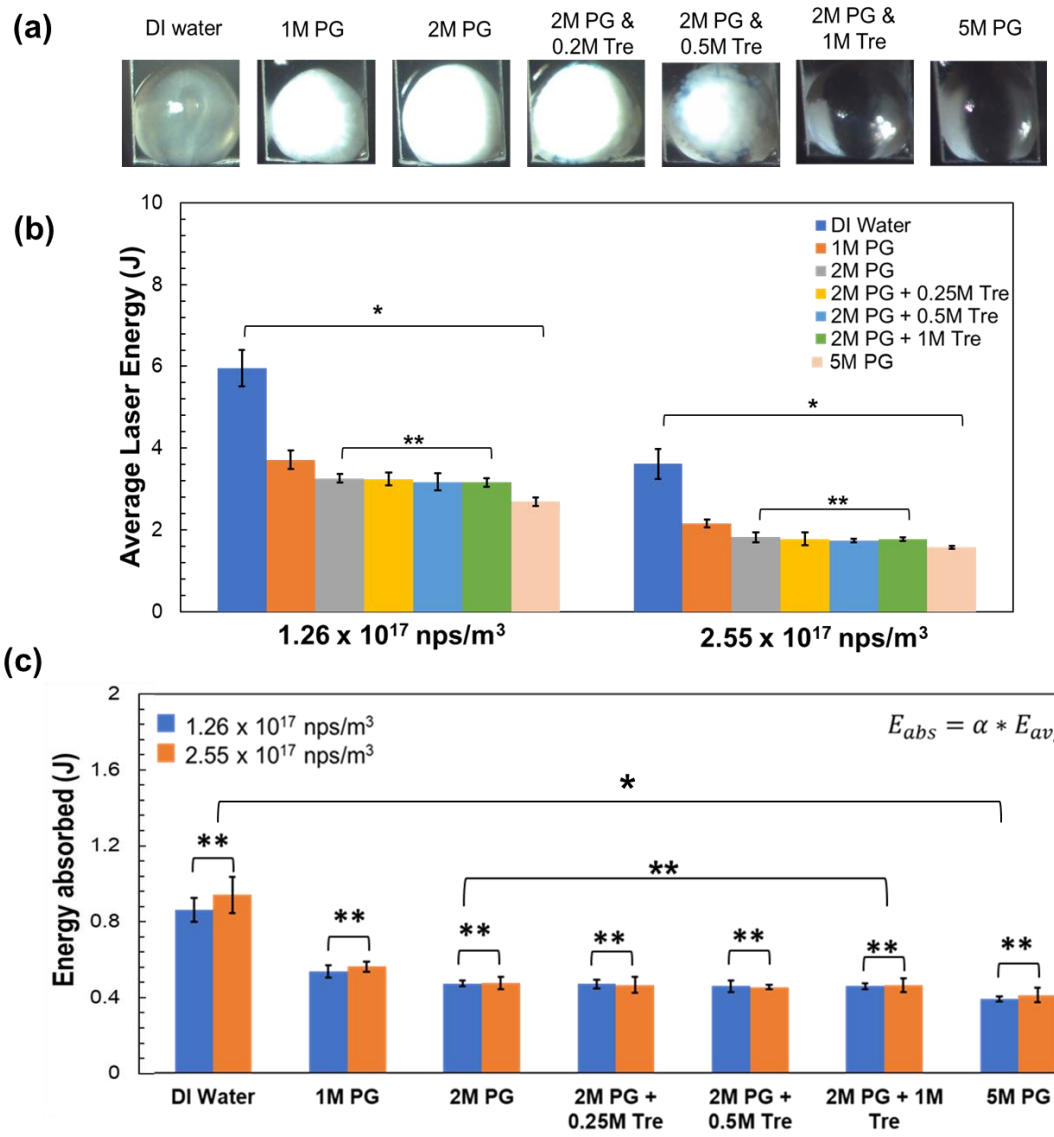

Figure 3.3. Average laser energy to avoid ice crystallization for 1µL droplets with different CPA and GNR combinations during laser nanowarming. (a) Images of 1µL rapidly cooled droplets of DI water, 1M PG, 2M PG, 2M PG + 0.25M Trehalose, 2M PG + 0.5M Trehalose, 2M PG + 1M Trehalose, and 5M PG immediately before laser warming. Cloudy and translucent droplets show ice formation, whereas clear and transparent droplets demonstrate successful vitrification. (b) Plot shows the average laser energy for successful rewarming (no ice crystallization or cloudy spots) of 1µL droplets containing the same solutions shown in (a) with two different GNR concentrations (1.26 x 10^{17} nps/m^3 and 2.55 x 10^{17} nps/m^3). The average laser energy has been measured previously measured using a laser power meter (c) Plot shows the amount of energy absorbed by the droplets under the same conditions as (a). The energy absorbed is calculated by using the energy absorption factor α (Figure 3.2), which is 14.4% and 25.9 % for 1.26 x 10^{17} nps/m^3 and 2.55 x 10^{17} nps/m^3 GNR concentrations, respectively. The error bars represent the standard error of the mean of laser energy that resulted in successful rewarming for both (a) and (b). Notation "* "means that there is significant difference between the groups (ANOVA, $P < 0.01$), whereas notation "**" means that there is not a significant difference between the data groups (ANOVA, $P>0.01$)

The average laser energy to rewarm these droplets can be seen in Figure 3.3b. This data set demonstrates the same trend presented in Figure 3.2a namely, the droplets with higher GNR concentration of 2.6 x 10^{17} nps/m^3 require less average laser energy to rewarm for all groups compared to those with lower GNR concentration of 1.3 x 10^{17} nps/m^3. However, for the same GNR concentration, the average laser energy decreases with increasing CPA concentration. In addition, for either GNR concentration, there is no significant difference between the E_{avg} for 2M PG, 2M PG and 0.2M Trehalose, 2M PG and 0.5M Trehalose, 2M PG and 1M Trehalose groups when compared to each other (ANOVA, $P>0.01$). Nonetheless, there is significant difference between E_{avg} for these groups when compared to DI water, 1M PG and 5M PG (ANOVA, $P<0.01$). Figure 3.3c shows the energy absorbed (E_{abs}), which is the product of α and E_{avg} for the same groups in Figure 3.3b. The data suggests that there is no significant difference between the E_{abs} for the same CPA concentration across the two GNR concentrations (ANOVA, $P>0.01$) but there is a significant difference when compared across the different CPA concentrations (ANOVA, $P<0.01$).

To further explore these results, a simplified energy balance was applied. The energy absorbed $E_{abs} = E_{sensible} + E_{latent}$, where $E_{sensible}$ is the energy needed to raise the temperature of the droplet from liquid nitrogen (-196 °C) to room temperature and E_{latent} is the energy required for phase change from ice to water. For a vitrified droplet such as 5M PG or 2M PG and 1M Trehalose, E_{latent} will be negligible, which makes $E_{abs} = E_{sensible}$. However, for a crystallized sample, E_{abs} will be a sum of $E_{sensible}$ and E_{latent}, where the latter increases as a function of ice formation. For example, the E_{abs} for a 1 µL droplet of 5M PG

was found to be 0.39 J. Comparing this with $E_{sensible}$ for a 1 µL droplet with properties of a vitrified material with density, ρ = 990 kg/m^3, specific heat, C = 2000 J/Kg K, temperature difference ΔT = 220 K, $E_{sensible}$ =ρCVΔT= 0.40 J. Taking this into account, E_{abs} for the same CPA concentration should be the same across the two GNR concentrations as similar ice formation occurs in droplets with the same CPA concentration when cooled at the same rate. This explains the decreasing trend for E_{abs} for DI water, 1M and other PG groups as ice formation decreases across these groups. This is most dramatically illustrated when comparing E_{abs} for DI water of ~ 1 J (highest ice formation) which is considerably higher than 5M PG droplets (effectively no ice) at ~ 0.4 J.

3.3 Relationship between average laser energy and droplet volume

We then investigated the impact of increasing volume on the average laser energy needed to successfully rewarm transparent droplets of 2M PG and 1M Trehalose. Figure 3.4a shows the E_{avg} needed to rewarm droplets varying in volume from 0.25µL to 2µL with a fixed GNR concentration of 1.3 x 10^{17} nps/m^3. The data suggests that there is a strong linear (R^2 = 0.96) relationship between E_{avg} (J) and droplet volume V (µL), which can be written as $E_{avg} = 1.5 * V$. The energy absorption factor α can be found for each volume by using equation $\alpha = \frac{\int SAR\, dV}{E_{avg}/_{Pulse\ width}}$, and this is also shown in Figure 3.4a for respective volumes.

The increasing trend in E_{abs} is expected as the energy needed to rewarm the droplets should increase with increase in volume.

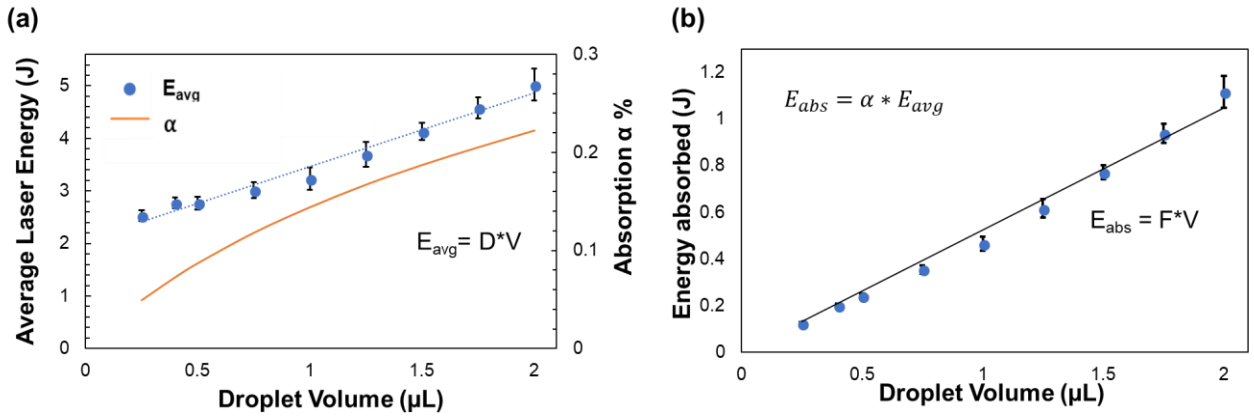

Figure 3.4. Average laser energy needed to avoid ice crystallization for varying droplet volumes. (a) Plot shows the average laser energy that led to successful rewarming (without ice formation) of varying droplet volumes with 2M PG + 1M Trehalose with a GNR concentration of 1.26 x 10^{17} nps/m^3. The data suggests that there is a strong linear (R^2 = 0.96) relationship between average laser energy and droplet volume, where D = 1.5 J/μL. (b) Plot shows the amount of energy absorbed by the droplets under the same conditions as (a). The energy absorbed is calculated by using the energy absorption factor α (Figure 3.2b), which is 14.4%. The data suggests that there is a strong linear relationship (R^2 = 0.99) between energy absorbed and droplet volume, where F= 0.5 J/μL. Energy balance for the droplet will show that energy absorbed equals the sensible energy (ρVCΔT) and latent energy (x_{ice} ρVH_{fusion}). The error bars represent the standard error of the mean of laser energy that resulted in successful rewarming for both (a) and (b).

The value of α also increases with volume since there are more nanoparticles within the droplet to absorb the laser; however, the increase is not large enough to offset the energy requirement to rewarm the additional volume. Figure 3.4b shows the E_{abs} for droplets under the same conditions as Figure 3.4a, indicating a strong linear relationship (R^2 = 0.99) between E_{abs} and droplet volume (V, μL) of $E_{abs} = 0.5 * V$. This is not unexpected based on the energy balance approach shown previously which suggests the energy needed should scale directly with volume.

3.4 Modeling and experiments of droplet cooling

A finite element (FEM) heat transfer model was developed in COMSOL to analyze the possible cooling and warming scenarios for the CPA and GNR-laden microliter sized droplets. Figure 3.5a shows an image of 1μL droplet of 2M PG on a cryotop. The contact angle was measured as 83° ± 4° and was used to build the geometry of the droplet (Figure

3.5b) in COMSOL with a width of 1.65mm and height of 0.73mm. With assumed convective boiling conditions in liquid nitrogen (h = 9,000 W/m^2 K, nucleate boiling[83-84]), the model yielded a cooling rate of 93,000 °C/min at the center of the droplet (Figure 3.5c). The modeling results indicate that the droplet would equilibrate with liquid nitrogen (-196°C) within 0.4s. This cooling rate from the modeling far exceeds the 23,900 °C/min required for vitrification of 3M PG[7], but is far slower than 290,000 °C/min needed for 2M PG[7] (See Figure 1.1), as experimentally validated (Figure 3.5d-e). We also used an Open Pulled Straw, which has a known cooling rate of 20,000 °C/min[51], to experimentally test if either 2M, 2M PG and 1M Trehalose and 3M PG solutions (V=2µL) would vitrify when plunged in liquid nitrogen. As expected, the 2M solution did not vitrify, but interestingly, neither did the 3M PG solution. Only 2M PG and 1M Trehalose vitrified completely at 2 µL volumes. This further supported the argument that the CCR for 3M PG is over 20,000 °C/min. Since there are no good estimates for CCR for 2M PG and 1M Trehalose, we estimated 20,000 °C/min as the minimum rate needed for vitrification.

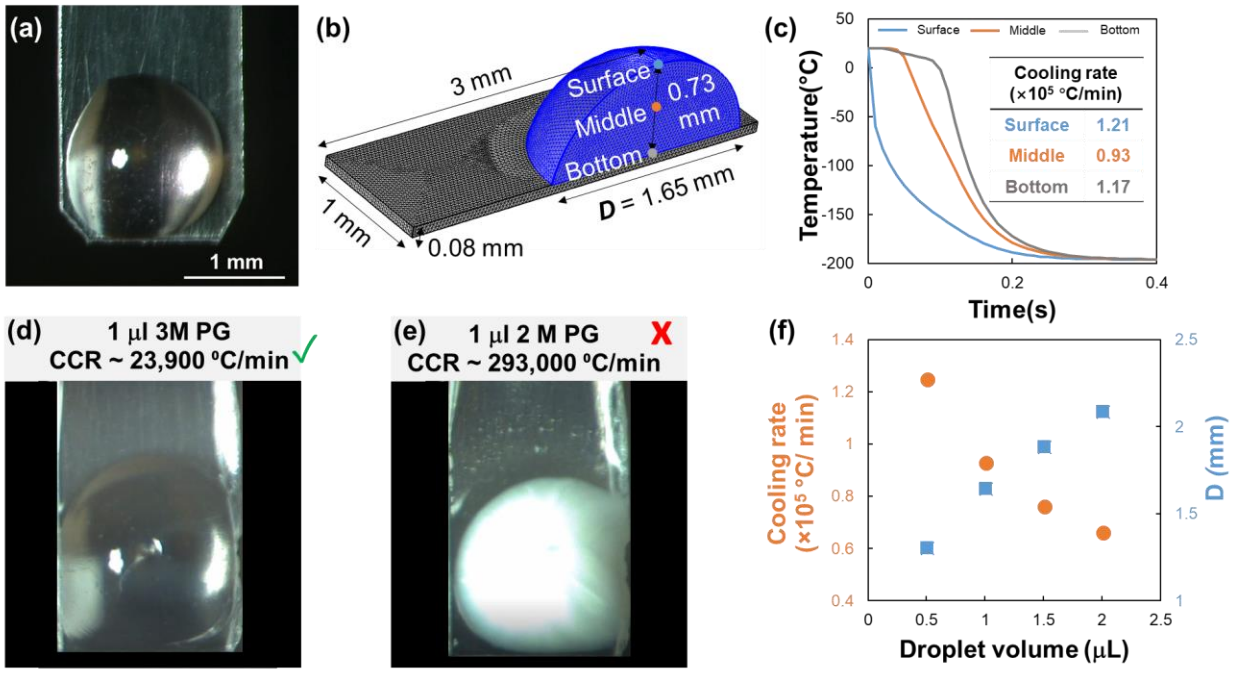

Figure 3.5. FEM Modeling of cooling with Cryotop. (a) Picture of 1 µL droplet on cryotop, with the measured contact angle being 83° ± 4°. (b) Geometry of the droplet and cryotop for COMSOL modeling. Three locations including "top", "middle" and "bottom" in the droplet are selected to represent the spatial temperature distribution. (c) Cooling temperature profile and variable rates within a 1 µL droplet. The cooling rates are calculated between 0 and -140 °C, with the convective heat transfer coefficient set to 9,000 W/m^2K. (d) Successful vitrification of 1 µl of 3M PG using cryotop, with the modelled cooling rate of the droplet exceeding the CCR of 3M PG. (e) Vitrification failure of 1 µL 2 M PG using cryotop, with the modelled cooling rate of the droplet below the CCR of 2 M PG. (f) Cooling rate at the middle of the droplet decreases with increasing droplet volume. Given that the maximum laser beam diameter is 2 mm, the maximum droplet volume is 1.8 µL such that the droplet diameter (D_{drop}) is smaller than the width of the cryotop (*i.e.* 2 mm).

Figure 3.5f shows the cooling rates obtained via modeling for varying droplet volumes. The data shows that even the smallest volume of 0.5 µL couldn't satisfy the cooling rates of 290,000 °C/min needed for 2M PG[7] to vitrify. While both experimental and computational data suggests that droplets of 2M PG and 1M Trehalose and 3M PG with volume up to 2 µL can be vitrified with the cryotop, a 2 µL droplet forms a diameter larger than 2mm (spot size of the laser), so the maximum droplet volume that can be used for laser nanowarming should be 1.8 µL (Figure 3.5f). This is not a hard limit for the droplet volume, since there may be approaches to expand the beam size using either special lenses, filters, and/or obtaining a pulsed laser with larger beam size. Therefore, laser nanowarming of volumes > 1.8 µL may be possible in the future if the cells within the droplet have experienced survivable ice formation during cooling and the laser warming is sufficiently fast and uniform.

3.5 Modeling of laser warming of droplets

Next, we modeled the laser warming of 1µL droplets of 2M PG and 1M Trehalose with a GNR concentration of 1.3 x 10^{17} nps/m^3 under different laser energy conditions. Figure 3.6a plots the temperature change at the surface, middle and bottom of the droplet over time using the same average laser energy conditions found in Figure 3.2a (250V and 1.6ms)

that resulted in rewarming without ice formation. The image of the droplet inside the plot is representative of the droplet appearance after the laser pulse is fired. Figures 3.6b-c are two extreme cases showing temperature change within the droplet when the laser energy is lower (*i.e.* underheating (250V and 1ms)) and when the laser is higher than E_{avg} (*i.e.* overheating (250V and 2.5ms)). Figures 3.6d-f also show the temperature within the droplet for representative cases of successful warming under the same average laser energy conditions but for different pulse widths (1 ms, 5.3 ms and 14.5 ms). Control of the pulse width (range is 0.5ms to 30ms) along with appropriate power and GNR concentration selection allows rates from 400,000 °C/min to 27,000,000 °C/min to be explored. In addition, as GNR concentration increases, the temperature gradient within the droplet (*i.e.*, between the top and bottom of the droplet) increases dramatically due to laser attenuation within the droplet (See Fig 3.7 for multiple GNR concentration cases, exhibiting larger thermal gradients).

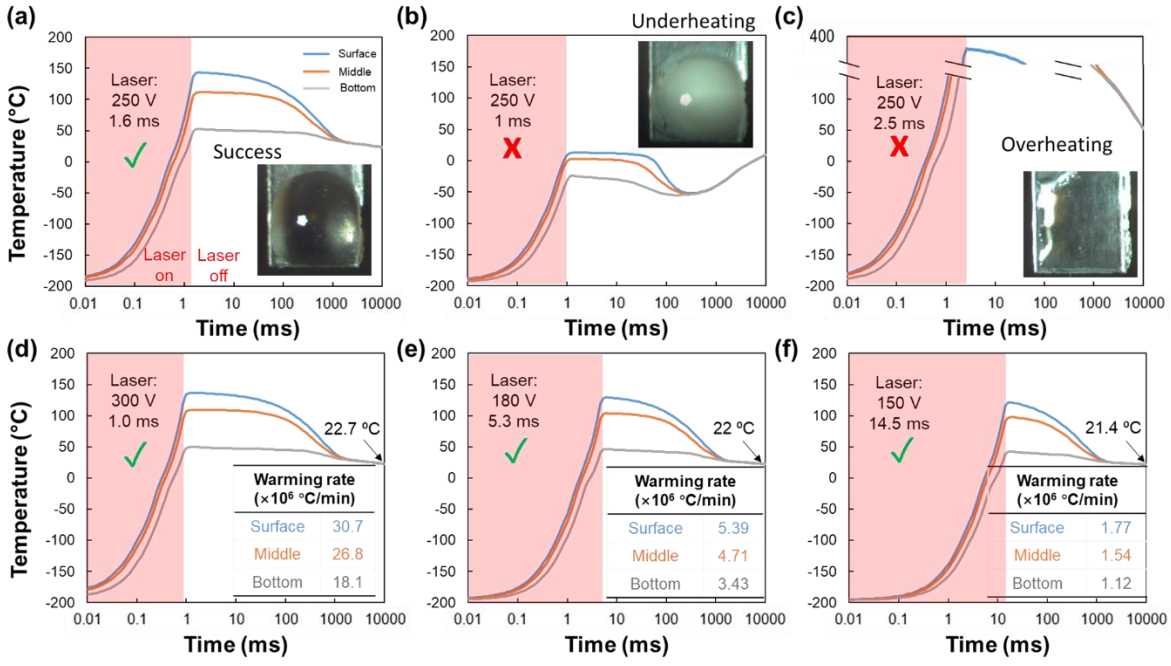

Figure 3.6. FEM Modeling of laser nanowarming of 1 µL droplet with cryotop. The CPA and GNR concentration is 2M PG + 1M Trehalose CPA and 1.26 x10^{17} nps/m^3, respectively. (a-c) Pulse laser settings, pictures, and spatial temperature profiles (model) for rewarming success, underheating, and overheating cases, respectively. (d-f) Different laser settings (*i.e.* voltage and pulse width) and spatial temperature profiles (model) using the same single total pulse energy (3.1 J). All plots share the same legend as (a).

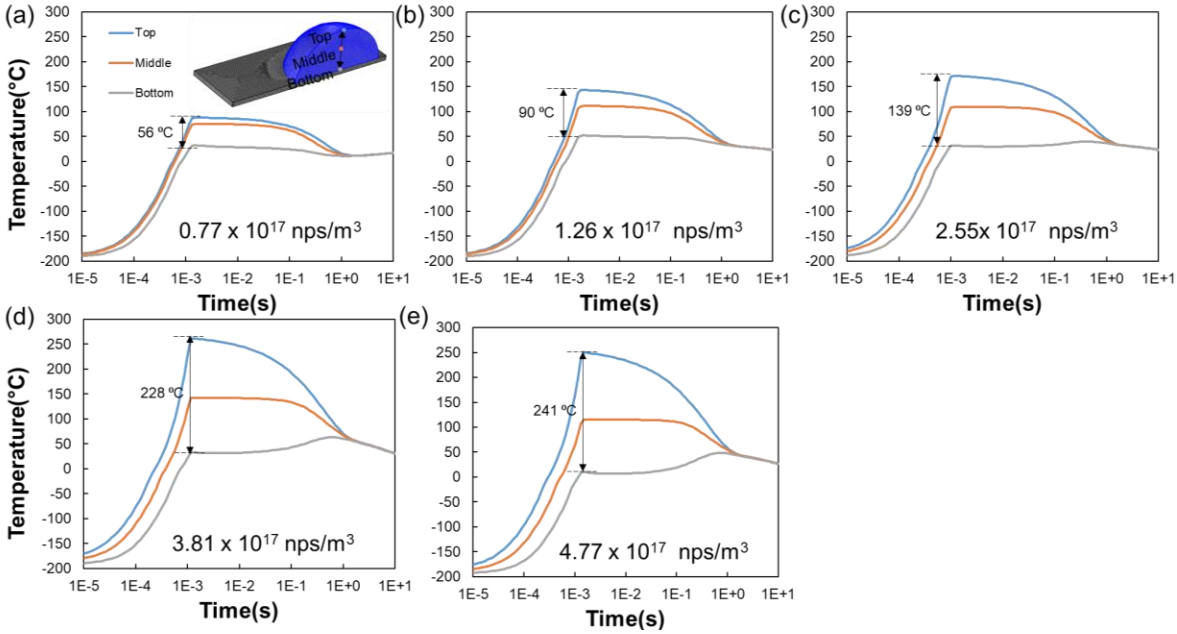

Figure 3.7. Predicted temperature difference in droplets with different GNR concentration for laser rewarming success. As GNR concentration increases from (a) to (f), the temperature difference between "top" and "bottom" increases from 56 ºC to 241 ºC. All plots share the same legend as (a). All droplet predictions are based on COMSOL modeling as described in the text.

3.6 Laser warming of droplets with Human Dermal Fibroblast cells

Figure 3.8a plots the viability of HDF cells post laser warming as a function of laser energy when warmed in 1µL droplets with 2M PG and two different concentrations of Trehalose (0.5M and 1M) and GNR (0.77 x 10^{17} np/m^3 and 1.76 x 10^{17} np/m^3). The highest average viability for 2M PG and 1M Trehalose group for GNR concentrations of 0.77 x 10^{17} np/m^3 and 1.76 x 10^{17} np/m^3 was 97% and 91% which occurred at laser energy of 5.4J and 1.9J, respectively. Just as expected, droplets with lower GNR concentration required higher amounts of energy per pulse for successful rewarming.

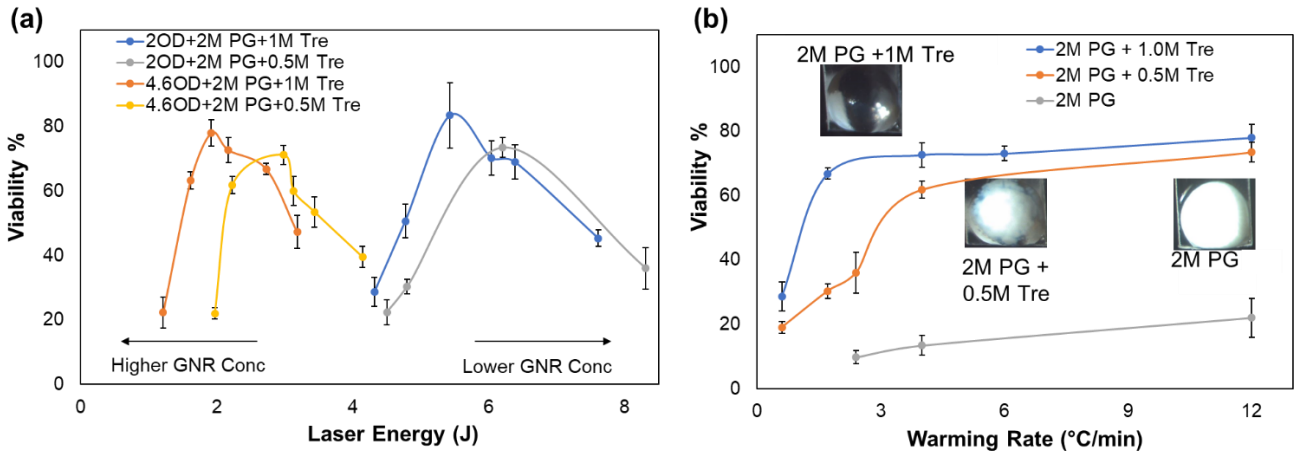

Figure 3.8. Laser warming of 1 µL droplets with Human Dermal Fibroblast cells. HDF cells in suspension were mixed with 2M PG and varying concentrations of Trehalose (0M, 0.5M and 1M) and GNR (0.14mM or 0.77 x 10^{17} np/m^3 and 0.37mM or 1.76 x 10^{17} np/m^3) for 3 min. 1 µL droplets of this cell solution with concentration of 10,000 cells/mL were cooled with the cryotop and then laser warmed under different laser conditions. The viability of the HDF cells was measured by using Trypan Blue assay post laser warming. The viability of HDF for the control group (mixed with PG and Trehalose but not laser warmed) was 85% and results here have been normalized to it. (a) The plot shows the relationship between laser energy and post laser warming viability rate of HDF cells for two different CPA and GNR concentrations. (b) The plot shows the relationship between warming rate and post laser warming viability rate of HDF cells for three different CPA conditions with the same GNR concentration of 0.37mM (1.76 x 10^{17} np/m^3). At least 3 trials (100,000 cells/mL) were carried out for each condition, and the error bars here represents the standard error of mean viability rate.

This is also consistent with relationship shown in Fig. 3.2a, according to which E_{avg} needed to rewarm 1µL droplets of 2M PG and 1M Trehalose with two GNR concentrations would be 4.4J and 2.0J. Similarly, for the 2M PG and 0.5M Trehalose group for GNR concentrations of 0.77 x 10^{17} np/m^3 and 1.76 x 10^{17} np/m^3 the highest average cell viability was 85% and 83%, warmed at a laser energy of 3.0J and 6.2J, respectively. For both CPA concentrations, the lower GNR concentration led to higher average viability rate. This can be attributed to the larger thermal gradients that are created with higher GNR concentrations (See Fig. 3.7). Figure 3.8b plots the viability of HDF cells post laser warming as a function of warming rate when warmed in 1µL droplets of 2M PG and with three different concentrations of Trehalose (0M, 0.5M, and 1M) and a GNR concentration

of 1.76 x 10^{17} np/m^3. Based on our previous experiments, we were able to find the optimal laser energy needed to rewarm a certain size droplet containing a specific CPA and GNR concentration. By keeping the laser energy, the same, we were able to manipulate the warming rates (WRs) by increasing or decreasing the pulse width for these droplets. We estimated these rates by using this rough estimation: WR = 200°C/(Pulse Width). Inside the plot, there are images of rapidly cooled droplets just prior to laser warming, showing a 2M PG droplet completely crystalized, a 2M PG and 0.5M Trehalose droplet partially crystalized, and a 2M PG and 1M Trehalose with no crystallization. There is clear trend demonstrating the highest cell viability at the highest warming rate for each group. For the fully crystalized 2M PG group, the highest viability rate of 26% was seen at 12,000,000 °C/min, which was much lower compared to the other groups. Despite crystallization occurring within droplets of 2M PG and 0.5M Trehalose, the cell viability of 86% at 12,000,000 °C/min was like the cell viability of 91% for 2M PG and 1M Trehalose group. However, as the warming rate fell below 4,000,000 °C/min, there is sharp decline in cell viability across all PG groups. For warming rates between 1 and 4,000,000 °C/min cell viability was between 30% to 70%, and for rates lower than 1,000,000 °C/min cell viability fell below than 30%. Considering the cell viabilities, the threshold warming rates for 2M PG, 2M PG and 0.5M Trehalose and 2M PG and 1M Trehalose might be approximately 12,000,000, 4,000,000 and 1,700,000 °C/min, respectively. However, a more careful calorimetric analysis might be needed to state this more accurately.

The key finding from this experiment was that despite sub-optimal cooling which led to ice formation in 2M PG and 2M PG and 0.5M Trehalose droplets, cell viability was retained when a significantly high laser warming rate (> 10,000,000 °C/min) was used. This is an

important finding since the conventional thinking in field of cryobiology has always been to avoid ice formation using faster cooling and/or high concentration CPAs. However, as the biomaterials become larger, faster cooling becomes harder to achieve and increasing CPA concentration may not be ideal due to toxicity concerns. Simply put, laser nanowarming can be a powerful new tool to help rescue biomaterials like zebrafish embryos (*i.e.* too big) and coral larvae (*i.e.* CPA sensitive) that cannot be cooled optimally without any ice formation. By providing ultra-rapid warming rates, laser nanowarming prevents any further damage by ice crystallization during rewarming.

3.7 Biomaterial size for extracellular vs intracellular warming

Using the FEM model, we were able to analyze the size constraints for biological specimens that can be rewarmed with the extracellular laser warming approach. Figure 3.9 plots the warming rates achieved inside biological samples (*i.e.* oocytes, embryos, islets) of varying diameters, D_{cell}, placed at the bottom of a 1µL droplet, with extracellular GNR concentration of 1.3 x 10^{17} nps/m^3 and being irradiated with average laser energy conditions of 250V and 1.6ms (E_{avg} = 3.2J).

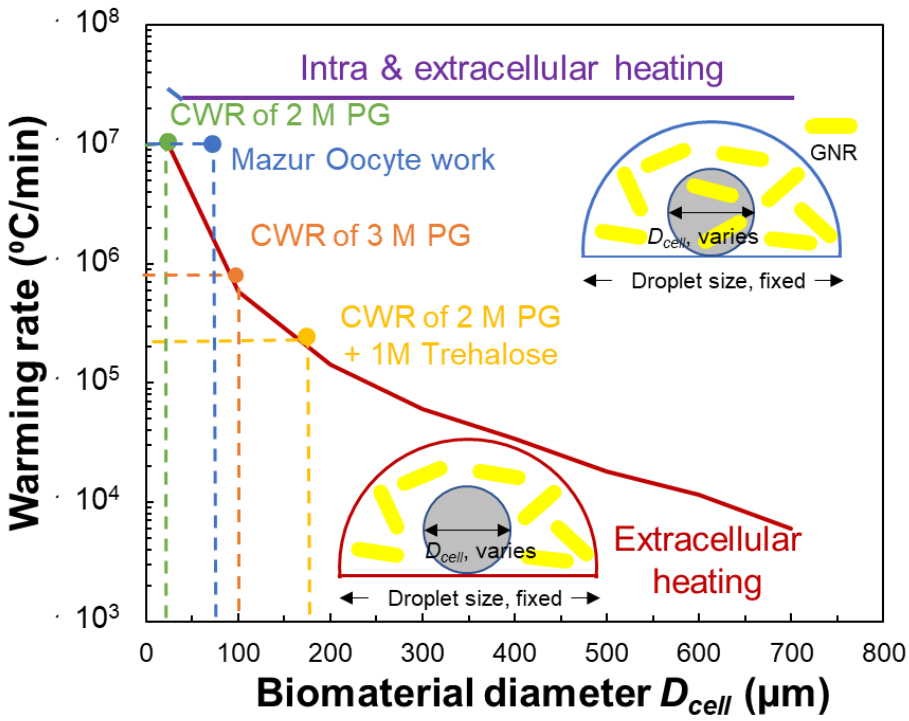

Figure 3.9. Modeling of warming rate for different sized biomaterial within a 1 µL droplet by extracellular laser warming. The GNR concentration is 1.26 x 10^{17} nps/m^3 and laser settings are 250V and 1.6 ms pulse width. The warming rate reported here is from predictions at the center of the biomaterial. The CWRs for 2M PG and 3M PG are approximately 11,400,000 °C/min and 930,000° C/min, respectively. Mazur's oocyte work with India Ink used a warming rate of 10^7 C/min is also shown[54]. Using an open pulled straw, we were able to find that the minimum cooling rate (CCR) to vitrify 2M PG and 1M Trehalose was 20,000 °C/min. Since there are no robust measurements in the literature, the CWR of 2M PG and 1M Trehalose can only be approximated as 200,000 °C/min (*i.e.* 10x CCR). The modeling results show that the maximum size of the biomaterial that can be rewarmed extracellularly is 180µm. While not ideal, increasing the concentration of CPA may help reduce the CWR needed and thus increase the threshold size of the biomaterial that can be rewarmed via extracellular laser warming. Comparatively, intra cellular laser warming can easily rewarm biomaterials up to 800µm; however, uniform GNR loading throughout the biomaterial can present its own challenges[11].

To prevent crystallization, the warming at the center of the specimen must surpass CWR of 11,400,000 °C/min, 930,000 °C/min and 200,000 °C/min when using 2M PG, 3M PG and 2M PG and 1M Trehalose, respectively (See Fig 1.1 in Chapter 1). Using these rates as a threshold, droplets with 2M PG and 3M PG can't prevent crystallization via extracellular warming for D_{cell} larger than 20 µm and 100 µm, respectively. Similarly, D_{cell} increases to 180 µm for a droplet with 2M PG and 1M Trehalose. The CWR are needed to

avoid crystallization within droplets; however, each biomaterial may remain viable even when rewarmed at rates slightly lower than these. For example, Mazur's laser warming work on 0.1 μL droplets still demonstrated high survival for 76% of mouse oocytes when rewarmed at 3,000,000 °C/min, compared to 93% survival rate for mice oocytes rewarmed at a rate of 10,000,000 °C/min using the same 2.3M CPA (a combination of ethylene glycol, Ficoll, etc)[54]. Additionally, the extracellular heating approach can work for larger specimens if the CPA concentration of the droplet is increased; however, this increases the risk of losing samples like embryos and oocytes due to toxicity. In contrast, the intra- and extra-cellular heating approach, *i.e.*, GNRs present inside and outside the biomaterials, can produce ultrahigh warming rates (20,000,000 °C/min) regardless of the biomaterial size, provided that the GNRs are distributed uniformly throughout the droplet and biomaterials. In this case, low CPA concentration such as 2M PG can be used without crystallization during the rewarming process (Figure 3.9).

Methods

Rapid cooling and laser warming of droplets

Rapid cooling and laser warming were performed as described by Khosla et al.[11], with small modifications as shown in Figure 3.1. Instead of a zebrafish embryo, microliter-sized droplets with varying CPA and GNR concentrations were pipetted onto the 3.0 x 2.0 x 0.08 mm blade of a modified cryotop (See Appendix A1 for design of modified cryotop). A specially designed automated system was used to rapidly cool the droplets by plunging them into liquid nitrogen for at least 10 seconds to allow for equilibration to liquid nitrogen temperature (See Appendix A1for detailed description of cryojig and methodology). For rewarming, a 1064nm Nd: YAG laser (iWeld 980 Series, 120 joule, LaserStar Technologies, FL, USA) was used to provide a high energy singular millisecond pulse.

This laser is equipped with a stereomicroscope with an eyepiece crosshair reticule to allow for visualization and alignment of the specimen within the laser chamber, along with a phototube to record high speed video. Once the jig raises the cryotop into the laser's focus, the laser is automatically fired. The energy provided by a single pulse can be varied by changing the input voltage and pulse time. A laser calibration table was generated using a laser power meter (Nova II, Ophir, Jerusalem, Israel) to determine the amount of energy in joules produced by the laser at a given voltage and pulse time (See Appendix A2 for laser calibration).

This entire process of cooling and laser warming droplets is captured by the camera. There are two distinct time points in the video which are used to observe ice formation during this process. The first is "prewarming" wherein the droplet is quickly raised into the laser's focus from the liquid nitrogen; this transition takes less than 0.3s. For our purposes, a vitrified droplet appears transparent without any white spots, whereas ice formation in the droplet appears white or cloudy (either partially or completely). For example, a vitrified 1µL droplet of 2M PG and 1M Trehalose can be seen in Fig. 3.5d, and a crystalized 1µL droplet of 2M PG can be seen in Fig. 3.5e.

The second observation point is "post-warming," wherein the droplet is seen immediately after the laser is fired. It should be noted that the video recording during the millisecond(s) of laser warming is blocked by a protective filter due to possible damage to the camera. Our physical definition of success is that the droplet remains clear, *i.e.* without the appearance of ice post laser warming. A first warming failure mode we term crystallization exists when the droplet shows ice (white spots) due to underheating because the laser energy was too low to completely rewarm the droplet to its melting temperature. A second

failure mode exists if the droplet disappears or get damaged if the laser energy exceeds the rewarming threshold. Examples of all three cases can be seen in Figures 3.6 a-c. For each laser warming case, the voltage and pulse width were varied until there was no ice formation within the droplet during rewarming (n=5). For example, a laser pulse with voltage of 250V and pulse width of 1.6ms successfully rewarmed a vitrified 1µL droplet with 2M PG, 1M Trehalose and $1.26x10^{17}$ nps/m^3 GNR. This technique was used to obtain the laser energy conditions for physical success at different GNR concentrations, CPA concentrations, and droplet volumes.

Laser warming of droplets with Human Dermal Fibroblasts

Standard techniques can be used to cryopreserve these HDF cells, but for our technique to be valid and translatable, we use HDF cells as a model to test experimental conditions needed for biological success of laser nanowarming. The cells were cultured by standard methods in our lab[85] and suspended in culture medium. To prepare test samples, the HDF cells were mixed with 2M PG and varying concentrations of Trehalose (0M, 0.5M and 1M) and GNR (N = 0.77 x 10^{17} np/m^3 and 1.76 x 10^{17} np/m^3) for at least 3min. Using the same protocol described earlier, 1 µL droplets with a cell concentration of 100,000 cells/mL were frozen with the cryotop and then laser warmed at various laser energy and pulse width conditions. After each warming trial, the laser warmed droplets mixed with 1M PG solution. After performing at least 10 trials for each different CPA, GNR, and laser warming condition, the cells were washed with PBS to remove PG. It should be noted that cell solutions were kept on ice before and after laser warming until cell viability was evaluated. To measure viability post laser warming, the cells were first concentrated by centrifugation and the majority of supernatant was removed. After which the cell solutions were mixed with Trypan Blue (Sigma Aldrich T8154) in a 1:1 ratio and placed inside the

Cell Counter (Countless, Thermo Fisher Scientific) to evaluate cell viability, following a similar to the protocol established in literature[86].

Model to study rapid cooling and laser warming

The MCA-3 (Kyowa Interface Science, Japan) was used to measure the contact angle of 1 µL droplets when pipetted onto the blade of a cryotop (polypropylene). It was found to be 83° ± 4° and was used to model the dimensions of a 1 µl droplet on cryotop. The geometries of the droplet and cryotop were then used to construct a geometric model of the droplet in COMSOL as shown in Figure 3.5b. Considering symmetry, only half of the droplet was used in the model, with the height of the droplet 0.73 mm, the diameter of the contact area between the droplet and cryotop 1.65 mm, and the dimensions of the cryotop 3mm x 1mm x 0.08mm. Constant properties of the cryotop were used in the model with density 1040 kg/m^3, thermal conductivity 0.033 W/mK and specific heat 1300 J/kgK. Due to the lack of specific measurement of 2M PG and trehalose, the droplet was assigned temperature-dependent thermal properties of 2M Glycerol in Phosphate-buffered saline from published measurements [11, 87]. The governing equation used to solve the cooling temperature profile is

$$\rho c \frac{\partial T}{\partial t} = \mathrm{k}\nabla^2 T$$

where T is the temperature (K), ρ is the density (kg/m^3), c is the specific heat (J/kg/K), and k is the thermal conductivity (W/m^{2}K). The initial temperature was 293 K, and ambient temperature was set to 77 K. We then assumed the boundary condition to the entire surface of the droplet and cryotop was governed by convection with a heat transfer coefficient of 9,000 W/m^{2}K. This value is consistent, but on the high end of recorded values (1,000 – 10,000 W/m^{2}K)[84] in literature as we are plunging the sample[83]. Three locations within the

droplet – including "surface", "middle", and "bottom" – are selected to represent the spatial temperature distribution as shown in Figure 3.5b. The temperature range to calculate the cooling rate is -140 °C ~ 0 °C.

The governing equation used to solve the warming temperature profile is

$$\rho c \frac{\partial T}{\partial t} = \mathrm{k}\nabla^2 T + SAR$$

$$SAR = C_{abs} * N * I$$

$$I(x, y, z) = I_0(x, y) * \exp(-C_{ext} * N * z),$$

where $I_0(x, y)$ is the Gaussian distribution of the laser intensity (W/m^2), C_{abs} and C_{ext} are the absorption and extinction cross section area of GNR, z is distance travelled vertically by the laser, and *N* is the number density of GNR (nps/m^3). The heat source term "SAR" is only applied in the droplet volume with selected pulse width, since the cryotop is transparent to 1064 nm laser[71]. In addition, convective heat transfer with surroundings (293 K) is applied at the surface with the heat transfer coefficient 100 W/m^{2}K. To model the warming rate for different-sized specimens with extracellular warming, the droplet size is fixed to be 1 μL and the biomaterial is assumed to be a sphere placed on the surface of the cryotop as shown in Figure 3.5. The heat source term "SAR" is only applied outside the specimen, and the warming rate at the center of the specimen is reported. The temperature range to calculate the cooling rate is -140 °C ~ 0 °C, since the possibility of crystallization is highest in this range.

Conclusion

Table 1 summarizes the physical conditions necessary for laser nanowarming including the concentration of nanoparticles and CPA, droplet volumes and laser energy conditions. We were able to show the ability of the cryotop to vitrify to up to 1.8µL droplets for 2M PG and 1M Trehalose, which is our ideal laser nanowarming CPA. Numerical modeling shows that the CCR and CWR of 20,000 °C/min and 200,000 °C/min can be achieved for our ideal (2M PG and 1M trehalose) droplet.

Table 3.1. Physical conditions required for successful laser rewarming of gold nanorod impregnated droplets cooled with cryotop.

	Cryotop Cooling	
Droplet volume (µL)	0.1 ~ 1.8	
Cooling rate (ºC/min)	66,000 ~ 210,000	
PG concentration (M)	≥ 2.0	
Sugar additive (M)	0.1 ~ 1.0	
	Laser warming	
	Extracellular heating	**Intra & extracellular heating**
Laser pulse energy (J)	2.0 ~ 6.0	
GNR concentration ($\times 10^{17}$ nps/m^3)	0.77 ~ 4.8	
Pulse width (ms)	0.5 ~ 30	
*Biomaterial diameter (µm)**	≤ 180	≤ 2,000
Warming rate (ºC/min)	70,000 ~ 20,000,000*	400,000 ~ 20,000,000**

* The GNR concentration 1.26 x 10^{17} nps/m^3 and laser settings 250V, 1.6 ms pulse width are used to obtain the warming rate and maximum specimen diameter with CCR set to 20,000 ºC/min (see Table 2).** The warming rates are obtained by varying pulse width from 1 ms to 30 ms. A successfully rewarmed droplet remains clear and transparent (*i.e.* no ice crystallization occurs) whereas a failed droplet becomes cloudy (*i.e.* ice crystallization occurs)

In addition to using the visual analysis of droplets, by achieving over 90% viability for HDF cells post warming, we were able to test the ability of laser nanowarming quantitively

by successfully rewarming droplets that were either vitrified or contained some ice. As visual analysis of ice crystallization within droplets is intrinsically qualitative, we have added a biological read-out based on % viability of HDF cells post warming to assess overall success. We hope in future studies, to add further metrics of ice formation within droplets using X-ray diffraction[88], high speed video and/or other techniques. In addition, we hope to follow the same protocol we used to optimize the survival of HDF cells under different GNR loading and laser warming conditions for other systems like zebrafish embryos and pancreatic islets. Further, the model provides a size limit of 180 μm for biomaterials that can be rewarmed by extracellular means only. Compared to intracellular warming, extracellular warming reduces the need for complex loading procedures like microinjections of GNR used in our previous work with zebrafish embryos[11]. However, it limits the size of specimens that can be rewarmed without crystallization. In addition, extracellular warming creates thermal gradients across the droplet and encapsulated biomaterials which can be damaging, especially for larger samples and faster warming rates.

When we compare devices such as the cryotop,[50] Open Pulled Straw,[51] Cryoloop[89], Quartz Micro Capillary,[52] and copper grids[12] with recent laser warming approaches, we find that our laser nanowarming approach can provide the highest warming rates and largest volumes with CPA < 3M (Table 2). This technology has the potential to provide a platform to cryopreserve a wide variety of biomaterials ranging from microns to millimeters in size, thereby providing a new biomedical tool for cryopreservation, assisted reproduction, aquaculture, and biodiversity.

Table 3.2. Comparing the representative cooling and warming capabilities of existing cryopreservation approaches.

Device	Sample Volume	System	Vitrification Solution	Cooling Rate °C/min	Warming Rate °C/min	Ref
Traditional Straw	250 µL	Bovine oocytes	4M PG	2,500	2,700	21
Copper Grids	0.5 µL	Bovine oocytes	5.5 M EG & 1M sucrose	3,000	3,500	7
Cryo-loop	0.5 µL	Bovine oocytes, human oocytes	0.65M sucrose, 2.8M DMSO & 3.3M EG	10,000	20,000	31
Open Pulled Straw	2 µL	Bovine embryos	3M PG	22,500	35,000	20
Cryotop	0.1 µL	Mouse oocytes	7M EAFS**	69,000	117,000	23
Quartz Micro-Capillary	0.1 µL	Mouse oocytes	2M PG & 0.5M Trehalose	250,000*	120,000*	21
Cryotop + Laser Warming (India Ink)	0.1 µL	Mouse oocytes	2.3M EAFS**	69000	10 million*	23
Cryotop + Laser Warming (GNR)	1 µL	Zebrafish embryos	2.3M PG	90,000*	13 million*	6

Increasing Rates over time

*Cooling and warming rates presented were calculated by using FEM modeling. ** EAFS vitrification solution is a mixture of ethylene glycol, acetamide, Ficoll, and sucrose. The preparation has been described in ref 23. Also note PG is Propylene glycol and EG is Ethylene Glycol.

Chapter 4: Improvement in long term survival of frozen zebrafish embryos post laser nanowarming

This chapter details the changes and optimizations made in injection and freezing protocols that led to significant improvements to survival rate up to 5 days post laser warming. Additionally, there is also data showing live and viable embryos spawning from two adult fish that were cryopreserved and rewarmed as embryos. Most of the work in this chapter is being prepared as the following manuscript for submission and review:

Khosla, K., Kangas, J., Zhan, L., Liu, Y., Daly, J., Hagedorn, M., & Bischof, J. (2019). Improvement in long term survival of zebrafish embryos post laser nanowarming (in preparation)

Abstract

The ability to cryopreserve fish embryos can transform the fields of aquaculture, species preservation and biomedical research. We have previously shown the ability to successfully rewarm rapidly cooled and microinjected zebrafish embryos using laser nanotechnology. Here we present our optimized protocols for a Single Injection of cryoprotectants and gold nanorods that have increased the survival rates of laser warmed embryos up to Day 5. The results from this new protocol (n = 282) demonstrated viable embryos with consistent structure at 1 hr (40%), continuing development at 3 hr (22%), movement at 24 hr (11%), hatching at 48 hr (9%) and swimming at Day 5 (3%). In addition, we also present data showing that two of the laser warmed embryos grew and spawned embryos with over 85% survival rate, which is comparable to average survival rate of control groups. This is the first demonstration we are aware of that cryopreserved fish embryos can hatch, grow to adulthood and successfully spawn. Our future efforts are geared towards improving survival rates to adulthood and developing apparatus to cryopreserve fish embryos in a high throughput manner.

Results & Discussion

4.1 Comparison between the "Single Injection" and "Double Injection" protocols

Figure 4.1a shows images of both good and bad cases of injection in zebrafish embryos at High cell stage with 18nL of the injection solution (10.1M PG, 4.6M MeOH, $9.4x10^{17}$ np/m^3). MeOH has been widely used in cryopreservation of fish germplasm and has shown the ability to reduce chilling injury[22]. As shown in the image, "good injection" shows no leakage of CPA or yolk within the embryo, whereas a "bad injection" leads to yolk and CPA leaking out due to damage caused by the needle piercing and damaging membranes. After injections are finished, the embryos that looked like the "bad injection" case in Fig. 2a were discarded and only embryos that looked like "good injection" case were used in our studies. Our initial study[11] used a Double Injection of CPA and GNR in both the yolk and surrounding perivitelline fluid. We attempted to replicate these results by using the exact protocol[1] and compared survival rates with a new Single Injection protocol. The new approach relies on a singular injection of CPA and GNR into the yolk followed by immersion in a precooling bath to reduce perivitelline fluid. The injection solution is a mixture of PG (10.1M), MeOH (4.6M) and GNR ($3.8x10^{17}$ np/m^3) and was used for the Single Injection group only. For the Double Injection experimental group, the injection solution consisted of 13.1M PG and $9.4x10^{17}$ np/m^3 GNR. For both groups, 9nL of the respective solution was injected into the yolk. For the Double Injection group, 72nL was injected into the perivitelline fluid.

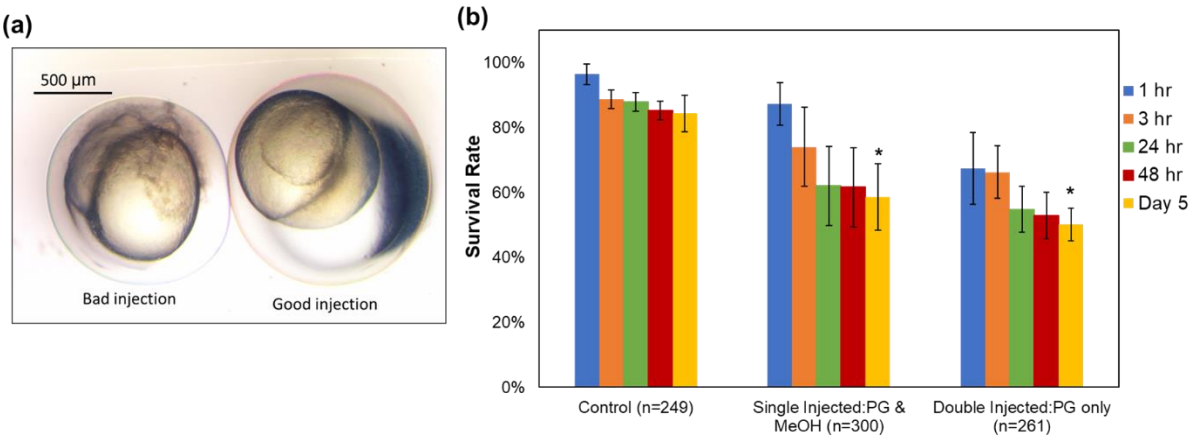

Figure 4.1. Comparing the "Double Injection" (Khosla et al 2017) protocol to current "Single Injection" protocol. (a) Example images of good case and bad case of an injected embryo are shown within 30mins of an injection of CPA and GNR into the yolk using the current Single Injection protocol. (b) Survival of fish embryos up to Day 5 using three treatments: i) Control (uninjected), ii) Single Injection of 9nL of 10.1M PG, 4.6M MeOH, $9.4x10^{17}$ np/m^3 in the yolk, iii) Double Injection of 13.1M PG, and $9.4x10^{17}$ np/m^3 GNR in volumes of 9nL in the yolk and 72nL in perivitelline fluid. The survival rate for the Single Injection group was significantly higher (ANOVA, $p<0.05$) compared to the survival rate of Double Injection group. Notation "**" means groups have don't have significant difference (ANOVA, $p> 0.1$), whereas "*" means that groups have significant difference (ANOVA, $p <0.05$).

Figure. 4.1b shows the average survival rates of embryos injected at the High cell stage using either Single Injection or Double Injection protocol. We used morphological and developmental changes through Day 5–such as presence of swim bladder and ability to swim normally, straight alignment of trunk musculature, presence of normal heart and gills–to determine the attrition after injections. Morphological screening has long been the benchmark within the zebrafish community to understand mutagenetic changes[77]. As shown in Fig 4.1b, the Single Injection group (n=300) had a significantly higher (ANOVA, $p<0.05$) average survival rate of 58% compared to 50% for the Double Injection (n=261) group at Day 5. This demonstrates that the new Single Injection approach significantly reduces toxicity and subsequent death from the injection itself. The control group (n=249) consists of uninjected embryos who are cultured at 28°C alongside the experimental groups to isolate any clutch specific issues. Whenever the control group's Day 5 survival rate was

below 80%, the experimental data from the entire group was rejected and not presented in our cumulative results. The reported error bars are the standard deviations of the mean survival rate.

4.2 Testing the biocompatibility of other nanoparticles

Using the single injection approach, we tested the biocompatibility of the various Polyethylene Glycol (PEG)-coated nanoparticles (nanoComposix, Inc, San Diego CA) to evaluate if they could be used in future studies to change the optical properties of the zebrafish embryos. In this study, we compared our highly absorbing PEG-coated GNRs to highly scattering hollow gold nanoshells (HGNS) and silica core filled gold nanoshells (GNS (Si core)). To prepare the injection solutions, 10.1M PG and 4.6M MeOH were mixed in with the respective GNP to achieve a particle concentration of 9.4×10^{17} np/m^3. Figure 4.2 shows the average survival rates of embryos injected at the High cell stage using the Single Injection protocol. The average survival rate at Day 5 for embryos injected with the PEG-GNR (n=107), PEG-HGNS (n=128) and PEG-GNS (silica core, n=105) was 55%, 53% and 53%, respectively. Comparing the Day 5 average survival rates, no significant difference was found (ANOVA, $p>0.1$) for embryos injected with PEG-GNR, PEG-HGNS and PEG-GNS (silica core), suggesting that highly scattering GNP are biocompatible similar to PEG-GNR, which has been shown to be biocompatible in our earlier study[11].

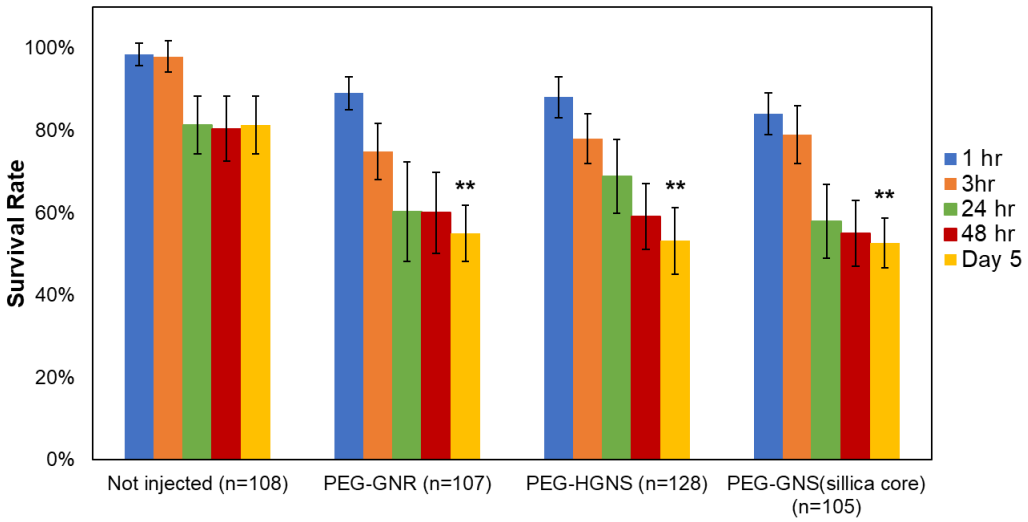

Figure 4.2. Biocompatibility of different injected gold nanoparticles. Three different laser absorbers (PEG-coated GNR, PEG-coated HGNS, and PEG-coated GNS (silica core)) were injected in volumes of 9nL with 10.1M PG and 4.6M MeOH into the yolk. The concentration of GNPs inside the yolk was $1.4x10^{17}$ np/m^3. The survival rates monitored up to Day 5 along with a non-injected control group. All the embryos were injected at the High cell stage. No statistical difference ($p > 0.1$, ANOVA) was found between survival rates of embryos injected with either PEG-coated GNR, PEG-coated HGNS, or PEG-coated GNS (silica core). This suggests that other PEGylated gold nanoparticles could be used in future laser warming settings.

4.3 Impact of increasing injection volume

By changing the injection volume, we can change the concentration of the CPAs within the yolk. The amount of water present in the yolk was known and was used to estimate injection concentration of GNR and CPA within the embryo[20, 73]. For this study, we injected the standard injection solution (10.1M PG, 4.6M MeOH and $9.4x10^{17}$ np/m^3 GNR) in the yolk at High cell stage (3hr post fertilization) in volumes of 9nL, 18nL, and 30nL, respectively. Figure 4.3a shows a table of injected volumes and the corresponding PG, MeOH and total CPA concentration in the yolk.

(a)

Injected Volume in Yolk (nL)	PG Conc (M) in Yolk	MeOH Conc (M) in Yolk	Total Molarity in Yolk (M)
9	1.5	0.7	2.2
18	2.6	1.2	3.8
30	3.7	1.7	5.4

(b)

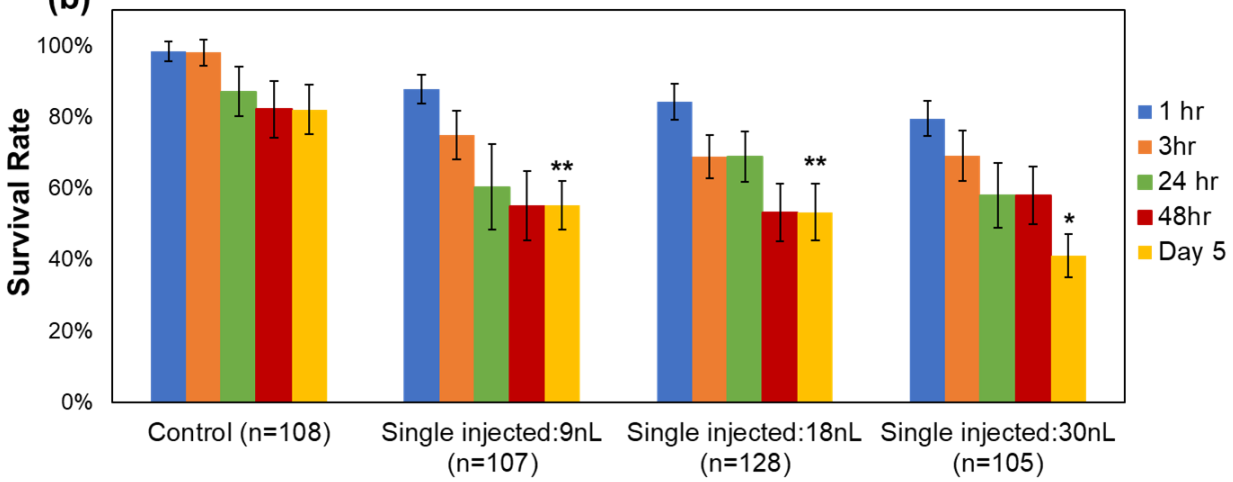

Figure 4.3. Changing the injected volume in the yolk. (a) Table showing the concentration of PG and MeOH in the yolk for 9nL, 18nL and 30nL volume cases. The amount of water within the yolk has been characterized in previous studies and was used to find the yolk CPA concentration[20, 73]. (b) Survival of fish embryos up to Day 5 using four treatments: i) control (not injected), ii) single injection of 9nL in the yolk, iii) single injection of 18nL in the yolk, and iv) single injection of 30nL in the yolk. There is no significant difference between the Day 5 survival rate for the 9nL and 18nL injection cases (ANOVA, $p>0.1$). However, survival rate for 30nL group was significantly different (ANOVA, $p<0.05$) compared to the 9nL and 18nL groups. Notation "**" means groups have don't have significant difference (ANOVA, $p> 0.1$), whereas "*" means that groups have significant difference (ANOVA, $p <0.05$).

By increasing the CPA concentration in the yolk, the possibility of ice formation in the yolk should also decrease. Figure 4.3b shows the survival rates over 5 days for "Single Injection: 9nL" (n=107), "Single Injection: 18nL" (n=128) and "Single Injection: 30nL" (n=105) as 55%, 53% and 41%, respectively. There is no significant difference (ANOVA, $p>0.1$) between the Day 5 survival rate for the 9nL and 18nL injection cases. However, survival rate for 30nL group was significantly different (ANOVA, $p<0.05$) compared to the 9nL and 18nL groups. Therefore, in addition to using 9nL injections in the yolk, we

will also evaluate the ability of 18nL injection, which creates an overall CPA concentration of 3.8M in the yolk, to maintain long term viability in future laser warming studies.

4.4 Impact of injecting at different stages of development

A successful injection should lead to uniform distribution of GNR and CPA. It is expected that the nanorods will diffuse from the yolk into the blastodermal cells; however, this may be dependent on what developmental stage is chosen for injection. Since the yolk's membrane permeability changes across different developmental stages due cytoplasmic streaming (1-100- cell stage) and the development of the yolk syncytial layer (post High cell stage)[20], we wanted to study the biodistribution of GNPs after microinjection at early development stages such as 1-8 cell stage (0-45 mins post fertilization), later epiboly stages such as 50% epiboly (5.25 hr post fertilization), and 100% epiboly (10 hr post fertilization). Figure 4.4 shows the survival rates over 5 days for embryos injected with 9nL of the standard injection solution between 1-8cell stage (n=60), 512-High cell stages (n=60), 50% epiboly (n=60), and 100% epiboly (n=60). When comparing the Day 5 survival rates for the High cell, 50% epiboly and 100% epiboly groups, no statistical difference ($p > 0.1$, ANOVA) was found. By comparison, the 1-8 Cell stage yielded a significantly lower survival ($p < 0.001$, ANOVA), suggesting that the earlier stage embryos are not robust enough to withstand the toxic and osmotic shock caused due to the injections. However, it was promising to see that the later stage embryos injected at 50% epiboly and 100% epiboly were able to exceed the average survival rate of the embryos injected between 512 and High cell stage and will be considered for future laser warming experiments.

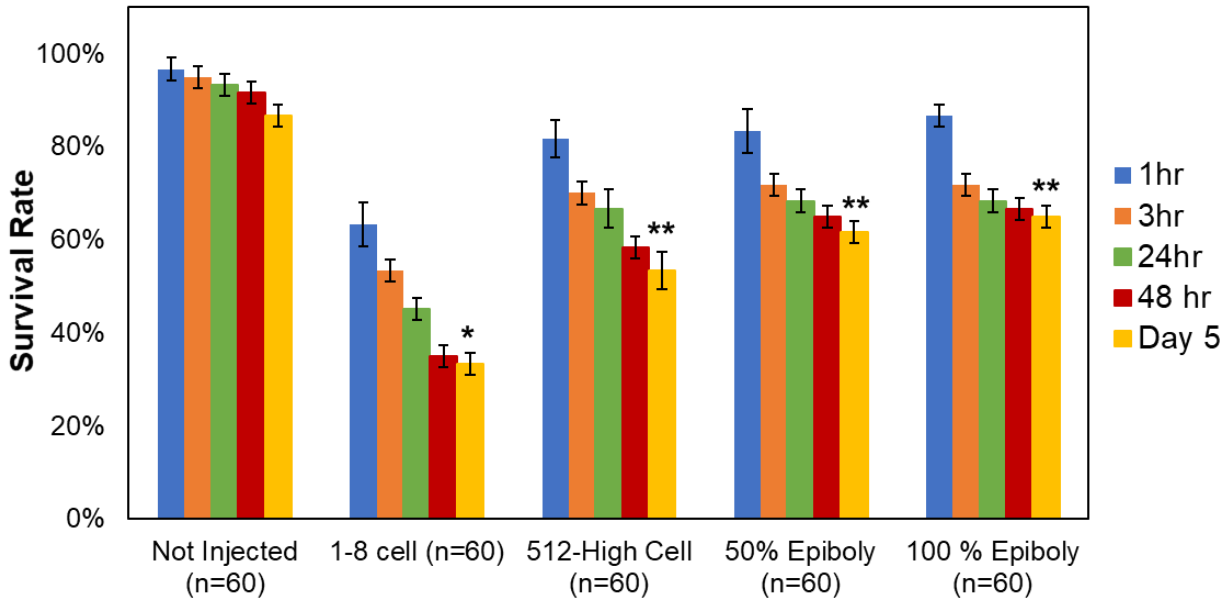

Figure 4.4. Injecting at different developmental stages. Using the single injection protocol, 9nL of 10.1M PG, 4.6M MeOH, and 9.4 x 10^{17} np/m^3 was injected into embryos at different developmental stages and compared to a non-injected control for survival out to Day 5. Comparing Day 5 survival rates for the High cell, 50% epiboly and 100% epiboly groups, no statistical difference ($p > 0.1$, ANOVA) was found. By comparison, the 1-8 Cell stage yielded a significantly lower survival ($p < 0.001$, ANOVA). In laser warming experiments, the High cell stage was used to inject embryos. Notation "**" means groups have don't have significant difference (ANOVA, $p > 0.1$), whereas "*" means that groups have significant difference (ANOVA, $p < 0.05$).

4.5 Impact of a pre-cooling bath

For the Single Injection protocol, no injection of CPA and GNR is made in the perivitelline fluid. Therefore, a "Pre-Cooling" bath is used to remove the perivitelline fluid and replace it with CPA. Fig 4.5a lists the varying concentrations of CPA used to prepare Pre-Cooling "Bath 1" (2M PG, 1.2M MeOH & 0.5M Tre) and "Bath 2" (1M PG, 1.7M MeOH, 1M Tre). Fig 4.5b is an image of a non-injected embryo placed in embryo medium followed by an image of the embryo (taken 30s after being placed in Bath 1) with a collapsed chorion, suggesting the loss of perivitelline fluid. Fig 4.5c shows the survival rates of embryos either non-injected or injected (based on the Single Injection protocol) and then exposed to Bath 1 or Bath 2 for 5mins. After, the embryos are put into a "Post-Warming" bath (1/2x concentration of Precooling Bath) then followed by three washes in embryo

medium. For the non-injected groups, the average survival rates at Day 5 for embryos exposed to Bath 1 (n=60) and Bath 2 (n=51) were 57% and 34%, respectively. For the injected groups, the average survival rates at Day 5 for embryos exposed to no Bath (n=129), Bath 1 (n=95) and Bath 2 (n=86) were 61%, 50% and 25%, respectively. For both injected and non-injected groups, embryos exposed to Bath 1 had a significantly higher survival rate (ANOVA, $p<0.05$) than the embryos exposed to Bath 2, suggesting that additional toxicity and osmotic shock from Bath 2 was causing additional damage to embryos.

(a)

Bath	PG Conc (M)	MeOH Conc (M)	Tre Conc(M)
1	2.0	1.2	0.5
2	1.0	1.7	1.0

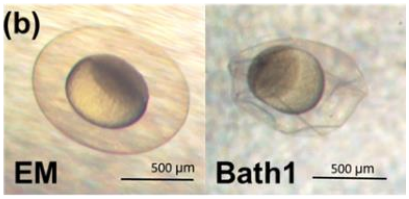

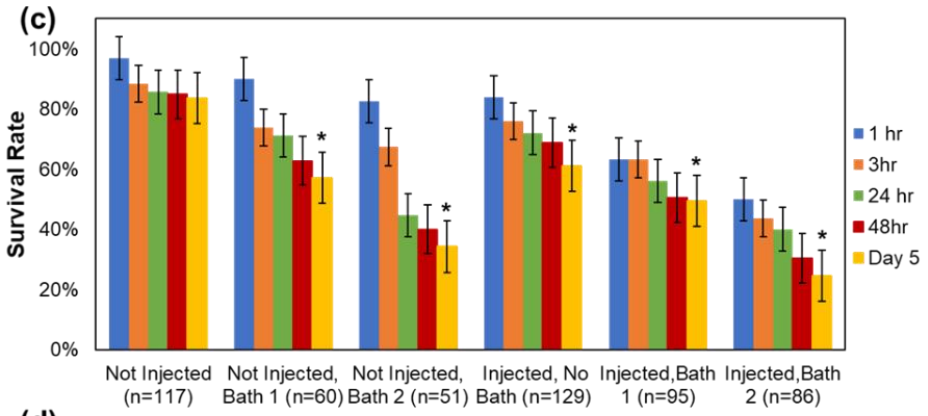

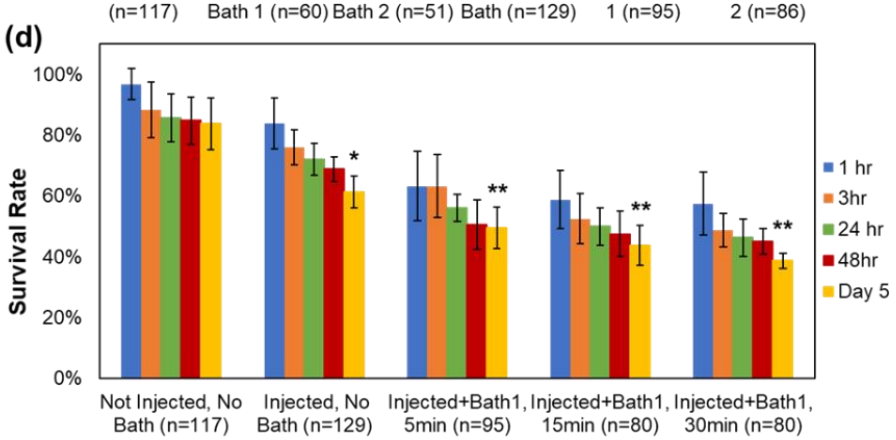

Figure 4.5. Impact of the prefreezing bath. (a) Table comparing the concentrations of PG, MeOH and Tre in "Bath 1" and "Bath 2". (b) Images of a non-injected embryo in embryo medium and immediately after being placed in Bath 1. (c) Survival rates up to Day 5 for embryos placed in

"Bath 1" and "Bath 2" for 15 min are reported here along with a non-injected and non-bath control. The injected embryos were injected based on the Single Injection protocol at the High cell stage. For both injected and non-injected groups, embryos exposed to Bath 1 had a significantly higher survival rate (ANOVA, $p<0.05$) than the embryos exposed to Bath 2. (d) Survival rates up to Day 5 for injected embryos placed in Bath 1 for 0 min (no bath), 5 min, 15 min, and 30 min are reported here along with a non-injected non-bath control. The injected and no bath (0 min) group showed a significantly higher survival rate (ANOVA, $p<0.05$) than the embryos exposed to Bath 1 for longer times. However, there was no significant difference between survival rates for injected embryos exposed to Bath 1 for 5 min, 15min and 30 min. Notation "**" means groups have don't have significant difference (ANOVA, $p> 0.1$), whereas "*" means that groups have significant difference (ANOVA, $p <0.05$). Also note that the survival of the embryos was evaluated after being rehydrated in "Post warming" wash out bath and washed to remove the CPA.

Comparing the average Day 5 survival rate of non-bath exposed injected embryos to that of Bath 1 exposed injected embryos, we found a significant difference ($p<0.05$, ANOVA). The survival rates of injected embryos submerged in Bath 1 (50%) were 2x higher than the survival rates of in injected embryos from Bath 2 (25%). We wanted to further evaluate the loss in survival rates of embryos based on time spent in Bath 1. Fig 4.5d shows the average Day 5 survival rates of embryos for the following groups: non-injected, no bath control (n=117), injected embryos placed in Bath 1 for 0min (n=129), 5mins (n=95), 15mins (n=80) and 30mins (n=80) to be 84%, 61%, 49%, 44% and 39%, respectively. The injected and no bath (0 min) group showed a significantly higher survival rate (ANOVA, $p<0.05$) than the embryos exposed to Bath 1 for longer times. However, there was no significant difference (ANOVA, $p>0.1$) between survival rates for injected embryos exposed to Bath 1 for 5 min, 15min and 30 min. This suggests that the embryos can be exposed to Bath 1 for longer times without necessarily inducing additional damage. Previous studies have shown that for embryos at 100% epiboly development stage, the yolk is impermeable while the blastoderm was semi-permeable [20, 73]. In future studies, we will use both 15min and 30min baths to study if any improvement in post warming survival rates is seen.

4.6 Cooling and laser warming of embryos

Figure 4.6 shows a step-by-step overview of the Single Injection protocol and associated protocols for baths, cooling and laser warming. After the injection, embryos are kept at 28°C for 2 hr before immersion in Bath 1 (2M PG, 1.2M MeOH, and 0.5M Tre) for 5 min. The embryos are then encapsulated in a 1µL droplet with the same CPA concentration as the precooling bath and a GNR concentration of 4.2 x 10^{17} np/m^3 (3xGNR in yolk). Our modeling data supported using 3x higher concentration of GNR in the encapsulating droplet than the GNR in the yolk to generate the necessary warming rates. The droplet and embryo were placed onto our "cryojig," which automatically and reproducibly cools the embryo by immersion in LN2. The embryo is held at -196°C for over 10s to ensure equilibration. After this, we rewarm the embryo and the droplet under laser settings (300V power, 1ms pulse time, I=1.1 x10^9 W/m^2 fluence rate) similar to those in our original work[11]. The entire laser warming process is recorded using an overhead camera to isolate any misfires. Post laser warming, the embryo is placed in the "Post Warming Wash Out" bath (1M PG, 0.6M MeOH, 0.25M Trehalose) for 10 mins, followed by three washes in standard embryo medium.

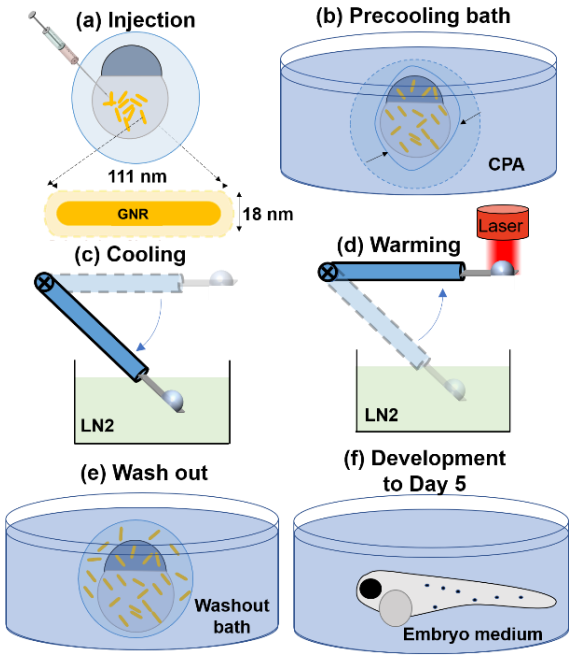

Figure 4.6. Overview of the cryopreservation and laser warming process. The process includes: (a) microinjection of 1064 nm resonant GNR and CPA (PG & MeOH) into the yolk, (b) placing the embryo in a CPA bath for 5min to replace the perivitelline fluid, (c) rapid cooling with the modified cryotop to prevent ice formation, (d) laser warming which yields rapid and uniform warming inside the embryo to outrun any ice formation, (e) post-warming wash out consisting of rehydrating and washing the embryo to remove toxic CPAs from perivitelline fluid (f) after which an embryo can grow and develop over 5 days in embryo medium at 28°C.

Fig. 4.7a compares the survival rate of embryos for both injection-only and laser warmed groups. Comparing injection-only groups, the Single Injection group (n=300) had higher average numbers at all time points and was significantly higher at Day 5 (ANOVA, $p<0.05$) at 58% compared to 50% for the Double Injection (n=261) group. This suggests that the Single Injection reduces injury from the injection itself. Now comparing the laser warmed groups at 1 hr, there was no significant difference (ANOVA, $p>0.1$) between the average survival rate of 31% and 40% for Double Injection and Single Injection groups, respectively. However, comparing at Day 5, the Single Injection group had significantly higher (ANOVA, $p<0.05$) average survival at 3% (9 fish out of 282) vs. 1% (2 fish out of 271) for the Double Injection group. Importantly, 11 fish from both groups managed to hatch and swim post laser warming. Thus, both Single Injection and Double Injection

approaches can deliver intact embryos post laser warming. It should be noted that we use survival rates at 1 hr only to distinguish intact vs non-intact embryos (no visible membrane damage). To measure viability, we consider embryos that develop to Day 5 and have no major developmental mutations[1]. Thus, the Single Injection approach improves the average survival and overall viability at Day 5 (3x higher than Double Injection).

Fig. 4.7b shows the impact of dechorionation on injected-only and laser-warmed embryos. Comparing the average survival rates for "injected and dechorionated only" (n=60), "laser warmed and dechorionated at 1hr" (n=32) and "dechorionated and laser warmed" (n=53) to the control groups (ie chorion intact), we found that the survival rates are significantly lower (ANOVA, $p<0.05$). We used standard protocols of enzymatic digestion for removing chorion using 2% pronase[80]. For the case where the chorion was removed at 1 hour after laser warming, the percentage of surviving embryos after 1 and 3hr was 26% (n=8) and 6% (n=2), respectively. For the case where embryos were dechorionated prior to laser warming, none of the embryos survived at any of the time points. Importantly, none of the laser warmed embryos that had their chorion removed prematurely (before 48 hr post-fertilization) survived beyond 24 hr. There is a significant difference (ANOVA $p< 0.05$) between the average Day 5 survival rates of dechorionated embryos for the two laser-warmed groups and the single injection-only group. The survival rate dropped significantly by removing the chorion, suggesting that the embryos are very fragile before post-warming and additional handling reduces viability.

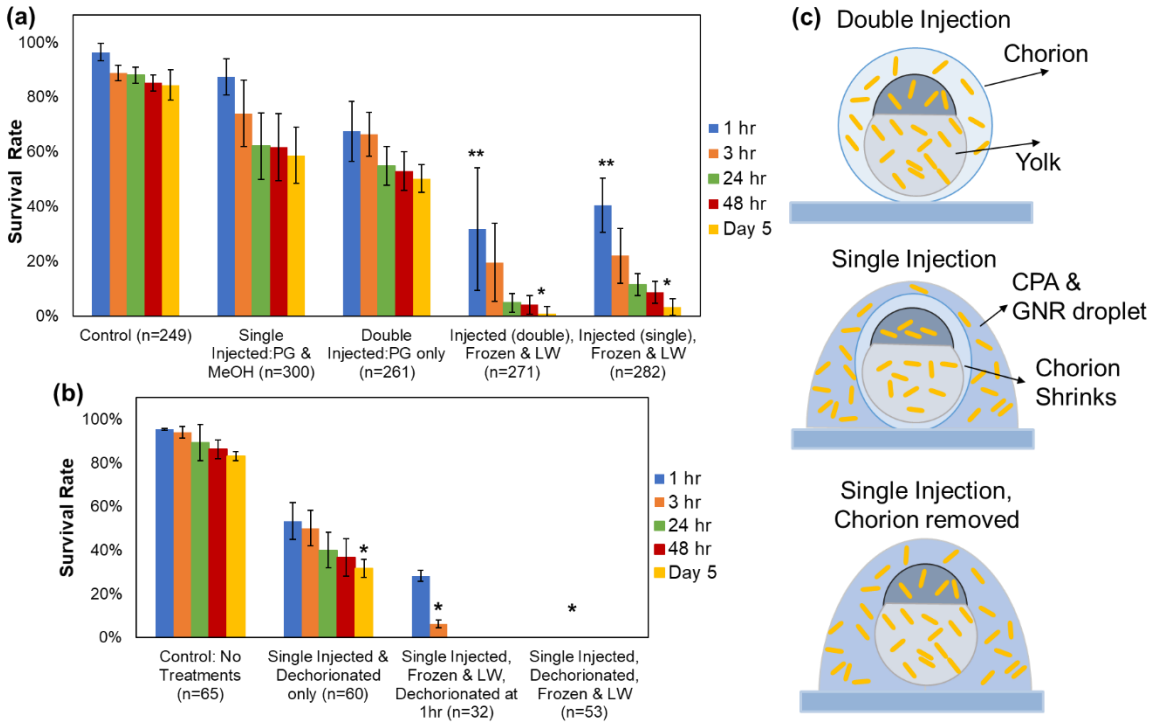

Figure 4.7. Freezing and Laser warming of embryos. (a) Comparing the survival of embryos obtained from previous Double Injection [11] and new Single Injection protocol. Survival of fish embryos up to Day 5 using five treatments: i) control (uninjected), ii) Single Injection of 9nL in the yolk, iii) Double Injection in volumes of 9nL in the yolk and 72nL in perivitelline fluid, iv) Double injected, followed by rapid cooling and laser warming, v) Single injected, followed by bath, rapid cooling and laser warming. The survival rate post laser warming for the Single Injection group was significantly higher (ANOVA, $p<0.05$) compared to the survival rate of Double Injection group. (b) Survival rate of zebrafish embryos using four treatments: i) control (uninjected), ii) Single Injection of 9nL in the yolk and then dechorionated enzymatically, iii) Single Injection of 9nL in the yolk, followed by cooling and laser warming, and then chorion removed after 1 hr, iv) Single Injection of 9nL in the yolk, then dechorionated enzymatically and followed by rapid cooling and laser warming. (c) Representative images to show the different protocols of injection, bath and chorion handling used in this study. Notation "**" means groups have don't have significant difference (ANOVA, $p> 0.1$), whereas "*" means that groups have significant difference (ANOVA, $p <0.05$).

4.7 Growth and Spawning of Laser Warmed Fish

Two fish from the single injected and laser warmed group that survived up to Day 5 were transferred to UMN zebrafish core. Here the fish were housed, fed, and grown to adulthood. They ultimately spawned at 4 months. Once their individual sex was identified, they were named Rodger (male) and Erin (female). Fig. 4.8a shows the development of Rodger at 3 hr, 52hr, Day 6 and 3 months after being rapidly cooled and laser warmed. In addition to

Rodger and Erin, a wild type male fish (8 months old) was also spawned three times with single transgenic blue glofish of the opposite sex. Fig 4.8b shows the average survival rates of embryos obtained from spawning of blue glofish with untreated male wild type fish (control, n=330), Rodger (n=585), and Erin (n=561) as 92%, 88% and 91%, respectively. Comparing the average Day 5 survival rates, no significant difference was found between control (92%), Rodger (88%) and Erin (91%) groups. This suggests that the laser warmed fish are capable to reproducing viable embryos normally.

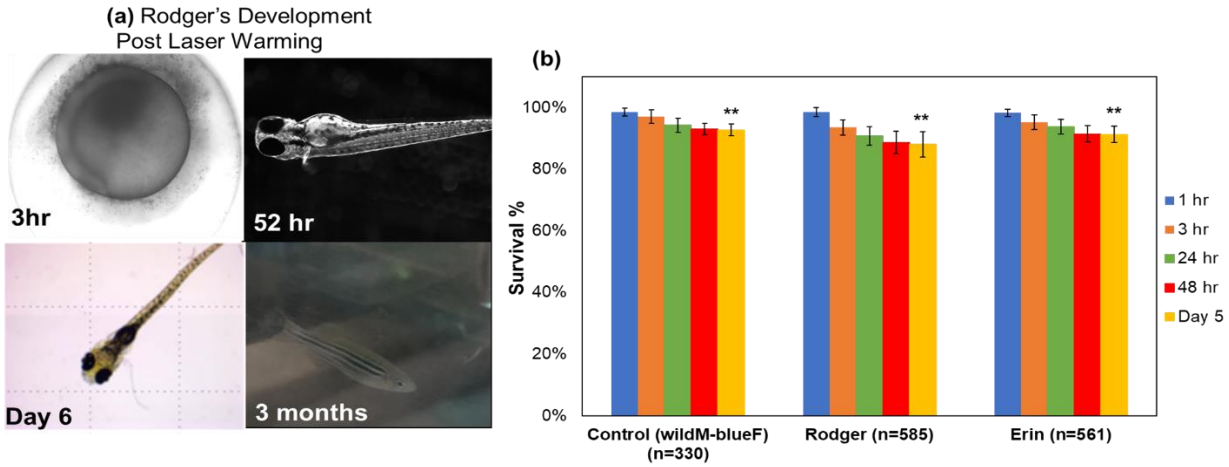

Figure 4.8. Spawning adult "cryopreserved and laser warmed" fish. (a) Images of Rodger fish at different stages of development: developing at 3 hr, hatched into a larva at 52 hr post laser warming, swimming with no developmental mutations at Day 6, and deeding at 6 weeks post laser warming. (b) Survival of zebrafish embryos up to Day 5 obtained from spawning with transgenic blue glofish™. The groups represent embryos from: control (wild AB male with blue glofish female), Rodger (with female blue glofish), and Erin (with male blue glofish). There is no significant difference between the survival rates of the embryos from control, Rodger and Erin groups. This suggests that the laser warmed fish are capable to reproducing viable embryos. Notation "**" means groups have don't have significant difference (ANOVA, $p > 0.1$), whereas "*" means that groups have significant difference (ANOVA, $p < 0.05$).

Methods

Injections in the Yolk

We inject a solution of CPA and GNR into the yolk for two reasons. First, we want to ensure that ice formation can be reduced by placing CPA directly into the yolk. Second, we want to place enough laser absorption particles like GNR so that uniform heating can occur. The injections are performed using the injection setup in the UMN Zebrafish Core. The protocol used in this study has been adapted from previous studies by the authors [11, 73]. The CPAs used to prepare the injection solution have been modified from 99% PG (13.1M) to now have 80% v/v PG (10.1M) and 20% v/v MeOH (4.6M). In addition to using our standard laser absorber (i.e. PEG-coated GNR from nanoComposix, San Diego CA), we also injected HGNS and GNS to test the biocompatibility of these particles individually. We also tested the robustness of various developmental stages (early cell division to high epiboly) to withstand injections. This was done to study if cytoplasmic streaming seen at earlier stages could be leveraged to deliver nanoparticles from the yolk into the cells. Finally, we also tested the survival rates achieved by increasing the injected volumes from 9nL to 18nL and 30nL. Previous studies have characterized the water content within the yolk and were used to estimate the concentration of both nanoparticles and CPA inside the yolk after injection. For example, when injecting 9nL of an injection solution consisting of PG (10.1M), MeOH (4.6M) and GNR ($9.4x10^{17}$ np/m^3) into the yolk, the resultant concentration would be diluted to 1.5M PG, 0.7M MeOH, and 1.4×10^{17} np/m^3 GNR in the yolk. Any embryos that were visibly leaking (i.e. streaming yolk that can be seen within the perivitelline fluid) were discarded from the study. All the laser warming studies used a 9nL injection.

Pre-Cooling Bath

After the injections had been completed and dead embryos removed, the live embryos were cultured at 28°C for at least 2 hours. This time allows the embryos to recover and patch any holes made in the yolk membrane. Then, the embryos were placed into a petri dish with a prefreezing bath solution. The main purpose of the bath was to remove the perivitelline fluid and replace it with CPA that can allow vitrification (no visible ice) upon cooling. In this study, we evaluated the impact of two different baths: Bath 1 (2M PG, 1.2M MeOH, 0.5M Tre) and Bath 2 (1M PG, 1.7M MeOH, 1.0M Tre). We also varied the time (0 min, 5 min, 15 min and 30 min) the embryos were exposed to the bath to evaluate its impact on their survival rates. Once the embryos had been exposed to bath, they could be placed on the cryotop to begin rapid cooling and laser warming. Once the laser warming was completed, the embryos were returned to the pre-freezing bath for at least 10 mins and then transferred to another rehydration bath (1/2 strength of pre-freezing bath) for 20 mins. The embryos were then finally washed in embryo medium at least 3 times and then cultured up to Day 5 based on our protocol.

Rapid Cooling and Laser Warming of Embryos

To initiate rapid cooling and laser warming, the embryos were placed onto the tip of the cryotop. For the single injected group, a 1µL droplet of 2M PG, 1.2M MeOH and 4.2 x 10^{17} np/m^3 GNR (3x GNR in yolk) was placed around the embryo. Our modeling data supported using 3x higher concentration of GNR in the encapsulating droplet than the GNR in the yolk to generate the necessary warming rates. The cryotop was attached to a motor arm of the cryojig (See Cryojig in Appendix A), which can rapidly immerse the embryo directly into LN2. Once the embryo was centered under the laser's focus, the cooling was initiated, and the embryo held in LN2 for at least 10 seconds to allow for equilibration to -

196C. To initiate laser warming, the cryojig brought the embryo back under the laser's focus and initiated the laser pulse (300V power, 1ms pulse time, I=1.1 x10^9 W/m^2 fluence rate). This entire process was recorded by an overhead camera, and the video was used to evaluate if any ice was formed inside the embryo. After the warming had been completed, the embryo was placed back into a dish containing the prefreezing bath and subsequently washed to remove CPA.

Survival Analysis

The protocol used in this study is like the method used in our previous studies of evaluating survival rates of zebrafish embryos after applied treatments [73]. The selected time points were: 1 hr, 3 hr, 24 hr, 48 hr and 5 days after the specific treatment for an experimental group (i.e. injection, bath, or laser warming). In this study, we have begun to report the survival rates at 48 hr since we expect the embryos to hatch and leave their chorions by this time point. In our previous study, many of our fish died prior to hatching from their chorions due to hardening. For the first 3 time points, embryos were considered alive if they were developing and moving within the chorion between consecutive time points. At the Day 5 time point, an embryo was considered normal in development if it had hatched and was able to swim upright in the water column, had proper cardiac development, eye and tail musculature development, fins, and a functional swim bladder. Any fish that did not match these criteria was considered abnormal in its development and not counted among the "survived" fish.

Animal Care

Wild type zebrafish (*Danio rerio)* embryos were obtained from the University of Minnesota Zebrafish Core. All care and welfare for the animals met NIH animal care standards. Full details of approved protocols are listed with the Zebrafish Core-IACUC

(protocol # 1506-32642A). Zebrafish parent clutches and their embryos were maintained at 28°C under standard conditions as described in Westerfield [80]. To grow fish in our lab space from Day 3 to Day 5, the authors developed their own IACUC protocol (1804-35844A). This protocol also covered the transfer, housing, feeding and spawning of the fish that survived up to Day 5 after laser warming in the Zebrafish core.

Spawning with Adult Fish

From the double injected and single injected group, a total of 11 fish survived up to Day 5. Since we didn't have resources for housing the fish initially, many of surviving fish were euthanized by Day 6. But once were able to get an IACUC protocol (1804-35844A), in place, we were able to house the two fish that made it to Day 5 from the single injected group. The two fish were placed in their own individual tanks and at approximately 6 weeks, the sexes of the fish were visually confirmed as male and female. The male fish was named Rodger and female fish was named Erin. When the each of the fish was approximately 4 months old, we attempted to get them to spawn with a single transgenic blue glofish^{TM} of the opposite sex. The day before the spawn, both Erin and Rodger were placed in spawning tanks with a single blue glofish^{TM} of the opposite sex and left overnight. We also spawned a wild type AB male fish with a blue female glofish^{TM} and used the embryos as a control group for this experiment. We attempted to spawn both Erin and Rodger 3 times, giving at least 3 weeks between a successive spawn. The fish started spawning as soon as the lights were turned on in morning and their embryos were collected soon after. The embryos were cleaned and placed in petri dishes with embryo medium. These spawned embryos were also cultured up to Day 5 and their survival rates were evaluated based our protocol.

Conclusion

The results from this study demonstrated an optimized method to reproducibly rewarm zebrafish embryos after cryopreservation using laser-assisted gold nanoparticle warming. Compared to our previous Double Injection protocol, the Single Injection of PG and GNRs allowed introduction of safer and more effective cryoprotectants and laser absorbers inside the embryo and increased the average survival rate up to Day 5. We also developed methods for using pre-cooling and post warming wash out baths to effectively load CPAs and remove perivitelline fluid. Finally, we also demonstrated the ability to these laser warmed fish to grow to adulthood and spawn viable embryos.

Chapter 5: Conclusion and Future Work

This chapter will discuss the overall results from the development of laser nanowarming technology and its application to cryopreserve zebrafish embryos. In addition, we also discuss our future work and its implications for other biological systems. This chapter was prepared individually by the author with the permission of other collaborators.

5.1 Need for Fish Cryopreservation

In Chapter 1, we described the importance of cryopreservation of aquatic germplasm as a tool to save biodiversity, enhance aquaculture, and maintain genetic research models. Through our literature review, we discussed the barriers to cryopreserve most fish embryos and the need to develop rapid cooling and laser warming methods to overcome them. We also briefly discussed the mechanism behind the gold nanoparticle assisted laser heating and warming rates that could be generated from its application.

Cryopreservation has consistently provided frozen germplasm to improve the reproductive efficiency of animals, from the routine production of genetically outstanding livestock with frozen sperm and embryos to modern milestones in propagating endangered species such as the black-footed ferret, cheetah, giant panda[90], and now zebrafish. Since the National Institutes of Health have dramatically increased funding to support the development of zebrafish as an increasingly important vertebrate model for human genetics and biomedical research, researchers have rapidly produced many new strains of wild type, transgenic and mutated zebrafish for studying vertebrate developmental biology and disease mechanisms. Even though zebrafish sperm cryopreservation is now possible, it only maintains half the genome, and there are no reproducible fish embryo cryopreservation protocols to supply the remaining genome despite decades of work [30].

Moreover, the need for developing techniques for the cryopreservation of teleost and other multi-compartment germplasm is pressing. At present, aquaculture is largely dependent upon wild fish populations or continuous maintenance of living cultures [30, 49]. Unfortunately, the availability and productivity of these systems is continually threatened by accidents, natural disasters, breeding failure and disease. Likewise, developing multiple brood-stocks to move toward year-round availability has proved to be

expensive, time consuming and, for many species, not possible. At a food-fish aquaculture workshop sponsored by MN Sea Grant (MNSG)[91], this was noted as a particular problem for percid farming in the Midwest.

For example, valuable genetic lines created for productivity and disease resistance, such as transgenic fish and hybrids[49], must be maintained in live-culture systems. Likewise, Minnesota-based researchers want to genetically engineer Carp embryos to study and control invasive fish species, but strains can take years to generate, which is costly in terms of space, maintenance, and research effort, and are subject to loss through genetic drift. In the case of zebrafish, an important research model, the Zebrafish International Research Center (ZIRC) at the University of Oregon commonly cryopreserves zebrafish sperm. However, sperm cryopreservation only maintains half the genome, and until now, zebrafish embryo cryopreservation has not been successful [34]. Systematic germplasm cryopreservation can address such problems in aquaculture by: (1) allowing the maintenance of large gene pools and reducing inbreeding; (2) reducing pressure on wild populations from collection activities; (3) maintaining a constant supply of animals (because some animals are unavailable in the wild during certain times of the year); (4) decreasing costs by reducing the facilities needed; (5) reducing the impact (e.g., contamination with antibiotics) of aquaculture sites upon wild populations and food resources; and (6) sustaining productivity by minimizing the impact of live-culture failures resulting from human error, natural disasters, breeding failure and epidemics [92].

Again, we can end this bottleneck through cryopreservation and laser-based rewarming technologies. Combined with developments in automation that will allow for indefinite

storage of millions of embryos, cryopreservation technology could have a huge positive effect on Minnesota's and the Midwest's aquaculture industry.

5.2 Proof of concept in Zebrafish

In Chapter 2, we demonstrated our ability to successfully rewarm cryogenically stable zebrafish embryos. The results from 14 trials (n = 223) demonstrated viable embryos with consistent structure at 1 hr (31%), and continuing development at 3 hr (17%) and movement at 24 hr (10%) post-warming. This compares starkly with 0% viability, structure, or movement at all time points in convectively warmed controls (n = 50, $p < 0.001$, ANOVA). Our approach used micro-injection of GNRs and cryoprotectants, followed by cooling to -196°C and then rapid warming with laser irradiation. Further results demonstrated the biocompatibility of PEG-coated GNRs compared to other laser absorbers like India ink and GNRs coated with cetyl-trimethylammonium bromide (CTAB). The characterization of GNRs along with the heat transfer modeling allowed estimation of the cooling (90,000 °C/min) and warming (14 million °C/min) rates that can be achieved by this method. However, survival of laser warmed fish up to Day 5 was not achieved.

In Chapter 4, we optimized our initial protocol, which used a Double Injection of CPA and GNR in both the yolk and surrounding perivitelline fluid. We were concerned that CPA and GNR leaked out after micro-injection in the chorion, creating non-uniform warming. This led to the exploration of a new Single Injection protocol. The new approach relies on one injection of CPA and GNR (9nL) into the yolk at the High cell stage (3 hr post fertilization), followed by immersion in a precooling bath. Comparing to injection-only and laser warmed groups, the Single Injection group had higher average numbers at all time points, and was significantly higher at Day 5 (ANOVA, $p<0.05$) compared to the

Double Injection groups. This suggested that the Single Injection reduces injury from the injection itself as well as improve the post warming outcomes. Importantly, 11 fish from both groups managed to hatch and swim post laser warming. Thus, both Single Injection and Double Injection approaches can deliver intact embryos post laser warming. However, the Single Injection approach improves the average survival and overall viability at Day 5 (3x higher than Double Injection) will be our primary approach in the future. Finally, two laser warmed embryos (Erin and Rodger) that lived to Day 5 from Single Injection group were grown to adulthood (currently living at 12 months) and spawned several times (at 4 months) to give embryos with over 85% survival at Day 5. Comparing the survival rates of the embryos spawned from the laser warmed fish with control groups was found to have no significant difference ($p>0.1$, ANOVA). This was the first demonstration we are aware of that cryopreserved fish embryos can hatch, grow to adulthood and successfully spawn.

5.3 Application to other systems

In Chapter 3, we generalized our rapid cooling and laser warming methods to droplets containing CPA and GNR which could potentially encapsulate a variety of biomaterials. We call this approach "Extracellular Laser Nanowarming" since laser absorbers like GNR don't have to be injected into the biomaterials as opposed to the "Intracellular Laser Warming" approach developed for Zebrafish embryos. We first showed that droplets containing low concentration cryoprotectants (such as 2M PG +/- 1M Trehalose) can be rapidly cooled by plunging into LN2 to achieve either a visually transparent (*i.e.* vitrified) or a cloudy with ice (*i.e.* non-vitrified) state. Both modeling and experiments were then used to characterize the process for different laser energy (2-6J), pulse length (1-20ms), droplet volume (0.2-1.8µL), cryoprotectant (2-3M) and gold concentration (0.77-4.8 $x10^{17}$ nps/m^3) to assess physical and biological success. Physical success was achieved

by finding conditions that minimize cloudiness and white spots within the droplets during cooling and warming as signs of damaging ice formation and ice crystallization, respectively. Using human dermal fibroblasts to find conditions that achieve ≥ 90 % cell viability normalized to controls post-warming, we showed the broad applicability of the extracellular method. Interestingly, we also showed that physical and biological success was possible even in cases of suboptimal CPA loading and cooling using this platform if crystallization could be prevented.

Table 5.1. Various biomaterials that can be cryopreserved and rewarmed using either Extra- or Intra-cellular Laser Nanowarming

System	Size (μm)	Min Droplet Volume (nL)	Convective warming possible ?	Droplets needed	GNP Absorber	Proof of Concept Status
HDF Cells	10	0.004	Yes, no CPA needed	N/A	Extracellular	Khosla et al 2018
Stem Cells	20	0.03	Yes, with 1M CPA	10 million	Extracellular	Untested
Mice Oocyte	80	2	Yes, with 2M CPA	N/A	Extracellular	Jin et al 2014
Coral Larvae	150	14	Yes, with 2M CPA	1 billion	Extracellular	Daly et al 2018
Pancreatic Islets	150	14	Yes, with 2M CPA	10 million	Extracellular	Zhan unpublished 2019
Drosophila Embryo	200	34	Yes with 2M CPA	N/A	Extracellular	Zhan unpublished 2019
Shrimp Nauplii	300	113	Yes with 3M CPA	100,000	Extracellular	Pers Comm-Cryoocyte
Zebrafish Embryo	1000	4189	No	10,000	Intracellular	Khosla et al 2017
Golden Shiner Embryo	1000	4189	No	10,000	Intracellular	Untested
Xenopus Oocyte	1200	7238	No	10,000	Intracellular	Untested
Walleye Embryo	2500	65,450	No	10,000	Intracellular	No Current Tech
Saugeye Embryo	2500	65,450	No	10,000	Intracellular	No Current Tech
Salmon Embryos	5000	523,599	No	10,000	Intracellular	No Current Tech

In Table 5.1, we list the various biomaterials that can be cryopreserved and rewarmed with our two approaches. To prevent crystallization, the warming at the center of the specimen must surpass CWR of 11,400,000 °C/min, 930,000 °C/min and 200,000 °C/min when using 2M PG, 3M PG and 2M PG and 1M Trehalose, respectively (See Fig 1.1 in Chapter 1). Using these rates as a threshold, droplets with 2M PG and 3M PG can't prevent crystallization via extracellular warming for D_{cell} larger than 20 μm and 100 μm, respectively. Similarly, D_{cell} increases to 180 μm for a droplet with 2M PG and 1M Trehalose. The CWR are needed to avoid crystallization within droplets; however, each biomaterial may remain viable even when rewarmed at rates slightly lower than these.

Additionally, the extracellular heating approach can work for larger specimens if the CPA concentration of the droplet is increased; however, this increases the risk of losing samples like embryos and oocytes due to toxicity. In contrast, the intra- and extra-cellular heating approach (i.e. GNRs present inside and outside the biomaterials) can produce ultrahigh warming rates (20,000,000 °C/min) regardless of the biomaterial size provided that the GNRs are distributed uniformly throughout the droplet and biomaterials. However, to rewarm Salmon embryos and other biomaterials over 2mm in size, we hope to use multiple lasers or lasers with larger spot sizes at the same time to uniformly rewarm them.

The extracellular approach has already been shown to successful in the cryopreservation of coral larvae[81]. Our collaborators in Hawaii showed for the first time that coral larvae can survive cryopreservation and resume swimming after laser warming. Using a laser warming rates of 4.5 million ºC/min and a 3.5 M CPA (1.3M PG, 1.2M DMSO, and 1M Tre in PBS), the coral larvae *Fungia scutaria* showed a survival rate of 43%[81]. Surviving larvae swam and continued to develop for at least 12 hours after laser warming.

5.4 Future Work

Our future work will be geared toward improving survival rates to adulthood and developing apparatus to cryopreserve fish embryos in a high throughput manner. We will explore the use of high-throughput 3D printing, microfluidic sorting, and laser nanotechnology cryopreservation and storage of zebrafish embryos. 3D printing and microfluidics are ideal tools to rapidly create droplets and flow chambers for manipulation and analysis of droplets of vitrified cellular systems. For this droplet microfluidic platform, we hope to encapsulate, transport, sort and store zebrafish embryos at both room and near-liquid nitrogen temperatures. After preservation and storage, the microfluidic technology will also be integrated with an ultra-fast laser warming system in our lab. Figure 5.1 shows

a schematic description of this proposed device, wherein the speed and reliability of 3D printing and microfluidics will be combined with laser nanotechnology to address the broader need for a scalable, high throughput platform that allows formation, manipulation, analysis and preservation of cellular drops using zebrafish embryos as a model system.

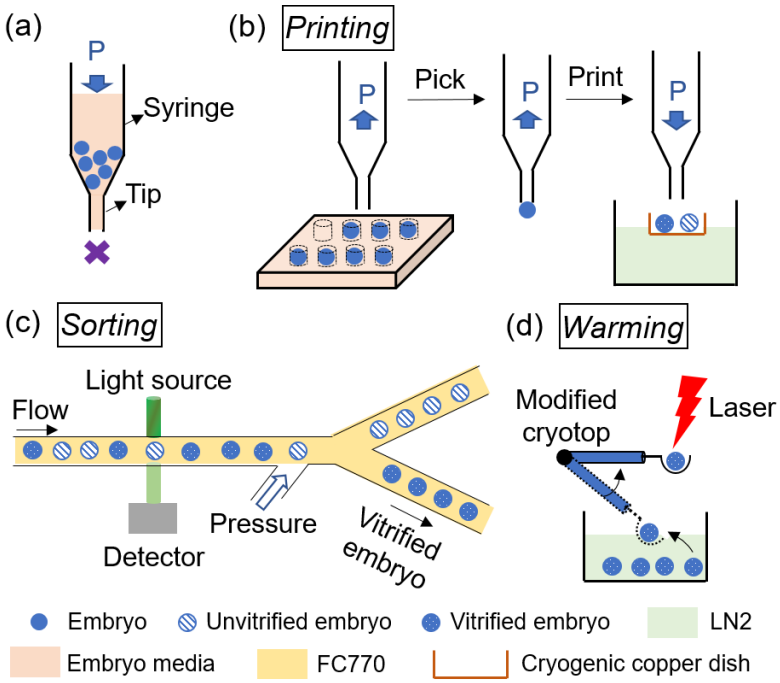

Figure 5.1. Schematic of high throughput zebrafish embryo printing, microfluidic sorting and laser warming process. (a) Zebrafish embryo settles and blocks the printing tip using conventional direct printing method. "P" indicates pressure and the arrow indicates the direction of pressure. (b) "Pick & Print" of embryo to cryogenic copper dish. (c) Microfluidic optical sorting of vitrified and unvitrified embryos. (d) Laser warming of the embryo with modified cryotop. **Image Credit: Li Zhan**

Using the "pick & print" method, we can print CPA droplet-encapsulated and injected embryos onto a cryogenic copper dish which is pre-chilled to LN2 temperature and obtain ~80% vitrification success, in contrast to 0% vitrification success when printed directly into LN2.

A microfluidic device flow with a characteristic length scale on the order of millimeters or less, is an ideal tool for manipulating and analyzing embryos. While vitrification of a zebrafish embryo on-chip during flow would be challenging due to its size, recent studies with a variety of other biological systems demonstrate clearly that microfluidic devices fabricated with low-cost materials can be used successfully for improved cryopreservation processes and cryogenic handling[93-94]. The narrow microfluidic flow channels accelerate processing, minimize destabilizing inertia effects, and enable high reproducibility. Moreover, the laminar nature of microfluidic flow, in conjunction with velocity gradients manifested on the order of cell size, enable cell manipulation and sorting using techniques that would not be effective at larger length scales, such as hydrodynamic manipulation [95]. Another important advantage of microfluidic cell sorting is that it is carried out in a closed, isolated environment, typically with cells in a carrier or buffer fluid, thereby minimizing contamination from the environment [95]. Already, room temperature optical sorting on microfluidic platforms is widely used for separating and sorting biological systems [96]. In this work, a label-free optical sorting method employing visible light and hydrodynamic fields will be used for sorting embryos under appropriate temperature conditions. There are sizable challenges introduced by the temperatures and time-scales for cryogenic processes that must be addressed as well.

This type of sorting, CPA loading, and printing system will also be helpful for our cryopreservation studies with Pancreatic Islets. The current clinical islet yields range from 300,000 to 700,000 IEQ per isolation. Often 2-3 transplants are necessary to restore normoglycemia. A viable aim is to implement a system that can process 100,000 in few to several hours. Such a device could then be multiplexed to achieve vitrification throughput

needed for full clinical applicability. Our current theoretical throughput for vitrification is ~72,000 islets/hr (15 droplets/min/tip x 8 tips x 10 islets/drop = 1,200 islets/min => 72,000 islets/hr).

For rewarming, the laser only allows repeatable warming for up to 30 droplets/min, meaning 300 islets/min or 30 embryos/min. Through robotics, 3D print multiplexing and optical modification, we hope to increase throughput several fold. To achieve high throughput laser warming of the printed and microfluidic sorted vitrified droplets, a customized delta robot will be designed and employed to pick the droplet from near cryogenic temperature, deliver the droplet to the laser for ultrafast rewarming and release rewarmed islets suspension back to culture media, as shown in Fig. 5.2.

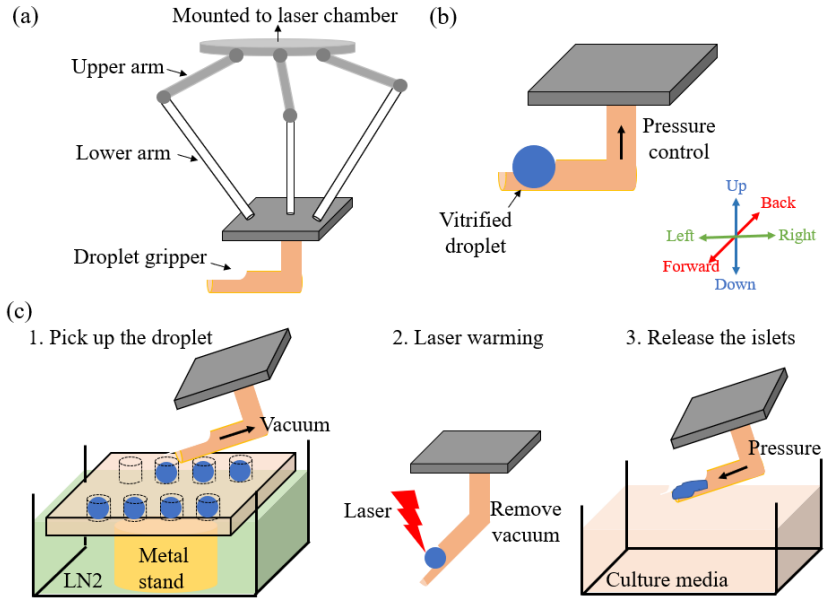

Figure 5.2. Schematic of a high throughput (higher than 120 droplets/min) laser warming setup. (a) Delta robot equipped with a droplet gripper to manipulate the droplets at very high speed. (b) Droplet gripper is connected to the pressure control device to manipulate the droplet. (c) Process of high throughput laser warming. **Image Credit: Li Zhan**.

Delta robots are widely used in picking and packaging in industry as they can manipulate small and light objects at very high speed, executing up to 300 droplets (i.e. 300 droplets x

10islets/droplet = 3000 islets/minute) per minute. Herein, we will mount a customized droplet gripper to the Delta robot to achieve droplet manipulation and high throughput laser warming. The Delta robot will be mounted to the laser chamber and programmed to move and control the pressure. Since our laser can allow up to 30 shots/min, the maximum of 300 islets or 30 embryos will be rewarmed in a 1 minute. To increase the number of islets or embryos rearmed per minute, we can devise a system to split the laser beam (2x needed power) into two separate beams using beam splitter (ie dielectric mirror or cubes). In conjunction with two delta robots, we could double the number of droplets being rewarmed from 30 to 60 per minute. Since the maximum power of the laser is approximately 20 times higher than the required power to rewarm a single droplet, a series of robots and beam splitters could be used to increase number of droplets rewarmed per minute drastically.

References

1. Fahy, G. M.; MacFarlane, D. R.; Angell, C. A.; Meryman, H. T. Vitrification as an Approach to Cryopreservation. *Cryobiology* **1984,** *21*, 407-426.
2. Lewis, J. K.; Bischof, J. C.; Braslavsky, I.; Brockbank, K. G. M.; Fahy, G. M.; Fuller, B. J.; Rabin, Y.; Tocchio, A.; Woods, E. J.; Wowk, B. G.; Acker, J. P.; Giwa, S. The Grand Challenges of Organ Banking: Proceedings from the First Global Summit on Complex Tissue Cryopreservation. *Cryobiology* **2016,** *72*, 169-182.
3. Boutron, P. More Accurate Determination of the Quantity of Ice Crystallized at Low Cooling Rates in the Glycerol and 1,2-Propanediol Aqueous Solutions: Comparison with Equilibrium. *Cryobiology* **1984,** *21*, 183-191.
4. Boutron, P.; Kaufmann, A. Stability of the Amorphous State in the System Water—1, 2-Propanediol. *Cryobiology* **1979,** *16*, 557-568.
5. Boutron, P.; Delage, D.; Roustit, B.; Körber, C. Ternary Systems with 1, 2-Propanediol—a New Gain in the Stability of the Amorphous State in the System Water-1, 2-Propanediol-1-Propanol. *Cryobiology* **1982,** *19*, 550-564.
6. Boutron, P.; Mehl, P. Theoretical Prediction of Devitrification Tendency: Determination of Critical Warming Rates without Using Finite Expansions. *Cryobiology* **1990,** *27*, 359-377.
7. Tucker, M.; Liebermann, J. *Vitrification in Assisted Reproduction: A User's Manual and Trouble-Shooting Guide*. CRC Press: **2007**.
8. Fahy, G.; MacFarlane, D.; Angell, C.; Meryman, H. Vitrification as an Approach to Cryopreservation. *Cryobiology* **1984,** *21*, 407-426.
9. Rall, W.; Fahy, G. Ice-Free Cryopreservation of Mouse Embryos at− 196 C by Vitrification. **1985**.
10. Hagedorn, M.; Kleinhans, F.; Artemov, D.; Pilatus, U. Characterization of a Major Permeability Barrier in the Zebrafish Embryo. *Biology of reproduction* **1998,** *59*, 1240-1250.
11. Khosla, K.; Wang, Y.; Hagedorn, M.; Qin, Z.; Bischof, J. Gold Nanorod Induced Warming of Embryos from the Cryogenic State Enhances Viability. *ACS nano* **2017,** *11*, 7869-7878.
12. Martino, A.; Songsasen, N.; Leibo, S. Development into Blastocysts of Bovine Oocytes Cryopreserved by Ultra-Rapid Cooling. *Biology of Reproduction* **1996,** *54*, 1059-1069.
13. Baudot, A.; Alger, L.; Boutron, P. Glass-Forming Tendency in the System Water–Dimethyl Sulfoxide. *Cryobiology* **2000,** *40*, 151-158.
14. Boutron, P.; Kaufmann, A. Stability of the Amorphous State in the System Water-Glycerol-Dimethylsulfoxide. *Cryobiology* **1978,** *15*, 93-108.
15. Boutron, P.; Mehl, P.; Kaufmann, A.; Angibaud, P. Glass-Forming Tendency and Stability of the Amorphous State in the Aqueous Solutions of Linear Polyalcohols with Four Carbons. *Cryobiology* **1986,** *23*, 453-469.
16. Baudot, A.; Boutron, P. Glass-Forming Tendency and Stability of Aqueous Solutions of Diethylformamide and Dimethylformamide. *Cryobiology* **1998,** *37*, 187-199.
17. Hopkins, J. B.; Badeau, R.; Warkentin, M.; Thorne, R. E. Effect of Common Cryoprotectants on Critical Warming Rates and Ice Formation in Aqueous Solutions. *Cryobiology* **2012,** *65*, 169-178.

18. Sutton, R. L. Critical Cooling Rates to Avoid Ice Crystallization in Solutions of Cryoprotective Agents. *Journal of the Chemical Society, Faraday Transactions* **1991,** *87*, 101.
19. Fahy, G. M. The Relevance of Cryoprotectant "Toxicity" to Cryobiology. *Cryobiology* **1986,** *23*, 1-13.
20. Hagedorn, M.; Hsu, E. W.; Pilatus, U.; Wildt, D. E.; Rall, W.; Blackband, S. J. Magnetic Resonance Microscopy and Spectroscopy Reveal Kinetics of Cryoprotectant Permeation in a Multicompartmental Biological System. *Proceedings of the national academy of sciences* **1996,** *93*, 7454-7459.
21. Mazur, P. Freezing of Living Cells: Mechanisms and Implications. *American Journal of Physiology-Cell Physiology* **1984,** *247*, C125-C142.
22. Zhang, T.; Rawson, D. M. Studies on Chilling Sensitivity of Zebrafish (Brachydanio Rerio) Embryos. *Cryobiology* **1995,** *32*, 239-246.
23. Janik, M.; Kleinhans, F. W.; Hagedorn, M. Microinjection of Cryoprotectants into the Yolk of Zebrafish Embryos (Brachydanio Rerio). *Biol Reprod* **2000,** *62*, 146-146.
24. Hagedorn, M.; Peterson, A.; Mazur, P.; Kleinhans, F. High Ice Nucleation Temperature of Zebrafish Embryos: Slow-Freezing Is Not an Option. *Cryobiology* **2004,** *49*, 181-189.
25. Tsai, S.; Rawson, D.; Zhang, T. Development of Cryopreservation Protocols for Early Stage Zebrafish (Danio Rerio) Ovarian Follicles Using Controlled Slow Cooling. *Theriogenology* **2009,** *71*, 1226-1233.
26. Liu, X. H.; Zhang, T.; Rawson, D. M. Differential Scanning Calorimetry Studies of Intraembryonic Freezing and Cryoprotectant Penetration in Zebrafish (Danio Rerio) Embryos. *Journal of Experimental Zoology* **2001,** *290*, 299-310.
27. Secretariat, C. In *Global Biodiversity Outlook 3*, Secretariat of the Convention on Biological Diversity, **2010**.
28. Reid, G. M.; Contreras MacBeath, T.; Csatádi, K. Global Challenges in Freshwater-Fish Conservation Related to Public Aquariums and the Aquarium Industry. *International Zoo Yearbook* **2013,** *47*, 6-45.
29. Tiersch, T. R.; Yang, H.; Jenkins, J. A.; Dong, Q. Sperm Cryopreservation in Fish and Shellfish. *Society of Reproduction and Fertility supplement* **2007,** *65*, 493.
30. Yang, H.; Tiersch, T. R. Current Status of Sperm Cryopreservation in Biomedical Research Fish Models: Zebrafish, Medaka, and Xiphophorus. *Comparative Biochemistry and Physiology Part C: Toxicology & Pharmacology* **2009,** *149*, 224-232.
31. Harvey, B.; Kelley, R. N.; Ashwood-Smith, M. Cryopreservation of Zebra Fish Spermatozoa Using Methanol. *Canadian Journal of Zoology* **1982,** *60*, 1867-1870.
32. Hagedorn, M.; Ricker, J.; McCarthy, M.; Meyers, S. A.; Tiersch, T.; Varga, Z.; Kleinhans, F. Biophysics of Zebrafish (Danio Rerio) Sperm. *Cryobiology* **2009,** *58*, 12-19.
33. Mazur, P.; Leibo, S. P.; Seidel, G. E. Cryopreservation of the Germplasm of Animals Used in Biological and Medical Research: Importance, Impact, Status, and Future Directions. *Biology of reproduction* **2008,** *78*, 2-12.
34. Saragusty, J.; Arav, A. Current Progress in Oocyte and Embryo Cryopreservation by Slow Freezing and Vitrification. *Reproduction* **2011,** *141*, 1-19.
35. Kimmel, C. B. Genetics and Early Development of Zebrafish. *Trends in Genetics* **1989,** *5*, 283-288.

36. Howe, K.; Clark, M. D.; Torroja, C. F.; Torrance, J.; Berthelot, C.; Muffato, M.; Collins, J. E.; Humphray, S.; McLaren, K.; Matthews, L. The Zebrafish Reference Genome Sequence and Its Relationship to the Human Genome. *Nature* **2013,** *496*, 498-503.
37. Amemiya, C. T.; Zhong, T. P.; Silverman, G. A.; Fishman, M. C.; Zon, L. I. Zebrafish Yac, Bac, and Pac Genomic Libraries. *The Zebrafish: Genetics and Genomics: The Zebrafish, Volume IIGenetics and Genomics* **1998,** *60*, 235.
38. Vilella, A. J.; Severin, J.; Ureta-Vidal, A.; Heng, L.; Durbin, R.; Birney, E. Ensemblcompara Genetrees: Complete, Duplication-Aware Phylogenetic Trees in Vertebrates. *Genome research* **2009,** *19*, 327-335.
39. Goishi, K.; Shimizu, A.; Najarro, G.; Watanabe, S.; Rogers, R.; Zon, L. I.; Klagsbrun, M. Aa-Crystallin Expression Prevents Γ-Crystallin Insolubility and Cataract Formation in the Zebrafish Cloche Mutant Lens. *Development* **2006,** *133*, 2585-2593.
40. Semina, E. V.; Brownell, I.; Mintz-Hittner, H. A.; Murray, J. C.; Jamrich, M. Mutations in the Human Forkhead Transcription Factor Foxe3 Associated with Anterior Segment Ocular Dysgenesis and Cataracts. *Human Molecular Genetics* **2001,** *10*, 231-236.
41. Muto, A.; Ohkura, M.; Abe, G.; Nakai, J.; Kawakami, K. Real-Time Visualization of Neuronal Activity During Perception. *Current Biology* **2013,** *23*, 307-311.
42. Amatruda, J. F.; Shepard, J. L.; Stern, H. M.; Zon, L. I. Zebrafish as a Cancer Model System. *Cancer Cell* **2002,** *1*, 229-231.
43. Berghmans, S.; Jette, C.; Langenau, D.; Hsu, K.; Stewart, R.; Look, T.; Kanki, J. P. Making Waves in Cancer Research: New Models in the Zebrafish. *Biotechniques* **2005,** *39*, 227.
44. Haldi, M.; Ton, C.; Seng, W. L.; McGrath, P. Human Melanoma Cells Transplanted into Zebrafish Proliferate, Migrate, Produce Melanin, Form Masses and Stimulate Angiogenesis in Zebrafish. *Angiogenesis* **2006,** *9*, 139-151.
45. Liu, S.; Leach, S. D. Zebrafish Models for Cancer. *Annual Review of Pathology: Mechanisms of disease* **2011,** *6*, 71-93.
46. Lee, L. M.; Seftor, E. A.; Bonde, G.; Cornell, R. A.; Hendrix, M. J. The Fate of Human Malignant Melanoma Cells Transplanted into Zebrafish Embryos: Assessment of Migration and Cell Division in the Absence of Tumor Formation. *Developmental Dynamics* **2005,** *233*, 1560-1570.
47. Stoletov, K.; Klemke, R. Catch of the Day: Zebrafish as a Human Cancer Model. *Oncogene* **2008,** *27*, 4509-4520.
48. Zon, L. I. Zebrafish: A New Model for Human Disease. *Genome research* **1999,** *9*, 99-100.
49. Houdebine, L.; Chourrout, D. Transgenesis in Fish. *Experientia* **1991,** *47*, 891-897.
50. Kuwayama, M.; Vajta, G.; Kato, O.; Leibo, S. P. Highly Efficient Vitrification Method for Cryopreservation of Human Oocytes. *Reproductive BioMedicine Online* **2005,** *11*, 300-308.
51. Vajta, G.; Holm, P.; Kuwayama, M.; Booth, P. J.; Jacobsen, H.; Greve, T.; Callesen, H. Open Pulled Straw (Ops) Vitrification: A New Way to Reduce Cryoinjuries of Bovine Ova and Embryos. *Molecular reproduction and development* **1998,** *51*, 53-58.

52. He, X.; Park, E. Y.; Fowler, A.; Yarmush, M. L.; Toner, M. Vitrification by Ultra-Fast Cooling at a Low Concentration of Cryoprotectants in a Quartz Micro-Capillary: A Study Using Murine Embryonic Stem Cells. *Cryobiology* **2008,** *56*, 223-232.
53. Mazur, P.; Seki, S. Survival of Mouse Oocytes after Being Cooled in a Vitrification Solution to− 196 C at 95 to 70,000 C/Min and Warmed at 610 to 118,000 C/Min: A New Paradigm for Cryopreservation by Vitrification. *Cryobiology* **2011,** *62*, 1-7.
54. Jin, B.; Kleinhans, F.; Mazur, P. Survivals of Mouse Oocytes Approach 100% after Vitrification in 3-Fold Diluted Media and Ultra-Rapid Warming by an Ir Laser Pulse. *Cryobiology* **2014,** *68*, 419-430.
55. Peyridieu, J.; Baudot, A.; Boutron, P.; Mazuer, J.; Odin, J.; Ray, A.; Chapelier, E.; Payen, E.; Descotes, J. Critical Cooling and Warming Rates to Avoid Ice Crystallization in Small Pieces of Mammalian Organs Permeated with Cryoprotective Agents. *Cryobiology* **1996,** *33*, 436-446.
56. Seki, S.; Mazur, P. The Dominance of Warming Rate over Cooling Rate in the Survival of Mouse Oocytes Subjected to a Vitrification Procedure. *Cryobiology* **2009,** *59*, 75-82.
57. Jobsis-vander Vliet, F. F. Discovery of the near-Infrared Window into the Body and the Early Development of near-Infrared Spectroscopy. *Journal of biomedical optics* **1999,** *4*, 392-397.
58. Weissleder, R. A Clearer Vision for in Vivo Imaging. Nature Publishing Group: **2001**.
59. Pissuwan, D.; Valenzuela, S. M.; Cortie, M. B. Therapeutic Possibilities of Plasmonically Heated Gold Nanoparticles. *Trends in Biotechnology* **2006,** *24*, 62-67.
60. Burda, C.; Chen, X.; Narayanan, R.; El-Sayed, M. A. Chemistry and Properties of Nanocrystals of Different Shapes. *Chemical Reviews* **2005,** *105*, 1025-1102.
61. Qin, Z.; Bischof, J. C. Thermophysical and Biological Responses of Gold Nanoparticle Laser Heating. *Chemical Society Reviews* **2012,** *41*, 1191-1217.
62. Dreaden, E. C.; Alkilany, A. M.; Huang, X.; Murphy, C. J.; El-Sayed, M. A. The Golden Age: Gold Nanoparticles for Biomedicine. *Chemical Society Reviews* **2012,** *41*, 2740-2779.
63. Shukla, R.; Bansal, V.; Chaudhary, M.; Basu, A.; Bhonde, R. R.; Sastry, M. Biocompatibility of Gold Nanoparticles and Their Endocytotic Fate inside the Cellular Compartment: A Microscopic Overview. *Langmuir* **2005,** *21*, 10644-10654.
64. Lipka, J.; Semmler-Behnke, M.; Sperling, R. A.; Wenk, A.; Takenaka, S.; Schleh, C.; Kissel, T.; Parak, W. J.; Kreyling, W. G. Biodistribution of Peg-Modified Gold Nanoparticles Following Intratracheal Instillation and Intravenous Injection. *Biomaterials* **2010,** *31*, 6574-6581.
65. De Jong, W. H.; Hagens, W. I.; Krystek, P.; Burger, M. C.; Sips, A. J.; Geertsma, R. E. Particle Size-Dependent Organ Distribution of Gold Nanoparticles after Intravenous Administration. *Biomaterials* **2008,** *29*, 1912-1919.
66. Hackley, V. Nist Rm 8011, Gold Nanoparticles, Nominal 10 Nm Diameter; Nist Rm 8012, Gold Nanoparticles, Nominal 30 Nm Diameter; Nist Rm 8013, Gold Nanoparticles, Nominal 60 Nm Diameter. *NIST SRM Spotlight* **2008**.

67. Qin, Z.; Wang, Y.; Randrianalisoa, J.; Raeesi, V.; Chan, W. C.; Lipiński, W.; Bischof, J. C. Quantitative Comparison of Photothermal Heat Generation between Gold Nanospheres and Nanorods. *Sci. Rep.* **2016,** *6*.
68. Browning, L. M.; Huang, T.; Xu, X.-H. N. Real-Time in Vivo Imaging of Size-Dependent Transport and Toxicity of Gold Nanoparticles in Zebrafish Embryos Using Single Nanoparticle Plasmonic Spectroscopy. *Interface Focus* **2013,** *3*, 20120098.
69. Bailey, J.; Ollis, D. Biochemical Engineering Fundamentals. *Chem. Eng. Edu.* **1986**.
70. Kleinhans, F.; Seki, S.; Mazur, P. Simple, Inexpensive Attainment and Measurement of Very High Cooling and Warming Rates. *Cryobiology* **2010,** *61*, 231-233.
71. Kleinhans, F.; Mazur, P. Physical Parameters, Modeling, and Methodological Details in Using Ir Laser Pulses to Warm Frozen or Vitrified Cells Ultra-Rapidly. *Cryobiology* **2015,** *70*, 195-203.
72. Jin, B.; Mazur, P. High Survival of Mouse Oocytes/Embryos after Vitrification without Permeating Cryoprotectants Followed by Ultra-Rapid Warming with an Ir Laser Pulse. *Sci. Rep.* **2015,** *5*.
73. Janik, M.; Kleinhans, F. W.; Hagedorn, M. Microinjection of Cryoprotectants into the Yolk of Zebrafish Embryos (Brachydanio Rerio). *Biol. Reprod.* **2000,** *62*, 146-146.
74. Murphy, C. J.; Sau, T. K.; Gole, A. M.; Orendorff, C. J.; Gao, J.; Gou, L.; Hunyadi, S. E.; Li, T. Anisotropic Metal Nanoparticles: Synthesis, Assembly, and Optical Applications. *J. Phys. Chem.* **2005,** *109*, 13857-13870.
75. Sun, Y.; Xia, Y. Shape-Controlled Synthesis of Gold and Silver Nanoparticles. *Science* **2002,** *298*, 2176-2179.
76. Boisselier, E.; Astruc, D. Gold Nanoparticles in Nanomedicine: Preparations, Imaging, Diagnostics, Therapies and Toxicity. *Chem. Soc. Rev.* **2009,** *38*, 1759-1782.
77. van Eeden, F. J.; Granato, M.; Odenthal, J.; Haffter, P. Developmental Mutant Screens in the Zebrafish. *Methods Cell Biol.* **1998,** *60*, 21-41.
78. Hirsch, L. R.; Stafford, R.; Bankson, J.; Sershen, S.; Rivera, B.; Price, R.; Hazle, J.; Halas, N. J.; West, J. Nanoshell-Mediated near-Infrared Thermal Therapy of Tumors under Magnetic Resonance Guidance. *Proc. Natl. Acad. Sci.* **2003,** *100*, 13549-13554.
79. Hagedorn, M.; Kleinhans, F.; Wildt, D.; Rall, W. Chill Sensitivity and Cryoprotectant Permeability of Dechorionated Zebrafish Embryos, Brachydanio Rerio. *Cryobiology* **1997,** *34*, 251-263.
80. Westerfield, M. *A Guide for the Laboratory Use of Zebrafish (Danio Rerio)*. 5 ed.; University of Oregon Press: **2007**.
81. Daly, J.; Zuchowicz, N.; Lendo, C. I. N.; Khosla, K.; Lager, C.; Henley, E. M.; Bischof, J. C.; Kleinhans, F. W.; Lin, C.; Peters, E.; Hagedorn, M. Successful Cryopreservation of Coral Larvae Using Vitrification and Laser Warming. **2018**.
82. Phatak, S.; Natesan, H.; Choi, J.; Brockbank, K. G.; Bischof, J. C. Measurement of Specific Heat and Crystallization in Vs55, Dp6, and M22 Cryoprotectant Systems with and without Sucrose. *Biopreservation and Biobanking*.
83. Flynn, T.; Draper, J.; Roos, J. The Nucleate and Film Boiling Curve of Liquid Nitrogen at One Atmosphere. In *Advances in Cryogenic Engineering*, Springer: **1962**, pp 539-545.

84. Jiao, A.; Han, X.; Critser, J. K.; Ma, H. Numerical Investigations of Transient Heat Transfer Characteristics and Vitrification Tendencies in Ultra-Fast Cell Cooling Processes. *Cryobiology* **2006,** *52*, 386-392.
85. Shah, N. B.; Dong, J.; Bischof, J. C. Cellular Uptake and Nanoscale Localization of Gold Nanoparticles in Cancer Using Label-Free Confocal Raman Microscopy. *Mol. Pharm.* **2010,** *8*, 176-184.
86. Louis, K. S.; Siegel, A. C. Cell Viability Analysis Using Trypan Blue: Manual and Automated Methods. In *Mammalian Cell Viability*, Springer: **2011**, pp 7-12.
87. Choi, J.; Bischof, J. C. Review of Biomaterial Thermal Property Measurements in the Cryogenic Regime and Their Use for Prediction of Equilibrium and Non-Equilibrium Freezing Applications in Cryobiology. *Cryobiology* **2010,** *60*, 52-70.
88. Anzar, M.; Grochulski, P.; Bonnet, B. Synchrotron X-Ray Diffraction to Detect Glass or Ice Formation in the Vitrified Bovine Cumulus-Oocyte Complexes and Morulae. *PloS one* **2014,** *9*, e114801.
89. Lane, M.; Bavister, B. D.; Lyons, E. A.; Forest, K. T. Containerless Vitrification of Mammalian Oocytes and Embryos. *Nature biotechnology* **1999,** *17*, 1234.
90. Pukazhenthi, B. S.; Wildt, D. E. Which Reproductive Technologies Are Most Relevant to Studying, Managing and Conserving Wildlife? *Reproduction, Fertility and Development* **2003,** *16*, 33-46.
91. Moen, S.; Schreiner, D.; Coburn, J.; Jacob, N. Food-Fish Aquaculture In. **2017**.
92. Hagedorn, M. Avian Genetic Resource Banking: Can Fish Embryos Yield Any Clues for Bird Embryos? *Poultry science* **2006,** *85*, 251-254.
93. Zhao, G.; Fu, J. Microfluidics for Cryopreservation. *Biotechnology advances* **2017,** *35*, 323-336.
94. Li, S.; Liu, W.; Lin, L. On-Chip Cryopreservation of Living Cells. *ALA: Journal of the Association for Laboratory Automation* **2010,** *15*, 99-106.
95. Lee, W.; Tseng, P.; Di Carlo, D. *Microtechnology for Cell Manipulation and Sorting*. Springer International Publishing: **2017**.
96. Shields IV; Wyatt, C.; Reyes, C. D.; López, G. P. Microfluidic Cell Sorting: A Review of the Advances in the Separation of Cells from Debulking to Rare Cell Isolation. *Lab on a Chip* **2015,** *15*, 1230-1249.
97. Choi, J. H.; Bischof, J. C. A Quantitative Analysis on the Thermal Properties of Phosphate Buffered Saline with Glycerol at Subzero Temperatures. *International Journal of Heat and Mass Transfer* **2008,** *51*, 640-649.
98. Whitaker, S. Forced Convection Heat Transfer Correlations for Flow in Pipes, Past Flat Plates, Single Cylinders, Single Spheres, and for Flow in Packed Beds and Tube Bundles. *AICHE J.* **1972,** *18*, 361-371.
99. Steif, P. S.; Palastro, M. C.; Rabin, Y. The Effect of Temperature Gradients on Stress Development During Cryopreservation Via Vitrification. *Cell Preserv. Technol.* **2007,** *5*, 104-115.
100. Jones, D. R.; Ashby, M. F. *Engineering Materials 2: An Introduction to Microstructures, Processing and Design*. Butterworth-Heinemann: **2005**.
101. Richerson, D. W. Modern Ceramic Engineering: Properties, Processing, and Use in Design (Revised and Expanded). Marcel Dekker, INC. New York: **1992**.
102. Plitz, J.; Rabin, Y.; Walsh, J. R. The Effect of Thermal Expansion of Ingredients on the Cocktails Vs55 and Dp6. *Cell Preserv. Technol.* **2004,** *2*, 215-226.

Appendix A

This appendix describes the development of a cryojig device, experimental, and modeling work conducted by the author to design studies associated with laser nanowarming of zebrafish embryos systems. This work has been a part of the peer reviewed publication and is reproduced here with permission.

Khosla, K., Wang, Y., Hagedorn, M., Qin, Z., & Bischof, J. (2017). Gold nanorod induced warming of embryos from the cryogenic state enhances viability. *ACS nano*, *11*(8), 7869-7878.

A.1 Design of the cryojig

An automated system was required to move samples rapidly from liquid nitrogen into the laser's focus was needed to order to ensure two important experimental considerations. First, microliter sized samples were accurately placed in laser's focus to ensure that they uniformly radiated by an incoming laser pulse (d=2mm). Second, the laser warming was initiated quickly to ensure that the samples wouldn't devitrify due to ambient convective warming. Figure A1 shows the various iterations of the cryojig device developed throughout this project. Each version essentially performs the same function by allowing the user to hold and position the sample under the laser focus, rapidly immerse in LN_2 for cooling and followed by ultrarapid warming by positioning the sample accurately under the laser's focus. All the versions applied a microcontroller to control high precision servo motor to move the sample in and out of LN_2. Fig A2d shows an image of latest version of cryojig, placed outside the laser chamber. This version was designed and manufactured in conjunction with a local design group DSI, in (Chanhassen, MN). A unique feature of this version is that it automatically fires the laser, once the sample in aligned into the laser's focus. All the jigs are setup on a styrofoam base which is used to store LN_2 (fixed height of 55 mm). Since the focus of the laser (i990 Weld, LaserStar, Orlando FL) is fixed, the user must ensure that a sample is in focus, by aligning it in the center of the crosshairs while looking through the laser's scope. Once sample alignment is performed, the user can continue with the cooling. When the motor brings back the sample, the user looks it through the scope to make sure it is still aligned with the cross hairs. If the sample is not aligned, which happens only rarely, the trial is disregarded, and the user starts over.

The cryojig has an X-Y stage (TSX1D, Newport, Irvine CA) for minor adjustment if needed. The samples are placed onto a lab made cryotop, which is mounted to the motor through a press fit attachment. A lab made cryotop was designed since the commercially available could only hold 0.1 µL samples (0.5 mm x 1.0 mm), which was not large enough to hold a zebrafish embryo (d~1mm). Therefore, 1.5mm x 3mm plastic strips (C-Line, 61003) were attached to a thin wood skewer to make the lab version for all experiments in this study.

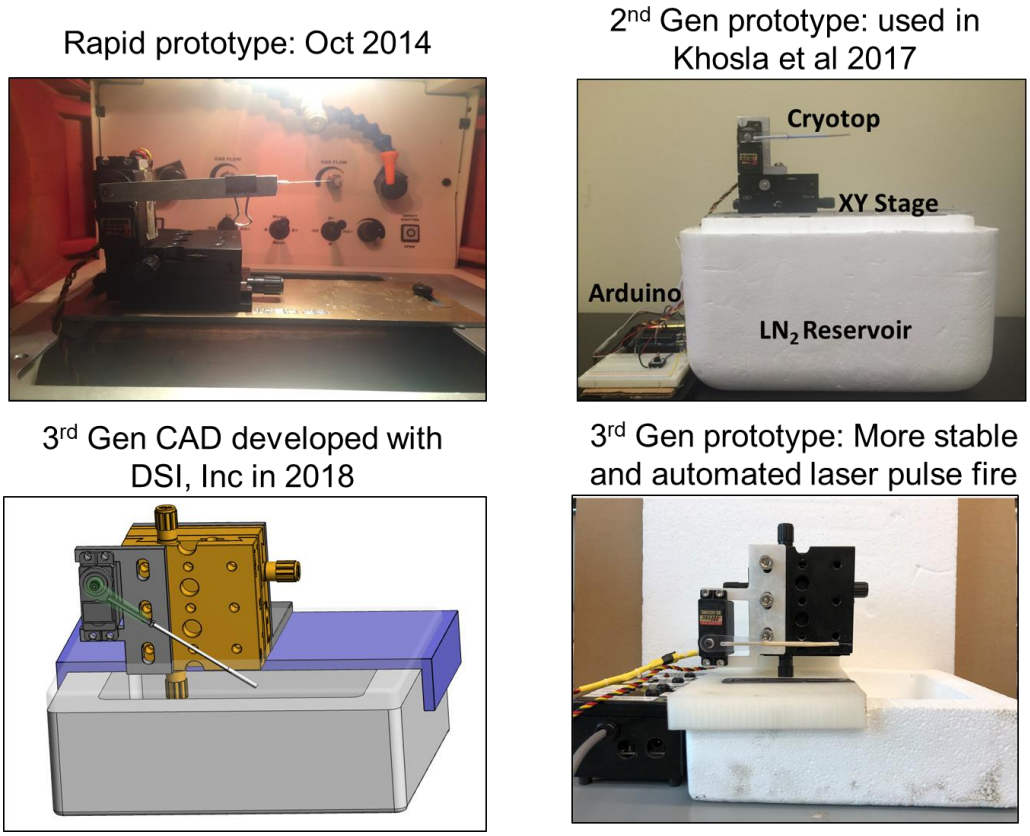

Figure A1: Different iterations of the cryojig. (a) Image of the rapid prototype of the cryojig placed inside the laser chamber first designed in 2014. (b) Image of the 2nd generation cryojig outside the chamber designed with precision machined parts to securely hold sample in place. (c) CAD image of 3rd generation jig with 3D printed parts for securing both motor and cryotop. Image is provided and reproduced with permission of DSI Inc (Chanhassen, MN). (d) Image of latest generation of the cryojig with ability to fire laser automatically as sample is aligned in the focus.

Using video recording, the time associated with moving the sample from liquid nitrogen into the laser was found to be ~ 0.3s. A calculation based on h = 100 W/m^2°C (forced convective coefficient in air), L = 400 µm (radius of the embryo), k = 1.0 W/m°C (thermal conductivity of vitrified solutions), showed that the Biot number, Bi = hL/k < 0.1. This in turn suggested that the system was thermally "lumped." A calculation using a lumped model, assuming 0.3 s exposure to the room temperature environment during positioning, suggested only about a 10 ºC change from the -196 °C storage temperature. This is well below the recrystallization range (> -100 °C) and insufficient to trigger devitrification as previously reported for similar systems.[71] A bill of materials to construct a cryojig is provided at in Appendix B along with CAD drawing for custom built parts.

A.2 Laser characterization

The laser i990 weld is a commercially available welding laser from LaserStar Inc (Orlando, Fl). Figure A2a shows an image of the laser and this same laser (but with varying power output) has been used by multiple groups working on laser warming studies (Mazur, Khosla, Daly studies). It is an Nd: YAG 1064nm wavelength capable of generating pulse with an average power of 80W with pulse times that can be changed from 0.5ms to 30ms. The choice of 1064nm laser was important since this wavelength is suitable for working with biological samples made up water, protein and fat, which are mostly transparent to wavelengths in the near infra-red region[61, 71]. Additionally, a pulse on the order of milliseconds can allow the possibility of generating warming rates on the order of 10 million to 100,000 °C/min. Since laser system is Class 4, it has a preinstalled operational chamber with a certification of Class 1. The laser system is sold with "Soft Touch Technology" or beam homogenizer which makes the laser beam profile a "flat top" instead

of gaussian. To ensure the laser spot size was accurate, a simple method of burning holes in black paper were used a different input settings of spot size. Figure A2b shows image of the paper with multiple holes along with the plotted relationship between the hole size and input spot size. The data provided a strong linear relationship (R^2=0.98), which the measured hole between within 5% of the laser spot size. To characterize the laser further studies were designed to measure the energy per pulse for various input parameters such as voltage and pulse width. Since the i990 weld laser has a fluence rate (W/m^2), most commercial laser energy sensors couldn't be used for repeated measurements without damage. Therefore, a technique was devised to only measure a fraction of energy by using a glass slide to reflect part of the laser beam towards the energy sensor (L50, Ophir, Jerusalem, Israel). Fig. A2C shows an image of the setup inside the laser chamber. By measuring the energy per pulse at lower magnitudes (150V-220V) directly with the sensor, a conversion factor ($\beta = \frac{E_{actual}}{E_{measured}}$) of 10.1 (N=100 trials) was obtained by using a power meter (NOVA II, Ophir). The laser energy plot for different voltage and pulse width conditions can be found in Figure A2d. For all these experiments, the spot diameter was set to 2 mm, to be able to easily encompass the droplet or embryo during future laser warming trials. Energy from a single pulse was later used to find the laser fluence rate, $I = E_{laser}$/ (Pulse Time x Spot Area).

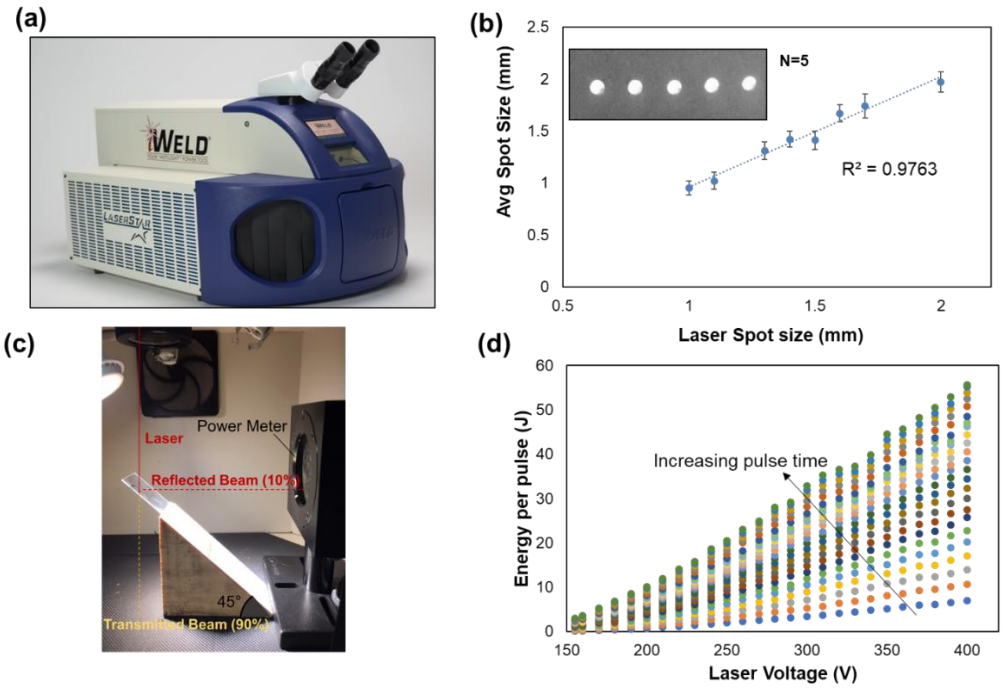

Figure A2. Laser calibration for 1064nm Nd: YAG i980 weld. (a) Image of the i990 weld with laser chamber closed (b) Plot for comparing the actual measured spot size by burning holes in paper vs the laser setting of spot size. (Inset) Image of burn holes made in paper at 400V, 2ms with 2mm spot size. (c) Image of the glass reflection setup used to measure the energy per pulse of the laser. (d) Plot for laser energy calibration representing the energy per pulse measured for ranges of input voltage (150-400V) and pulse width (0.5ms to 20ms).

A.3 Selection of GNR Concentration

As noted earlier the SAR needed to warm an embryo from liquid nitrogen to room temperature within a 1ms is 4.4 x 10^{11} W/m^3. In addition, we desired to have ≤ 20% variation of heating across the embryo to avoid thermal stress that can drive cracks. Since we used a near infrared (NIR) laser, we expected the embryo to be transparent to the laser light due to its high-water content,[61] leading to minimal attenuation. This allowed controlled absorption based on the addition of GNR in the path of the NIR light yielding an effective attenuation coefficient, for instance, μ_a = 38.9 cm^{-1} for a GNR concentration of N =1.2 x 10^{18} particles/m^3 (See Fig 1.2 in Chapter 2). Based on Beer's law, increasing the GNR concentration increases μ_a, which in turn will yield higher heating on the top *vs.* bottom of the embryo. This allowed us to estimate laser attenuation ($A= \mu_a D_{embryo}/log10$)

through GNR solutions with 0.3 x 10^{18} particles/m^3, 0.6 x 10^{18} particles/m^3, 1.2 x 10^{18} particles/m^3, and 1.8 x 10^{18} particles/m^3 as 5%, 9%, 19%, and 28%. While we could have used 0.3 x 10^{18} particles/m^3, 0.6 x 10^{18} particles/m^3concentration and achieve less than 20% variation in laser fluence rate, this would have required I = SAR/μ_a of 4.5 x 10^8 W/m^2 and 2.4 x 10^8 W/m^2 respectively, both of which are beyond the ability of the existing laser to produce (Fig. A2d). Thus, we selected the N =1.2 x 10^{18} particles/m^3 of GNR concentration since the required laser fluence rate of 1.1 x 10^8 was achievable while simultaneously leading to less than 20% laser attenuation through the embryo. In addition, we found that the differential absorption will yield differential heating and therefore create thermal stress. We further evaluated thermal stress for Case 2 and 3 using both N = 1.2 x 10^{18} particles/m^3 and 1.8 x10^{18} particles/m^3. It was found that thermal gradients in Case 3 will generate only 1.9 MPa of thermal stress (See Fig. A3). This was significantly lower than the critical stress of 3.2 MPa estimated for a crack to form. The thermal stress generated from N = 1.2 x 10^{18} particles/m^3concentration which had 28% attenuation (i.e. above 20% desired) yielded a thermal stress of 3.6 MPa which exceeds the critical stress to crack. In short, GNR concentration of N = 1.2 x 10^{18} particles/m^3allowed us to use the maximum power of the laser while achieving $\leq$ 20% attenuation and avoiding excessive thermal stress across the embryo.

A.4 Thermal Modeling Setup

A computational model was developed to understand the thermal effects of liquid nitrogen cooling and convective and laser warming. Due to the lack of specific measurement of 2M PG, the embryo was assigned temperature-dependent thermal properties of 2M Glycerol in Phosphate-buffered saline from published measurements.[97] These values include density

(ρ), thermal conductivity (k) and specific heat (C_p). The modified Cryotop (with a wider blade) was modeled to have properties of polypropylene,[71] which are assumed to be independent of temperature. This was done for faster computation, since our interest was primarily in the embryo. Using different boundary conditions, cooling and warming scenarios for the zebrafish embryo were modeled. To model the cooling rates that an embryo would experience with the Cryotop when plunged in liquid nitrogen, a heat transfer coefficient h=5,000 W/m^2 °C was assumed. This value is consistent with the heat transfer coefficient obtained from the liquid nitrogen boiling curves for the nucleate boiling regime.[83] Earlier studies have reported that heat transfer coefficient for such cases of boiling with liquid nitrogen is generally between 1,000 W/m^2 °C to 10,000 W/m^2 °C.[84]

Different warming conditions were studied with this computational model. For instance, "Convective Warming" corresponds to Case 1 in a well-stirred water bath at 25 °C with heat transfer coefficient h = 1900 W/m^2 °C, which was directly calculated for forced (i.e. plunged) water for a sphere based on Whitaker (Nusselt) correlations (h = Nu*k/D)[98]. Case 2 was called the "GNRs in Chorion" case, which corresponded to a condition with GNRs uniformly distributed outside the embryo, within the chorion. Case 3, "uniform GNR distribution", corresponded to an idealized case of uniform distribution of GNRs throughout the system (i.e., nanoparticles were present inside the yolk and blastoderm, and chorion). Cases 2 and 3 utilized the heat generation from GNRs due to laser warming which can be calculated using Equation A1:

$$\nabla.(K\nabla T) + SAR = \rho c_p \frac{\partial T}{\partial t} \qquad (A1)$$

The specific absorption rate, or SAR, represents the heat generation from GNRs when irradiated with a laser. SAR, as shown in equation 1 is a function of GNR concentration

(N, nps/m^3), absorption cross section (C_{abs}, nm^2) and laser fluence rate (I, W/m^2). Since there is no realistic way to measure the warming inside the embryo, this model was set up to mimic the experimental conditions. During laser warming, the embryos are injected with GNR ($\mu_a = NC_{abs}$, N =1.2 x 10^{18} particles/m^3), and warmed with a fluence rate of 1.1 x 10^8 W/m^2, which gives a bulk SAR of 4.4 x 10^{11} W/m^3 for model.

A.5 Thermal Stress Analysis

The key to viable zebrafish embryos is to provide both rapid and uniform warming to prevent structural damage. For instance, the first 100 degrees of warming are prone to damage from thermal expansion (i.e. mechanical stress), while from -100 °C to 0 °C, there is the risk of devitrification (i.e. amorphous water converting to ice crystals) and disrupting biological structures.[72] To study the stresses resulting from the cryoprotectants during warming and therefore reduce the possibility of cracking, we used the maximum thermal gradients from our modeling results with the thermal stress model developed by Steif and colleagues.[99] The thermal stress (σ_t), defined as a function of the maximum temperature difference inside the embryo (Equation A2), for all the three warming cases discussed in the paper were studied using the following equation:

$$\sigma_t = g\frac{E\beta\Delta T}{1-\vartheta} \qquad \text{(A2)}$$

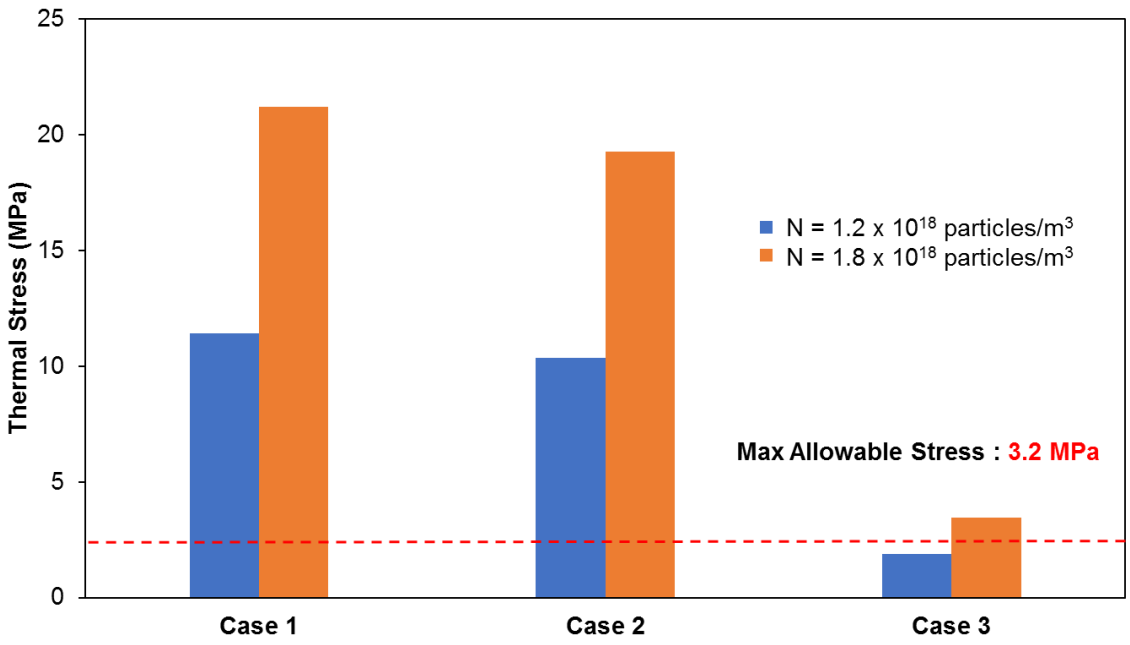

Figure A3. Thermal stress during various warming scenarios. For both N = 1.2 x 10^{18} and 1.8 x 10^{18} particles/m^3 GNR concentration, Case 1 corresponds to convective warming in a well stirred water bath at 25°C. Case 2 represents laser warming of embryos with GNRs present in chorion and droplet only. Case 3 represents laser warming of embryo with uniform distribution of GNR (i.e. inside yolk and chorion). Assuming a critical stress of 3.2 MPa from the literature[99], it became clear that only Case 3 for N = 1.2 x 10^{18} particles/m^3 had both a high and uniform warming rate needed to avoid ice formation and prevent cracking from thermal stress. By increasing the concentration of GNR to N = 1.8 x 10^{18} particles/m^3, all Cases were shown to exceed the critical thermal stress threshold.

In Equation A2, g = 0.4 is a geometric factor for sphere, whereas E = 1 GPa is the modulus of elasticity for an organic material, [100] ν = 0.2 is Poisson's ratio for a brittle material.[101] Finally, β is the volumetric thermal expansion coefficient for 2.2 M PG, which is calculated as function of temperature based on data in literature.[102] Even though the microinjection of GNR allows for uniform distribution of laser absorber (i.e. GNR), thermal gradients will still arise due to the variation in heat generation arising from attenuation of the laser as it passes through the embryo. For instance, when embryos have N = 1.2 x 10^{18} particles/m^3 of GNR, the top of the embryo would receive 100% laser energy compared to bottom that would receive only 80% of the laser energy, thereby producing temperature gradients. Steif

and colleagues also conducted experiments to analyze the spontaneous fracture of a thin film of cryoprotectant (7 M Dimethyl sulfoxide) on a cooling substrate from which they determined a critical stress of 3.2 MPa.[99]

The embryo will expand during warming and so the induced stresses will be compressive. It should also be noted that maximum stress corresponds with the circumferential stress for the sphere and, this stress is maximum at the geometric center of the sphere. Also, significant additional thermal stresses will be induced during cooling and will likely exist in the already cooled embryo. However, the current analysis was focused on warming, and therefore it does not consider the more detailed thermal stress analyses associated with cooling.

A.6 Zebrafish Histology

Figure A4 shows histology images of control and GNR injected ($N = 4.8 \times 10^{18}$ particles/m^3) zebrafish embryos that hatched and grew to Day 7. Silver enhancement precipitates metallic silver onto GNR thereby allowing visual assessment under light microscopy as a dark stain. As shown by the red arrows in Fig. A4a, no GNR were found in control, although natural pigmented "stripes" are present in all fish. In Fig. A4b yellow arrows point to areas of GNR deposit found in the yolk and tail of GNR injected fish. Since the yolk syncytial layer creates an impermeable membrane around the yolk, it was understandable to find stains in the yolk. In addition, a small amount of GNR was found in the tail vasculature as well. While ICP OES was considered, the total amount of gold per fish (0.2 ppb) was far below the limit of detection (250 ppb) of this technique and therefore was not attempted. These results suggest that small amounts of GNR are retained within the yolk and tail of the fish as they grow.

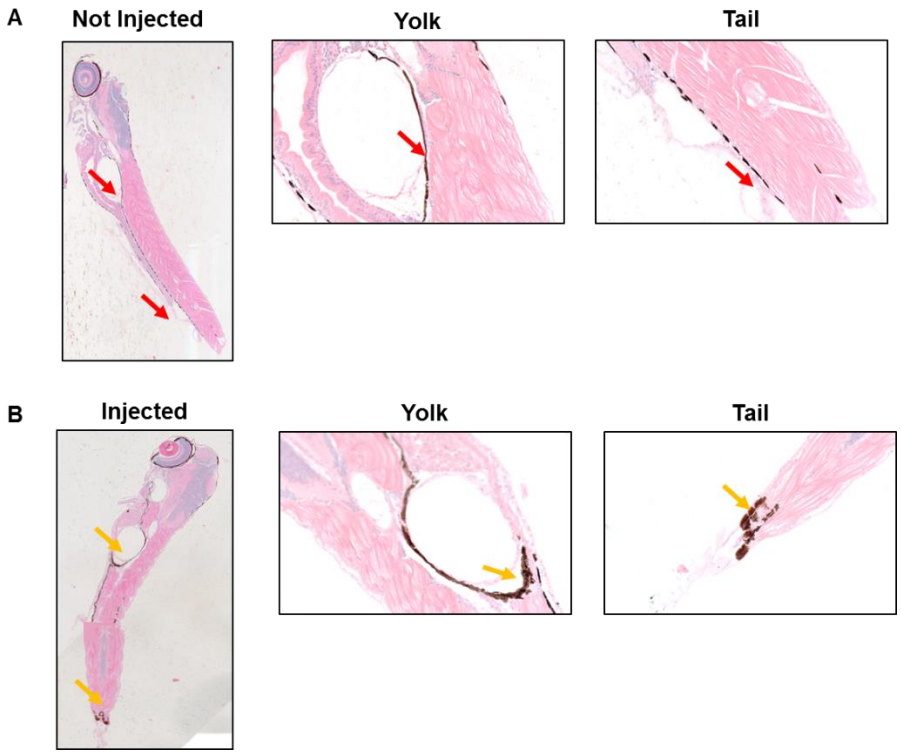

Figure A4: Silver stained histological sections of Zebrafish after embryo GNR micro-injection. (a) Control fish, where embryos were not injected and (b) Fish from GNR injected embryos showing the entire fish, yolk, and tail section. Red arrows show pigmented black zebrafish stripes present in all fish, while yellow arrows point to silver enhanced GNR present only in injected fish

Two sets of zebrafish embryos (n=5 each) were used to assess GNR distribution during development. The experimental group was injected with N =1.2 x 10^{18} particles/m^3 of GNR and 2 M PG while the other was left uninjected as a control. The embryos were cultured up to Day 7 and then euthanized in cold water. Both sets of zebrafish were fixed in Dietrich's fixative for 24 hours as suggested in Westerfield.[80] The fish were then embedded in paraffin blocks, sectioned (each 20 µm thick) and placed on glass slides. The sections were de-waxed and stained with LI Silver (Nanoprobes Inc., NY) based on a protocol developed in the literature.[85] The slides were then counterstained with nuclear Fast Red and covered with a glass slide. High resolution light microscopy images were taken of both sets of zebrafish to locate dark staining areas representing GNR.

Appendix B

This appendix shares details such as CAD drawings and BOM for the cryojig.

B1. Bill of Materials for Cryojig (no electronics)

Part Name	Quantity	Model #	Dimensions	Notes
Servo Motor	1	HiTech 5625MG		Servo City
Servo mount	1	Custom	See drawing	can be 3D printed
Linear Stage	2	TSX-1D		Metric, Newport
Styrofoam box	1	Generic	8in x 6.5in x 3in	leak proof andlarge enough to form base the motor and linear stage assembly (LIN
Base plate	1	custom	See drawing	can be 3D printed from UofM
Cryotop holder	1	custom	See drawing	can be 3D printed from UofM
SCHS M6	6		14 mm long	metric, socket head
SCHS 6-32 screw	3		8mm long	metric, socket head

B2. CAD drawing for Cryotop holder/mount

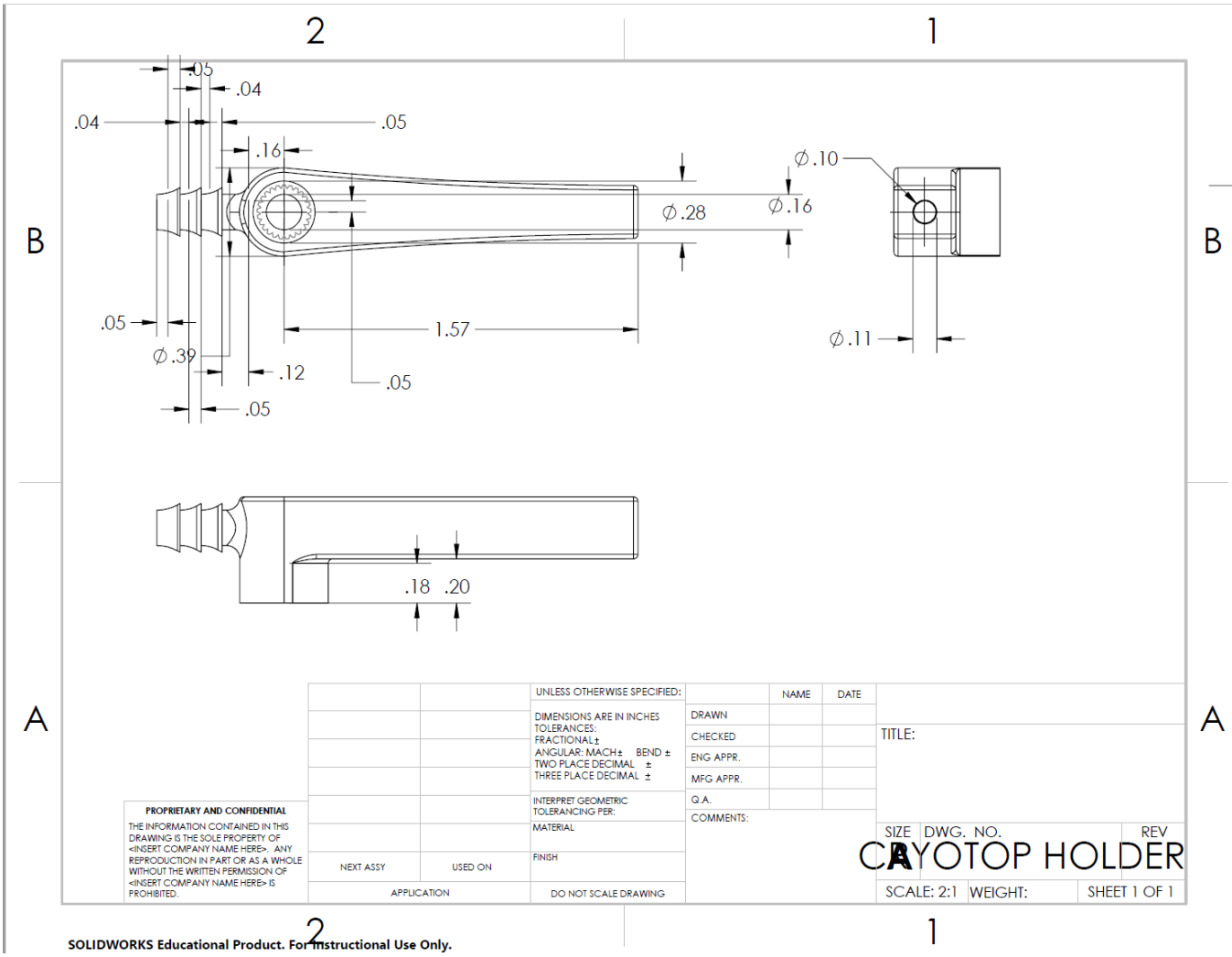

B3. CAD drawing for base plate

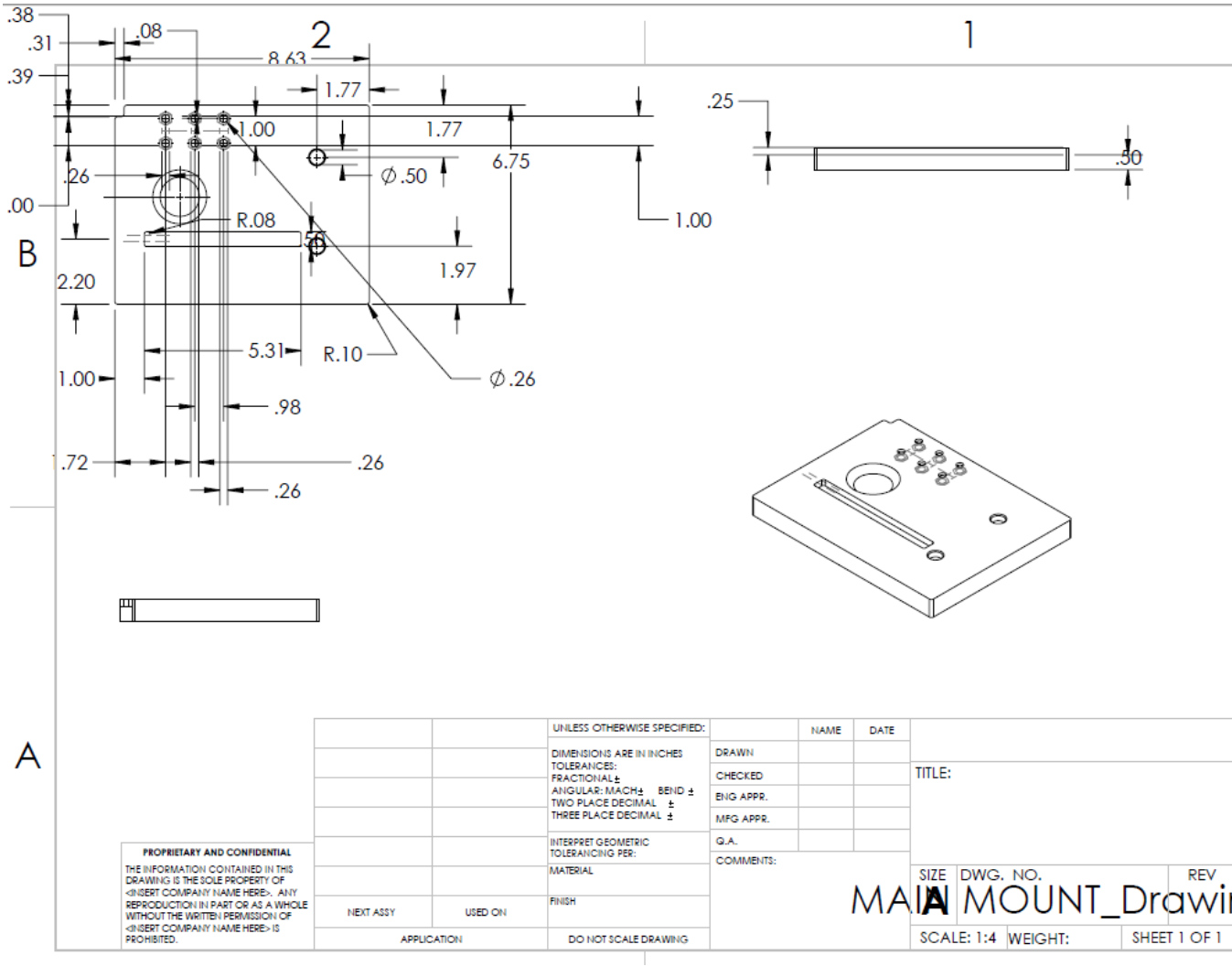

B4. CAD drawing for servo mount

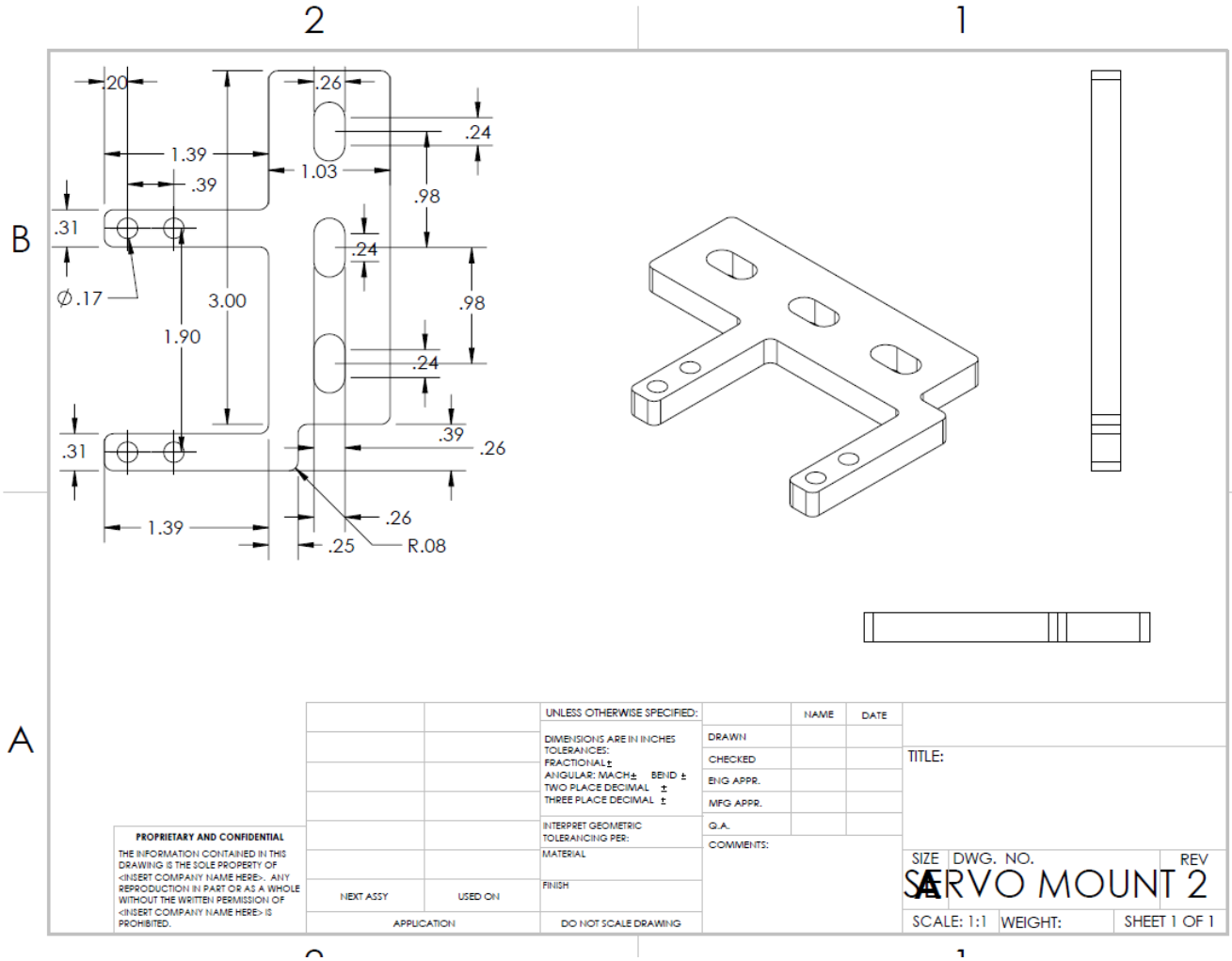

B5. Layout of the microcontroller box for cryojig

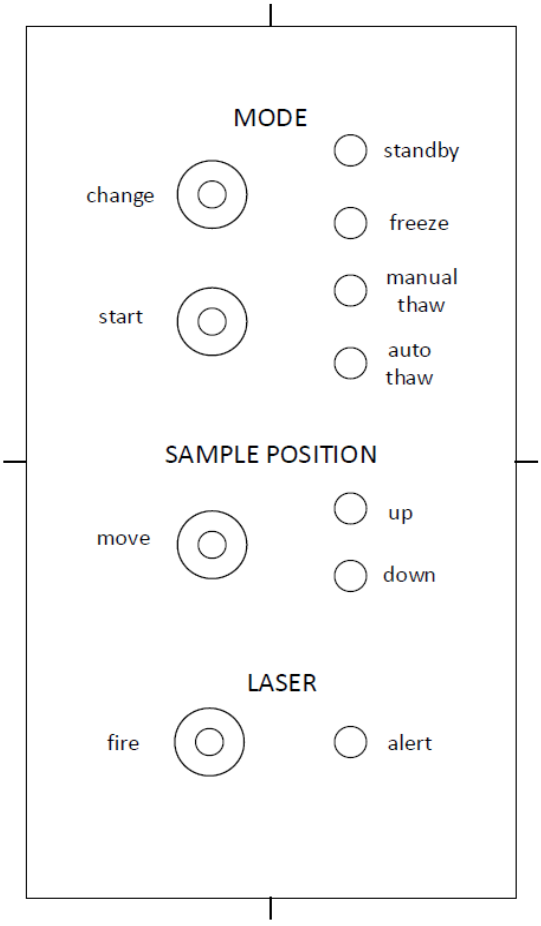

B6. CAD Model of the Cryojig

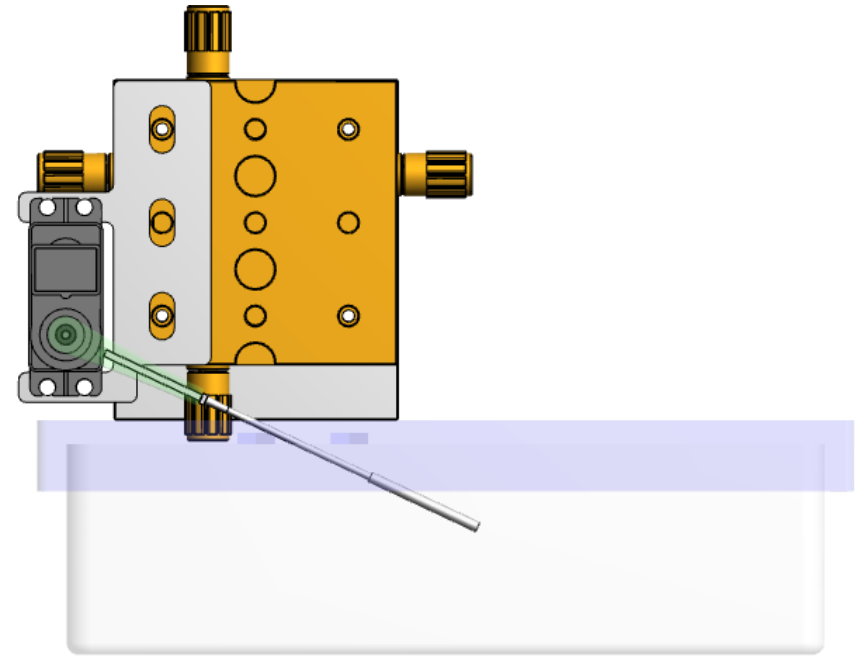

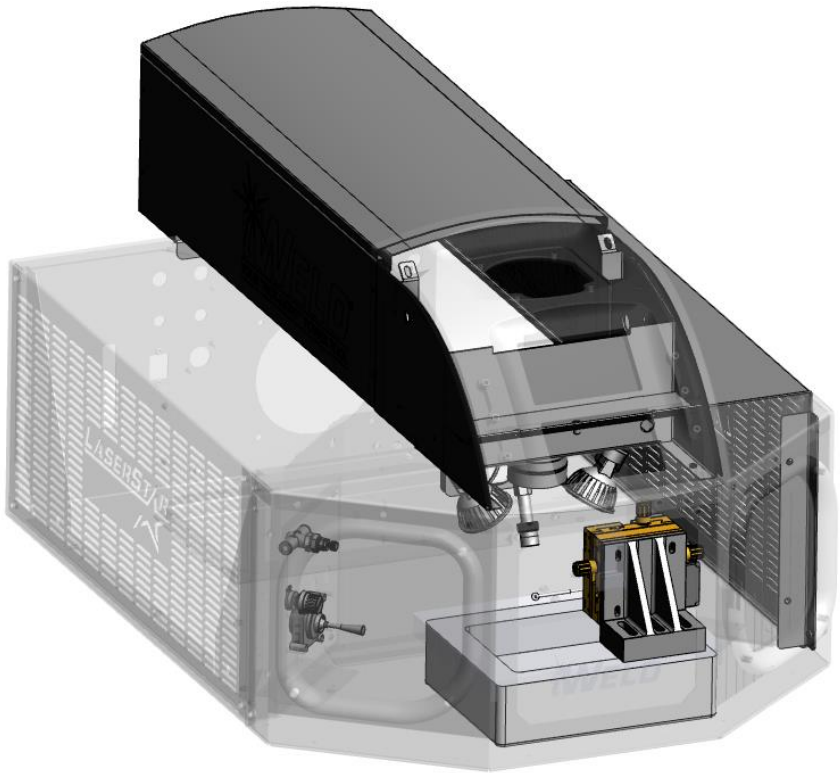

Appendix C

This appendix shares the cover page of a peer reviewed publications from our coral cryopreservation and laser warming work with our Smithsonian Collaborators. The author contributed significantly to this work and it led to the first ever instance of successful cryopreservation of coral larvae.

1. Daly, J., Zuchowicz, N., Lendo, C. I. N., **Khosla, K.**, Lager, C., Henley, E. M., ... & Hagedorn, M. (2018). Successful cryopreservation of coral larvae using vitrification and laser warming. *Scientific reports*, *8*(1), 15714. DOI: 10.1038/s41598-018-34035-0 Open access via Creative Commons Attribution 4.0 International License

SCIENTIFIC REPORTS

OPEN

Successful cryopreservation of coral larvae using vitrification and laser warming

Received: 8 June 2018
Accepted: 7 October 2018
Published online: 24 October 2018

Jonathan Daly[1,2], Nikolas Zuchowicz[1,2], C. Isabel Nuñez Lendo[1,2], Kanav Khosla[3], Claire Lager[1,2], E. Michael Henley[1,2], John Bischof[3,4], F. W. Kleinhans[5], Chiahsin Lin[6,7], Esther C. Peters[8] & Mary Hagedorn[1,2]

Climate change has increased the incidence of coral bleaching events, resulting in the loss of ecosystem function and biodiversity on reefs around the world. As reef degradation accelerates, the need for innovative restoration tools has become acute. Despite past successes with ultra-low temperature storage of coral sperm to conserve genetic diversity, cryopreservation of larvae has remained elusive due to their large volume, membrane complexity, and sensitivity to chilling injury. Here we show for the first time that coral larvae can survive cryopreservation and resume swimming after warming. Vitrification in a 3.5 M cryoprotectant solution (10% v/v propylene glycol, 5% v/v dimethyl sulfoxide, and 1 M trehalose in phosphate buffered saline) followed by warming at a rate of approximately 4,500,000 °C/min with an infrared laser resulted in up to 43% survival of *Fungia scutaria* larvae on day 2 post-fertilization. Surviving larvae swam and continued to develop for at least 12 hours after laser-warming. This technology will enable biobanking of coral larvae to secure biodiversity, and, if managed in a high-throughput manner where millions of larvae in a species are frozen at one time, could become an invaluable research and conservation tool to help restore and diversify wild reef habitats.

Coral reefs are imperiled globally by ocean warming and acidification resulting from the overuse of fossil fuels[1]. Since the early 1980s, three global bleaching events and scores of regional bleaching events have caused extensive coral stress and mortality[2–4]. On the Great Barrier Reef in Australia, above-average sea surface temperatures during 2016 and 2017 caused back-to-back mass bleaching events for the first time, resulting in the loss of an estimated 29% of shallow water coral cover in 2016 alone[5]. Even when coral survive bleaching, reproduction and fecundity are often profoundly affected for multiple breeding seasons[6], and the stress caused by warming can result in reduced reproductive output even in corals that do not visibly bleach[7]. Over three-quarters of the world's coral reefs are predicted to experience annual bleaching by the end of this century[8], so the need for innovative restoration tools to conserve and secure reef biodiversity is critical.

One of the most effective methods to secure biodiversity is low-temperature storage of reproductive material in biorepositories. Ultra-cold storage of living coral samples from healthy reefs can help mitigate the loss of genetic and species diversity caused by natural disasters and major bleaching events while avoiding problems like genetic drift that occur in multi-generational *ex situ* populations[9]. Storage of genetic material would also support and complement existing reef restoration programs, which encompass a range of strategies. These include research aimed at improving the ability of coral to adapt to changing environmental conditions (such as assisted gene flow, selective breeding, and hybridization)[10] and improving restoration methods by diversifying depauperate populations with frozen sperm. To be effective, these restoration efforts will require a broad base of species and genetic diversity. Therefore, it is vital to begin globally-linked programs that can secure reef biodiversity over

[1]Smithsonian Conservation Biology Institute, Front Royal, VA, 22630, United States of America. [2]Hawaii Institute of Marine Biology, 46-007 Lilipuna Rd, Kaneohe, HI, 96744, United States of America. [3]Department of Mechanical Engineering, University of Minnesota at Twin Cities, 111 Church St SE, Minneapolis, MN, 55455, United States of America. [4]Department of Biomedical Engineering, University of Minnesota at Twin Cities, 312 Church St SE, Minneapolis, MN, 55455, United States of America. [5]Department of Physics, Indiana University-Purdue University Indianapolis, Indianapolis, IN, 46202, United States of America. [6]National Museum of Marine Biology & Aquarium, Pingtung, 944, Taiwan. [7]Institute of Marine Biology, National Dong Hwa University, Pingtung, 944, Taiwan. [8]Environmental Science and Policy, George Mason University, Fairfax, VA, 22010, United States of America. Correspondence and requests for materials should be addressed to J.D. (email: dalyj@si.edu)